ESTIMATING HIGHWAY SUBSIDENCE DUE TO LONGWALL MINING

by

Juan José Gutiérrez Puertas

Ingeniero Civil, Universidad de los Andes, 2003

Master of Science, University of Pittsburgh, 2008

Submitted to the Graduate Faculty of

Swanson School of Engineering in partial fulfillment

of the requirements for the degree of

Doctor of Philosophy

University of Pittsburgh

2010

UNIVERSITY OF PITTSBURGH

SWANSON SCHOOL OF ENGINEERING

This dissertation was presented

by

Juan José Gutiérrez Puertas

It was defended on

March 25, 2010

and approved by

Luis E. Vallejo, Ph.D., Professor, Department of Civil and Environmental Engineering

Jeen-Shang Lin, Sc.D., Associate Professor, Department of Civil and Environmental Engineering

Julie M. Vandenbossche, Ph.D., Assistant Professor, Department of Civil and Environmental Engineering

Anthony Iannacchione, Ph.D., Associate Professor, Department of Civil and Environmental Engineering

Patrick Smolinski, Ph.D., Associate Professor, Department of Mechanical Engineering and Materials Science

Dissertation Co-Directors:

Luis E. Vallejo, Ph.D., Professor, Department of Civil and Environmental Engineering

Jeen-Shang Lin, Sc.D., Associate Professor, Department of Civil and Environmental Engineering

ESTIMATING HIGHWAY SUBSIDENCE DUE TO LONGWALL MINING

Juan José Gutiérrez Puertas, Ph.D.

University of Pittsburgh, 2010

Longwall mining is a common underground coal extraction technique in Appalachia. The extraction takes the form of panels whose width and length can reach approximately 450 m and 4000 m, with a thickness of about 2.0 m. Typical depth ranges from 180 m to 280 m. Longwall panels were mined underneath highway I-79 in the Cumberland and Emerald mines in southwestern Pennsylvania, causing large subsidence that affects traffic safety and can potentially damage highway structures such as pavements, culverts, and bridge abutments. Mining under the highway prompted the close monitoring by the Pennsylvania Department of Transportation of the impact of mining on the highway sections above the mines. A substantial amount of data was collected that formed the basis of this work. The data included time series of surveying data and inclinometer data in selected points. With the aid of a genetic algorithm, a three dimensional subsidence model was developed. The model gives the spatial and temporal distribution of surface subsidence in terms of the depth of mining, the panel width, the thickness of extraction, and the location relative to the face of the panels. Although the prediction of vertical deformations through the empirical model is feasible, the lateral deformation behavior of highway foundations did not always follow the premises adopted in existing subsidence prediction tools, often based on flat conditions. The complex topography of highway foundations, dominated by embankments with irregular cross sections, a sloped grade, and different orientations with respect to the direction of mining, gives each case a unique character that deems it very difficult to develop comprehensive empirical models to predict the location and magnitude of lateral deformations and strain/stress concentrations. The lateral component of subsidence prediction is very important as it is directly related to damage of the highway structures. A FEM model was developed in order to better understand the mechanisms of subsidence. The results of both empirical and numerical modeling are presented. The findings of this study have a broader scope than highway deformations, with potential applications on any type of earthen structures impacted by underground mining.

TABLE OF CONTENTS

LIST OF TABLES

LIST OF FIGURES

ACKNOWLEDGEMENTS

The successful completion of this study would have not been possible without the guidance and support provided to me by my advisors, Dr. Luis Vallejo and Dr. Jeen-Shang Lin. To them I extend my deepest gratitude.

Parallel to this study, I had the opportunity to meet experts from the Mining Engineering discipline, namely Dr. Anthony Iannacchione and Dr. Daniel Su. Their comments and insights were very useful to me in connecting my desk work to the real world.

I would also like to thank Roy Painter, Geotechnical Engineer with PennDOT, for always providing me with useful data and comments.

My deepest feelings go to my parents for their immense love. People that come to my mind and in many ways instilled in me the motivation to achievement in life are *abuelita Margot*, *tio Mimo*, *tia Paulina*, and *Ana Ximena*, my sister. My strongest mentor has always been my father, *Meko*, who shaped a big portion of who I am. My mother, *Yolanda*, is my dearest silent companion.

I want to express my deep love to my two *niñas*, *Jenny* and *Gabriela*. I dedicate this effort to both of you.

1.0 BACKGROUND

This dissertation is concerned with the prediction of highway subsidence caused by coal longwall mining in southwestern Pennsylvania. When underground mining is performed, the overburden, or earth portion from the mine to the surface, experiences a loss of equilibrium due to the extraction of material. For a new equilibrium condition to be achieved, the overburden moves towards the created cavity. If the extracted area is large enough, disturbances in the overburden reach the surface. Movements in the surface have both vertical and horizontal components and form a basin or trough (Kratzsch 1983; Peng and Chiang 1984; Peng 1992; Kratzsch 2008).

The formation of the subsidence trough is accompanied by settlements, strains, and displacements that have a negative impact on structures and natural resources lying within the area of influence of the extraction (Kratzsch 1983; Whittaker and Reddish 1989; Peng 1992; Kratzsch 2008).

Coal resources in southwestern Pennsylvania have recently been extracted under high traffic roads with subsequent structural damage and safety deleterious effects. Damages in highway structures due to the action of mining-induced subsidence include pavement cracking, compression bumps, damage to buried culverts, and cracking of bridge abutments (GeoTDR 2001).

Researchers have developed methods to predict subsidence and the consequent ground deformations and have applied them widely with reported success (Kratzsch 1983; Whittaker and Reddish 1989; Kratzsch 2008; Agioutantis and Karmis 2009).

1.1 LONGWALL MINING

Longwall mining is the most productive coal mining method in current practice. The high production rates are possible due to the extraction of large areas of coal seams in the form of rectangular panels. Coal seams in southwestern Pennsylvania have a thickness that ranges from roughly 1.5 m to 2.5 m. The typical width of a rectangular panel in this region may range between 350 m and 450 m, and its length can reach around 4000 m. The overburden thickness lies between 180 m and 280 m. Figure 1-1 gives a plan view of a series of longwall panels (Mine Subsidence Engineering Consultants 2007).

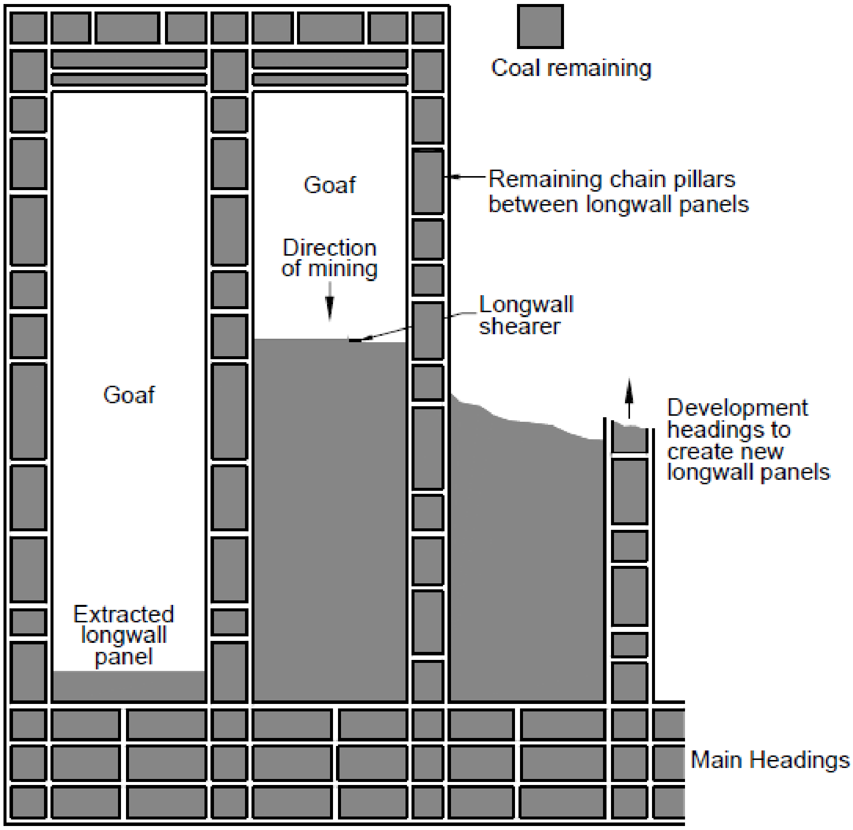

Figure 1-1 Plan view of longwall panels

(Mine Subsidence Engineering Consultants 2007)

The portion below relies heavily on a succinct description provided by Mine Subsidence Engineering Consultants, of Australia (Mine Subsidence Engineering Consultants 2007).

Before a longwall panel is mined out, a system of roadways is constructed around it. Between two adjacent panels, these roadways are called development headings, which are used to create new longwall panels. The roadways located at the entrance of the longwall panels are called main headings, and provide access to personnel and mining utilities. The direction of mining advancement is towards the main headings. The coal areas remaining between the roadways are called coal pillars.

In the process of mining, the piece of equipment cutting the coal is called the shearer, which travels back and forth along the mine face transversally to the panel long side, with a resultant net advancement in the direction of the long side of the panel. The personnel, shearer and a belt conveyor that takes the extracted coal out of the mine face are protected by a series of hydraulic supports and canopy that advance in the direction of mining. Behind the canopy the mine roof falls onto the gob. As the roof falls, upper strata fracture and sag whereas further upper strata bend, forming the subsidence trough. Figure 1-2 depicts a cross section of a longwall mine face.

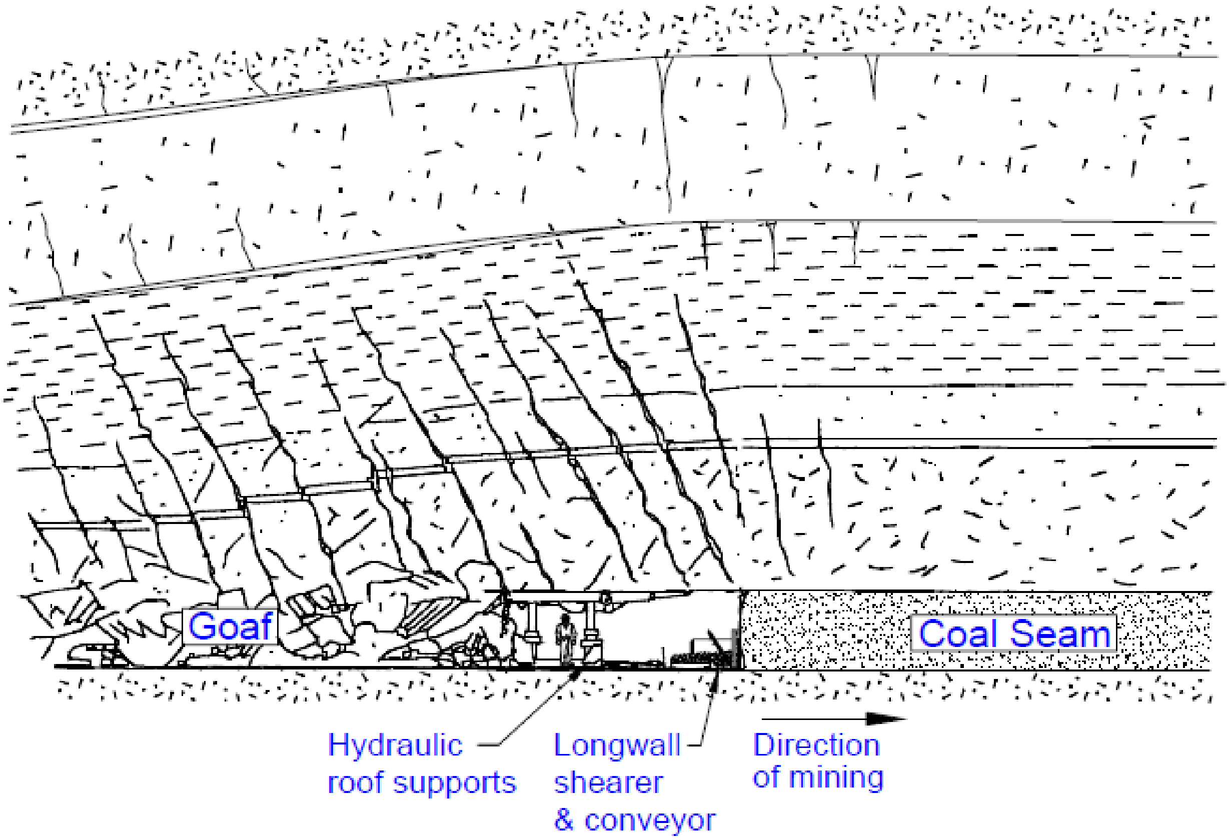

Figure 1-2 Cross section of a longwall face

(Mine Subsidence Engineering Consultants 2007)

1.2 THE SUBSIDENCE MECHANISM

Surface subsidence starts to develop slowly as the mined-out area is increased. The degree of affectation of the overburden is highest at the mine roof and diminishes upward. When a sufficiently large dimension in the cavity is reached, the roof collapses, forming a zone of fragmented angular rock that sags and closes the void created by mining. This is known as the caved zone, which ranges from 2 to 8 times the height of the extracted coal (Peng and Chiang 1984; Peng 1992). Above the caved zone is the fractured zone, in which vertical fractures and horizontal bed separations from large blocks. The fractured zone has a typical height of 28 to 42 times the extracted height. The combined height of the caved and fracture zones is roughly 30 to 50 times that of the extracted coal (Peng and Chiang 1984; Peng 1992).

While the mined-out area is still small, the disturbances caused in the overburden are accommodated by an arching effect of large rock fragments (Mine Subsidence Engineering Consultants 2007). As the area of mining grows, the magnitude of subsidence in the surface also increases. The level of subsidence reached while the arching effect is still in action is called subcritical. In subcritical conditions, increasing the mined-out area causes surface subsidence to increase. The dimensions of the panel at which the maximum potential subsidence is reached are called critical dimensions. Beyond the critical dimensions, the magnitude of subsidence does not change. This is known as supercritical subsidence (Whittaker and Reddish 1989; Mine Subsidence Engineering Consultants 2007). The current dimensions used in the coal industry longwall panels generally exceed critical dimensions, therefore it is common to have troughs that have a central flat area experiencing maximum potential subsidence.

1.3 SUBSIDENCE DEFORMATION INDICES

Surface subsidence is a fairly complex three-dimensional process characterized mainly by vertical and horizontal displacements, tilting, convex and concave curvature, and tensile and compressive strains (Kratzsch 1983; Whittaker and Reddish 1989; Mine Subsidence Engineering Consultants 2007; Kratzsch 2008). These deformation indices are defined below, and an illustration of their distribution is provided in Figure 1-3.

1.3.1 Subsidence

The term subsidence stands for the whole phenomenon of surface deformations. However, in practice it is often understood as the vertical displacement of the surface. It is given in units of length (Mine Subsidence Engineering Consultants 2007).

1.3.2 Tilt or slope

Tilt is mathematically computed as the first derivative of subsidence and reaches its maximum magnitude at the point of inflection of the subsidence profile, where the curvature changes from convex to concave. It is given in units of length over length (Mine Subsidence Engineering Consultants 2007; Agioutantis and Karmis 2009).

1.3.3 Horizontal displacement

The horizontal displacement is maximum at the inflexion point of the subsidence trough, where the curvature changes from convex to concave and the slope is also at its maximum (Mine Subsidence Engineering Consultants 2007). A traditional approach to estimate horizontal displacements is by linear correlation to slope (Luo, Peng et al. 1996; Agioutantis and Karmis 2009). It is given in units of length.

1.3.4 Curvature

Curvature is given by the second derivative of subsidence or the first derivative of slope. It is convex from the inflexion point towards the edge of the trough and concave towards the panel center. Its units are 1 over length (Mine Subsidence Engineering Consultants 2007).

1.3.5 Horizontal strain

Horizontal strain is defined as the first derivative of horizontal displacements. Its units are length over length (Agioutantis and Karmis 2009).

1.3.6 Angle of draw

The angle of draw is the angle formed by a vertical line projected from the panel edge to the surface and a line connecting the panel edge and a point experiencing no subsidence (Whittaker and Reddish 1989; Mine Subsidence Engineering Consultants 2007; Agioutantis and Karmis 2009).

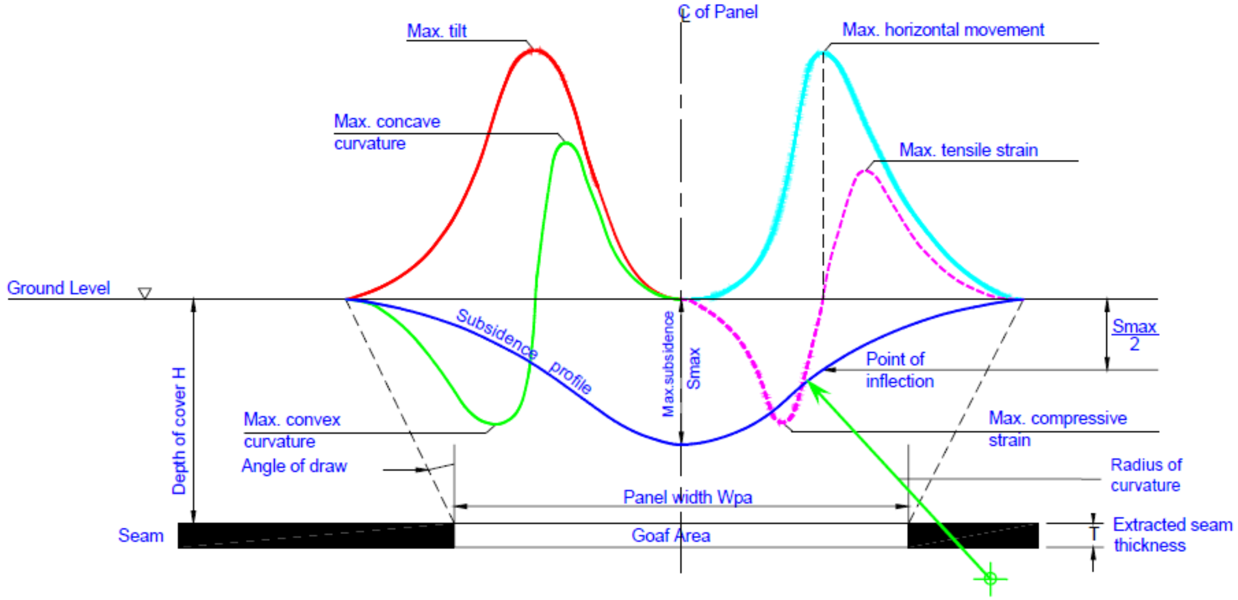

Figure 1-3 Subsidence deformation indices

(Mine Subsidence Engineering Consultants 2007)

Figure 1-4 depicts typical subsidence, horizontal displacements, and horizontal strain distributions for subcritical, critical, and supercritical conditions.

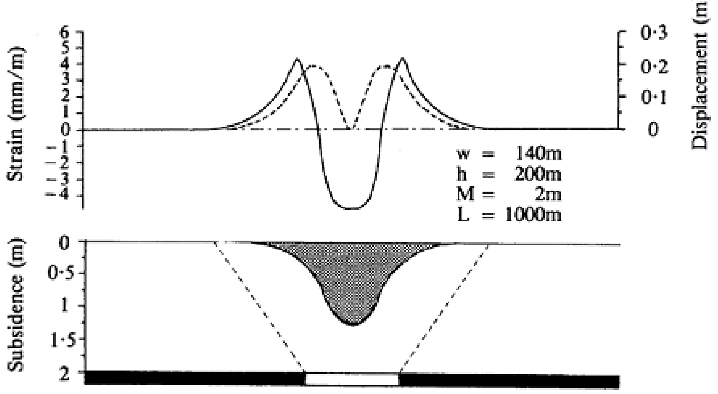

(a) Subcritical extraction

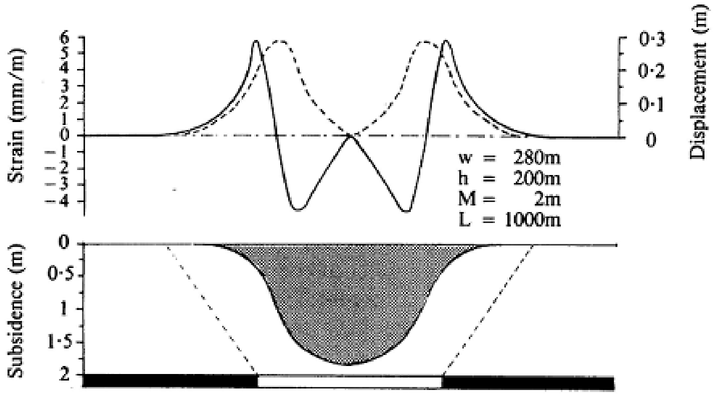

(b) Critical extraction

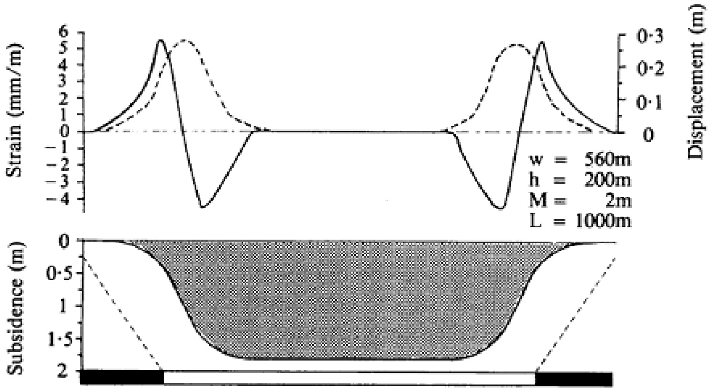

(c) Supercritical extraction

Figure 1-4 Subcritical, critical, and supercritical subsidence conditions

(Whittaker and Reddish 1989)

1.4 RESEARCH OBJECTIVES

The objectives of this dissertation are:

- To develop new three-dimensional empirical relationships for the prediction of longwall mining-induced highway subsidence (vertical displacements).
- To develop estimations of subsidence deformation indices, such as slope, horizontal displacement, curvature, and horizontal strain, based upon three-dimensional empirical relationships.
- To assess the feasibility of empirical relationships to correctly estimate surface deformation indices on a highway.
- To develop a three-dimensional Finite Element model for the purpose of subsidence estimation in order to aid the understanding of the key mechanisms governing the subsidence process.
- To develop a sensitivity analysis aimed at identifying key mechanisms and parameter interactions that explain surface subsidence.
- To study ways to account for subsidence deformation indices in the case of highway subsidence prediction whenever traditional assumptions fail or under-perform.

1.5 RESEARCH SIGNIFICANCE

Subsidence and surface strains induced by mining can affect the safety and integrity of buildings, roads, pipelines, dams, and reservoirs (Coulthard and Dutton 1988). The correct prediction of the magnitude, location, and direction of deformation indices in the subsidence trough is important in aiding the planning and protection of structures located at the surface and near subsurface. In the case of highways, structures that need protection and repairs due to the negative impact of mining are mainly pavements, culverts, and bridges (GeoTDR 2001).

Surface horizontal displacements, upon which strains and damage predictions are based, have traditionally been correlated linearly to the trough slope where the terrain can be assumed flat (Kratzsch 1983; Luo, Peng et al. 1996; Kratzsch 2008; Agioutantis and Karmis 2009). In the case of hilly terrain, predictions of horizontal displacements based on this assumption have been recognized as less reliable than subsidence or vertical displacement predictions, and methods have been proposed to correct horizontal displacements for hilly conditions (Luo, Peng et al. 1996; Luo and Peng 1999; Karmis, Agioutantis et al. 2008).

Corrected methods for hilly conditions in the prediction of horizontal displacements, upon which the ultimate damage predictions rely, have yielded successful results when shallow top soil thicknesses have been considered on top of bed rock (Luo and Peng 1999). However, the nature of highway foundations, dominated by large man-made earth works, may not be equated to the situation of natural bedrock with shallow topsoil upon which the existing method (Luo and Peng 1999) relies.

Embankments constructed with compacted soils along the highways that run across southwestern Pennsylvania can reach a large size, with heights above 30 m and base widths of more than 100 m. Structures of interest may be located at zones dominated or influenced to a varying degree by these massive structures. Given the different structural composition of highway foundations as opposed to natural terrain, it is important to understand the interactions between the response of the natural terrain and that of these man-made earth works to the mining process. A key question is whether conventional subsidence prediction models work in the case of highway subsidence, and whether it is possible to accurately estimate the magnitude and distribution of subsidence and deformation indices along highways. This dissertation aims at the development of a new subsidence (vertical displacement) prediction tool for highways in southwestern Pennsylvania. Also, a numerical approach is used to aid the understanding of subsidence mechanisms that cannot be captured by empirical relationships.

2.0 LITERATURE REVIEW

There are different types of subsidence prediction methods. Whittaker and Reddish classify them into five groups: Empirically derived relationships, profile functions, influence functions, analytical models, and physical models (Whittaker and Reddish 1989). Karmis, Haycocks, and Agioutantis consider three main groups: Theoretical models, numerical methods, and empirical or semi-empirical methods (Karmis, Haycocks et al. 1992). The former researchers consider the Finite Element Method as part of analytical methods; the latter consider profile and influence functions as part of empirical methods.

The present literature review focuses on two groups of subsidence prediction methods, namely empirical methods and numerical methods. Within empirical methods, both profile functions and influence functions are introduced.

2.1 LITERATURE ON EMPIRICAL MINE SUBSIDENCE PREDICTION

Empirical methods are popular due to their flexibility and ease of application (Karmis, Haycocks et al. 1992). Within empirical methods, profile functions and influence functions are the most widely used methods in longwall mining subsidence prediction (OSMRE 1986). Profile functions are two-dimensional functions that can be calibrated through proper parameters on a regional basis (Agioutantis and Karmis 2009). Influence functions provide a three-dimensional subsidence prediction, can also be calibrated on a regional basis, and provide the additional advantage of mathematically allowing superposition (Agioutantis and Karmis 2009).

Empirical methods, both profile and influence functions, require the initial estimation of maximum subsidence. The proportional subsidence distributions yielded by either method through proper functions are then multiplied by this parameter and the actual subsidence profiles or troughs can be obtained.

2.1.1 Maximum Subsidence

In empirical methods, the magnitude of maximum subsidence is the first step in subsidence prediction. The general expression for maximum subsidence is as follows (Kratzsch 1983; Peng 1992; Kratzsch 2008; Agioutantis and Karmis 2009):

$$S_{max} = a \cdot M \qquad \textbf{2-1}$$

where

S_{max} = Maximum potential subsidence.

$a =$ Maximum subsidence factor.

$M =$ Extraction thickness.

Engineers from different coal regions in the world have used typical values of the subsidence factor, a, depending on the coal basin. In the case of longwall mining allowing caving, British and German coalfields have experienced a subsidence factor of 0.9, French coalfields a value between 0.85 and 0.90, Polish 0.70, Russian ranging from 0.60 to 0.90, and American ranging from 0.50 to 0.60 (Whittaker and Reddish 1989). Subsidence literature concerned with data obtained in Appalachia shows that the subsidence factor for this region can reach magnitudes above 0.60 (Karmis 1987). From informal talks with an expert with substantial experience in southwestern Pennsylvania coal mines, the author learned that a generally accepted value for subsidence factor in southwestern Pennsylvania is 0.67.

In addition to the maximum potential subsidence factor, profile function methods require the estimation of maximum subsidence, $S*$, for the case of subcritical conditions. A widely accepted model in Appalachia for the whole range from subcritical maximum subsidence factors to supercritical maximum potential subsidence factors, where $S* = S_{max}$, was proposed by the Department of Mining and Minerals Engineering of the Virginia Polytechnic Institute and State University (Karmis, Triplett et al. 1983). The subsidence factor in this model is a function of the ratio of panel width over mine depth, W/H, and the percentage of hardrock, *H.R.*, which is defined as the percentage by thickness of the cumulative limestone, sandstone, and similar hardrock layers, considering a minimum layer thickness of 1.5 m. The software Surface Deformation Prediction System SDPS 6.0 (Agioutantis and Karmis 2009) uses this model (Figure 2-1). The magnitude of W/H found in Appalachia for critical conditions is 1.2 (Agioutantis and Karmis 2009). Values below 1.2 correspond to subcritical conditions; values above this threshold correspond to supercritical conditions.

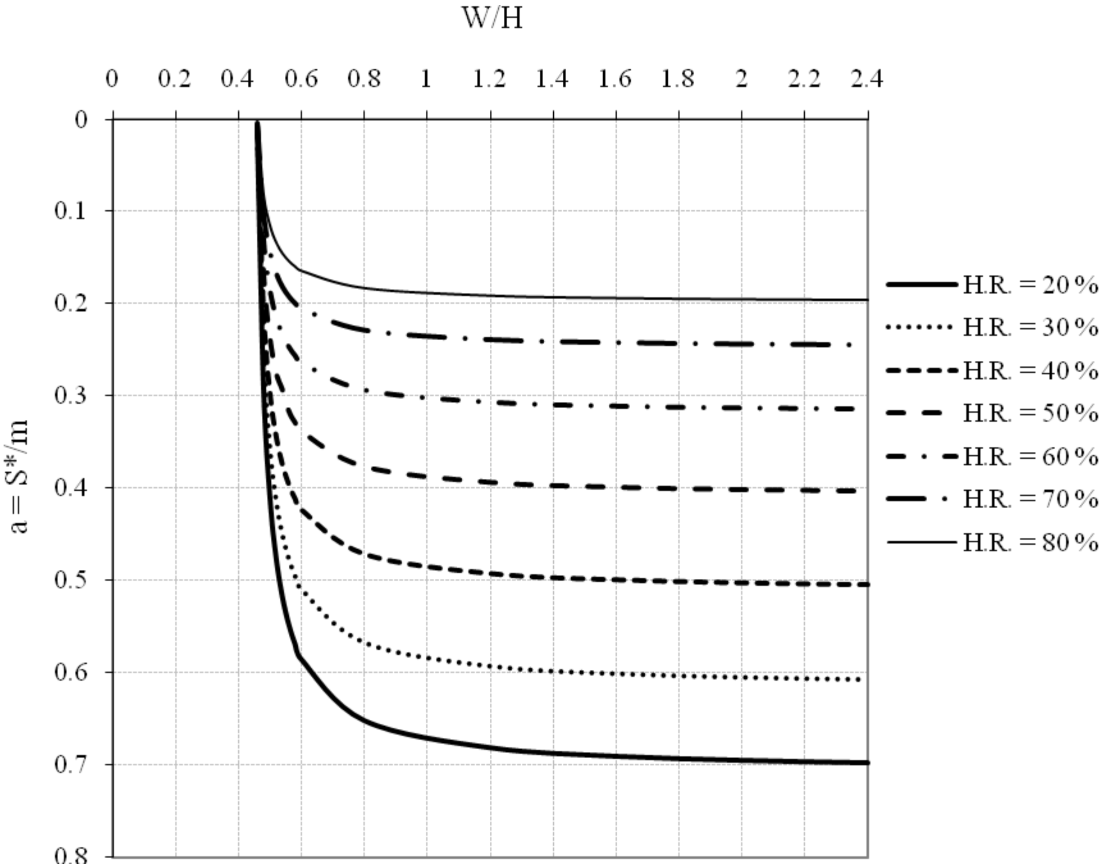

Figure 2-1 Current maximum subsidence factor prediction model

Based on SDPS version 6.0 (Agioutantis and Karmis 2009)

2.1.2 Profile Functions

The most widely used profile functions in the Appalachian coalfield are the exponential function and the hyperbolic tangent function (OSMRE 1986). The former was proposed by Chen and Peng in 1981, whereas the latter was proposed by the Department of Mining and Minerals Engineering at the Virginia Polytechnic Institute and State University (Karmis, Triplett et al. 1983). The software SDPS 6.0 uses the latter profile function.

2.1.2.1 Hyperbolic Tangent Function

The present portion on hyperbolic tangent function relies heavily on the description by the author who proposed its implementation (VPI&SU 1987). The hyperbolic function is given as follows:

$$S = 0.5S^* \left[1 - \tanh\left(\frac{cx}{B} \right) \right] \qquad \textbf{2-2}$$

where:

S^* = Maximum subsidence.

c = Fitting constant; 1.8 for critical and supercritical profiles, 1.4 for subcritical profiles.

x = Distance from the inflection point (negative towards the panel center).

B = Distance from the closest-to-edge point with maximum potential subsidence, S_{max}, and the inflection point.

Based on equation 2-2, the maximum subsidence is not located exactly at the panel center. A correction is therefore required, as follows:

$$S'_{max} = \frac{S^*}{S_{center}} S^* \qquad \textbf{2-3}$$

where:

S'_{max}= Corrected maximum subsidence.

S_{center}= Magnitude of subsidence at panel center before correction.

S^* = Estimated maximum subsidence.

The distance B can be estimated if the edge effect, or horizontal distance between the inflexion point and the vertical line projected from the panel edge, is known. The researchers that developed this prediction method also provided empirical relationships for the magnitude of the edge effect as a function of the ratio W/H (VPI&SU 1987). The edge effect needs to be subtracted from the total distance between the closest-to-edge point with maximum potential subsidence and the vertical line projected from the panel edge. This latter magnitude can be obtained from the fact that $W = 1.2H$ for critical conditions. Half of W is then the distance from which the edge effect is subtracted:

$$B = 0.6H - d \qquad \textbf{2-4}$$

where

B = Distance between inflection point and closest-to-edge point of maximum potential subsidence.

d = Edge effect or distance between the vertical line projected from the panel edge and the inflection point.

H = Overburden depth.

After taking the edge effect into account, and setting the origin (x = 0) at the panel center instead of at the inflexion point, the following expression is obtained for the subsidence profile:

$$S(x) = 0.5S'_{max}\left\{1 - tanh\left[\frac{c(x - 0.5W + d)}{B}\right]\right\} \qquad \textbf{2-5}$$

The order of steps for longwall subsidence prediction using the SDPS profile function is as follows (VPI&SU 1987):

1. Input M, W, H, % $H.R.$
2. Estimate $S^* = S^*(M, W, H, H.R.)$ and $d = d(W, H)$
3. If $W/H \geq 1.2$, then use $c = 1.8$, else $c = 1.4$
4. If $W/H < 1.2$, then use $B = 0.5W - d$, else $B = 0.6H - d$
5. $x' = x - 0.5W + d$
6. $S'_{max} = \frac{S^*}{S_{center}} S^*$

7. $S(x) = 0.5S'_{max}\left[1 - tanh\left(\frac{cx'}{B}\right)\right] = 0.5S'_{max}\left\{1 - tanh\left[\frac{c(x - 0.5W + d)}{B}\right]\right\}$

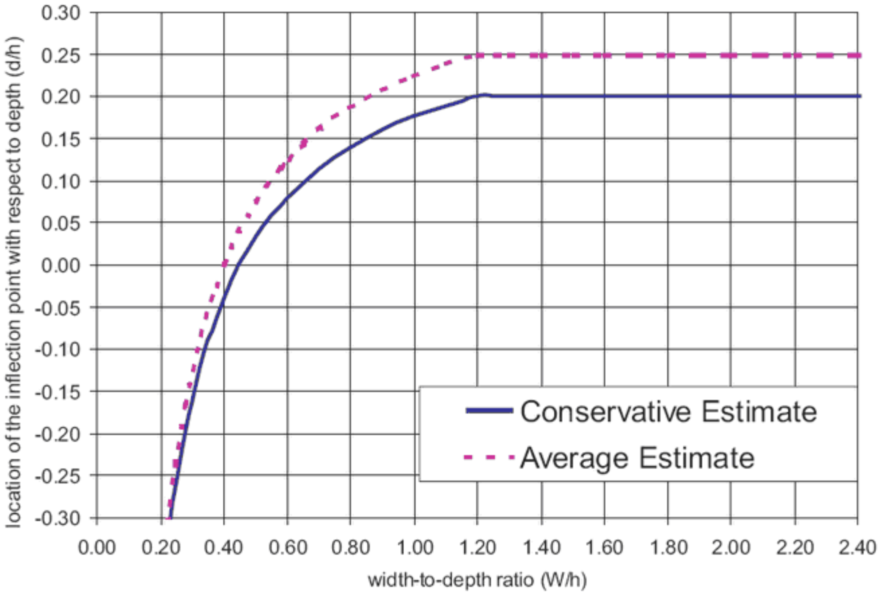

Figure 2-2 Edge effect estimation

(Agioutantis and Karmis 2009)

2.1.2.2 Exponential Function

The present portion on exponential function relies heavily on the report Guidance Manual on Subsidence Control (OSMRE 1986).

In 1983, Peng and Geng published data that considered forty cases from the Northern Appalachian Coalfield and produced the following expression for the maximum subsidence factor to account for the overburden properties (OSMRE 1986):

$$a_0 = 0.5(0.9 + P) \qquad \textbf{2-6}$$

where

$a_0 =$ Absolute maximum subsidence factor.

P = Combined Strata Coefficient,

$$P = \frac{\sum hQ}{\sum h} \qquad \textbf{2-7}$$

where

Q = Stratum Property Coefficient; the harder the rock, the lower the magnitude of this factor.

h = Thickness of each stratum in the overburden.

This method uses a correction that accounts for subcritical conditions. The expressions are as follows:

$$S^* = a' \cdot M \qquad \textbf{2-8}$$

$$a' = a_0 \cdot C \qquad \textbf{2-9}$$

$$C = \left[\left(\frac{L_L}{L_C}\right)\left(\frac{L_W}{L_C}\right)\right]^{1/2}\left[1.8\left(\frac{L_W}{L_C{}^{-0.1}}\right)\right]^{1/2} \qquad \textbf{2-10}$$

where:

a' = Subsidence factor adjusted for geometry

M = Extracted thickness

L_L = Length of the mined-out area

L_W = Width of the mined-out area

L_C = Critical dimension required for maximum potential subsidence to develop.

C = Parameter that is used to adjust the subsidence factor for panel geometry, with the condition that L_L/L_C and $L_W/L_C \leq 1$.

Chen and Peng (OSMRE 1986) use an exponential function:

$$S(x) = S * exp\left[-a_{pf}\,(x/L)^b\right] \qquad \textbf{2-11}$$

where:

a_{pf}, b= Empirical constants, which Chen and Peng found to be (a_{pf} , b) = (*8.97, 2.03*) based on longwall profiles from the Northern Appalachian coalfield.

x = Horizontal distance between a point on the profile and the origin, which is located at the point of maximum subsidence nearest the edge of the panel

L = Horizontal distance between the lip of the trough (zero subsidence) and the point of maximum subsidence nearest the edge of the panel (OSMRE 1986).

2.1.3 Influence Functions

This portion on influence function methods relies heavily on the SDPS theory (Agioutantis and Karmis 2009). The influence function preferred by the SDPS developers is the bell-shaped Gaussian function employed in the Budryk-Knothe influence function method. The influence function is expressed in terms of the two horizontal coordinates x, y, and the subsidence magnitude is the third dimension or vertical component, thus providing three-dimensional subsidence distribution prediction. The influence function is given by:

$$g(x,y,s,t)=\frac{1}{r^2}e^{-\pi\frac{(x-s)^2+(y-t)^2}{r^2}} \qquad \textbf{2-12}$$

where:

x, y = Location of an infinitesimal element of excavation.

s, t = Location of the point $P(s, t)$ where subsidence is calculated.

r = Radius of principal influence, $r=\frac{h}{tan\beta}$

Subsidence at a point $P(s. t)$ can be expressed as a definite integral:

$$S(x,y,s,t)=\frac{1}{r^2}\iint_A S_O(x,y)e^{-\pi\frac{(x-s)^2+(y-t)^2}{r^2}}dxdy \qquad \textbf{2-13}$$

where

A = Area of excavation

$S_o(x, y)$ = Function of roof convergence of the excavation area

The coordinates of the surface point on which subsidence is calculated can be taken as the origin, *P*(*0,0*), and since the convergence of the roof is constant and $S_O(x,y)=S_{max}$, the above function can be expressed as:

$$S(x,y)=\frac{S_{max}}{r^2}\int_{x1}^{x2}e^{-\pi\frac{x^2}{r^2}}dx\int_{y1}^{y2}e^{-\pi\frac{y^2}{r^2}}dy \qquad \textbf{2-14}$$

The step-by-step procedure for longwall subsidence prediction using SDPS influence function may be described as:

1. Calculate S_{max}. Estimate the influence angle, β (*90° – angle of draw*).
2. Input panel corner coordinates, overburden thickness, extraction thickness.
3. Input prediction points .
4. Estimate *S** = *S**(*M, W, H, H.R.*) and *d* = *d*(*W, H*) or input alternative *S*/M* factor
5. Calculate $r=\frac{H}{tan\beta}$, where *r* is the radius of influence, *H* is the overburden depth, and β is the angle of influence.
6. Calculate subsidence using equation 2-13.

From the influence function presented above, magnitudes and distribution of deformation indices such as slope, curvature, horizontal deformation, and horizontal strain, may be obtained.

2.2 LITERATURE ON NUMERICAL MINE SUBSIDENCE MODELING

Empirical methods do not take geological, mechanical properties or tectonic stresses into account. Consequently, the theories derived from empirical data may only be applied to the areas where the data were obtained or to very similar areas (Szostak-Chrzanowski 1988). Deterministic models (e.g. FEM), on the other hand, require a reliable knowledge of the mechanical properties, in-situ stresses and tectonics of the area. Despite efforts from various researchers, no successful method for ground subsidence prediction has been developed that relies on deterministic modeling alone (Szostak-Chrzanowski 1988). However, numerical methods can consider the effects of strata deformation and provide a tool for parametric studies (Karmis, Haycocks et al. 1992).

The present section contains a summary of the available literature on the topic of longwall subsidence prediction based on numerical modeling.

2.2.1 Linear elastic models

A linear elastic model was proposed for subsidence prediction in the Appalachian coalfield (Agioutantis, Karmis et al. 1987). The model is a 2D linear elastic approach in which radial zones were proposed for the different mechanical parameters, rather than the actual horizontal strata. The model is split into various slices emanating from the excavation rib. The researchers found the deformation shape to depend on the relative material properties, rather than on their absolute magnitude. A boundary condition for the convergence of the roof, defined by a deformation curve, was implemented. The code was developed in FORTRAN-77 and was based on a dam design program (Agioutantis, Karmis et al. 1987).

The zones proposed by these authors are:

- The intact zone, far away from the rib
- The affected zone
- The fractured zone or transition between tension and compression
- The intermediate zone
- The extraction zone

The procedure proposed by these authors produced correct profile and strain shapes, consequent with tuning of the relative properties of the above listed zones. However, the magnitudes needed to be scaled according to empirically predicted maximum values of subsidence and strain (Agioutantis, Karmis et al. 1987).

2.2.2 Anisotropic elastic models

In the process of extraction, macro and micro-fractures are formed in the rock mass, which reduce the magnitude of the rock modulus (Tajdus 2009). The situation in which the overburden is fractured to varying degrees is now common in Polish coalfields. Mine companies in that country have started mining shallow coal seams lying on top of old extracted seams, in an effort to avoid the costly operation of extracting deeper intact seams (Tajdus 2009). This motivated the study by Tajdús, aimed at back calculating Young's moduli for disturbed rock masses to be implemented in numerical methods. The calibration of the numerical models is based on pre-existing subsidence profiles. For validation purposes of the FEM model developed by Tajdús using Abaqus, the Knothe's influence function method is used. The FEM model considers layer thicknesses that exceed 20 m (Tajdus 2009).

Tajdús maintains the overburden zone classification found elsewhere as: the caved zone, the fractured zone, and the bending zone (Peng and Chiang 1984; Peng 1992; Tajdus 2009). The caved zone in this model is assumed to have a trapezoidal shape, and its height estimated as:

$$h_Z = \frac{100g}{c_1 g + c_2} \qquad \textbf{2-15}$$

where:

c_1, c_2 = Coefficients depending on strata lithology (strong and hard, medium strong, soft and weak).

g = Extraction height.

The behavior of this zone is assumed to be elastic isotropic, with the following expression for elastic modulus:

$$E_Z = \frac{10.39 {R_C}^{1.042}}{b^{7.7}} \qquad \textbf{2-16}$$

where Rc is the average compressive strength for the rock layers of the immediate roof and:

$$b = \frac{c_1 g + c_2}{100} + 1 \qquad \textbf{2-17}$$

For the fractured zone, an expression similar to the caved zone for the extent prediction is provided:

$$h_S = \frac{100g}{c_3 g + c_4} \qquad \textbf{2-18}$$

For the modulus of the fractured zone, a correlation was made with the GSI rock mass classification. Emphasis is made in the sense that the parameters of the bending zone are significantly lower than those in the intact rock mass.

Based on the specific conditions of previously disturbed overburden, this study claims that the original anisotropy of the bending zone caused by geologic processes, which was found to be insignificant, gave way to a very strong anisotropy as a result of fracturing due to the mining process. A transversally isotropic model with five elastic parameters $E_1 = E_2$, E_3, $v = v_{21} = v_{12}$, v_{31} and G_{13} was proposed (Tajdus 2009).

In the plane of isotropy, the shear elastic modulus is given by:

$$G_{12} = \frac{E_1}{2(1 + v_{12})} \qquad \textbf{2-19}$$

For the shear modulus G_{13}, the following expression was proposed (Tajdús 2009):

$$G_{13} = \frac{E_1 E_3}{E_1(1 + 2v) + E_3} \qquad \textbf{2-20}$$

The estimation of transversally isotropic elastic moduli is based on Hoek's rock mass classifications (Tajdus 2009):

$$E_m(GPa) = \left(1 - \frac{D}{2}\right)\sqrt{\frac{R_{ci}}{100}}10^{GSI-10/40} \text{ for } R_{ci} \le 100MPa, \qquad \textbf{2-21}$$

$$E_m(GPa) = \left(1 - \frac{D}{2}\right)10^{GSI-10/40} \text{ for } R_{ci} > 100MPa \qquad \textbf{2-22}$$

where:

R_{ci} = Uniaxial compressive strength

GSI = Geological strength index

D = Degree of disturbance

The magnitudes of elastic moduli needed to be lowered by a large factor, the E_1=E_2 values are roughly 0.2 GPa and E_3 roughly 1.6 GPa (Tajdus 2009), as opposed to typical values for laboratory specimen of undisturbed rock. The magnitude of these reduction factors ranges from roughly 10 to 100.

The described study included sensitivity analysis concluding that subsidence is sensitive to E_3 (anisotropic direction), whereas the trough slope is sensitive to the ratio E_1/E_3 or the anisotropy itself (Tajdus 2009).

2.2.3 Non-linear elastic models

An iterative non-linear elastic model was developed in Canada (Szostak-Chrzanowski 1988) using the author-developed code FEMMA. In this model, the tensile strength of rocks varies from 1/40 of the compressive strength above the mine roof to 1/10 near the surface. The in-situ Young's modulus of elasticity is estimated by multiplying the laboratory values by a factor of 1/5 to 1/3 (Szostak-Chrzanowski 1988).

The described model is based on the assumption of a weak zone, which is delineated by critical shear zones that occur at the boundary between tensile vertical stress and compressive vertical stress. The transfer of tensile stresses is limited by the further reduction of magnitude of the Young's modulus in the weak zone by a factor of 3 (Szostak-Chrzanowski 1988).

The iterative calculation process involves four steps (Szostak-Chrzanowski 1988):

1. Perform an elastic solution of the problem without mine opening.
2. Perform an elastic solution with the mine opening and determine:
    a. The weak zone, which is delineated by the highest shear stresses between the opening and the surface. This weak zone may be extended to account for faults.
    b. Critical tensile zone where the tensile strength is surpassed.
    c. Strains and displacements by combining steps 1 and 2.

3. Repeat step 2 introducing:
    1. *E/3* in the weak zone
    2. Isotropic *E=0* in the critical tensile zone above the opening

    A new state of stress and deformation is obtained and new elements with critical stresses may result.
4. Perform non-linear solution with anisotropy in the weak zone by placing *E=0* in the direction of tensional stresses in all tensional elements obtained in step 3. Depending on the expected maximum deformation of the roof, additional boundary conditions are introduced for vertical displacement.
5. Repeat step 4 until no tensional elements result.

The model was validated using three cases: a coal longwall panel in the Shoemaker Coal Mine in West Virginia, a longwall panel in a coal mine located in the central east coast of the People's Republic of China, and a lead and zinc mine in Southern Poland. The agreement was very good in all three cases (Szostak-Chrzanowski 1988).

2.2.4 Linear elastic and elastoplastic models with allowance of interface displacements

Besides the traditional factors that have been found to influence subsidence, namely the extraction thickness, mine width, overburden thickness, type of support, seam inclination, time, and angle of draw, the number of planes of weakness and the geomechanical properties of the overburden were highlighted in the study performed by Su, of Consol Energy (Su 1991). The main motivation behind his study was the fact that isotropic elastic models predict much flatter subsidence basins than the actual deformations.

The study by Su employed the finite element program MSC/NASTRAN version 66B and introduced shearing along planes of weakness. He concluded that shearing plays a very important role on subsidence prediction. He attributes the previous lack of success in subsidence Finite Element modeling to the fact that models had not incorporated shearing and separation along existing planes of weakness in the rock mass (Su 1991).

Weak layers in Su's work are modeled as GAP elements. The friction coefficient of the weak planes is assumed to be equal to 0.3 and cohesion is assumed to be little. On the rocks surrounding the excavation, elastoplastic behavior was used. The Drucker-Prager criterion was used as a failure criterion (Su 1991):

$$f(\sigma) = \frac{6\,sin\,\phi}{3 - sin\,\phi}\sigma_m + \sqrt{3}\left(J_2^{'}\right)^{\frac{1}{2}} - \frac{6c\,cos\,\phi}{3 - sin\,\phi} = 0 \qquad \textbf{2-23}$$

where

$$\sigma_m = \frac{\sigma_1 + \sigma_2 + \sigma_3}{3} \qquad \textbf{2-24}$$

$$\left(J_2^{'}\right)^{\frac{1}{2}} = \left\{\frac{1}{6}\left[\left(\sigma_1 - \sigma_2\right)^2 + \left(\sigma_2 - \sigma_3\right)^2 + \left(\sigma_3 - \sigma_1\right)^2\right]\right\}^{\frac{1}{2}} \qquad \textbf{2-25}$$

ϕ = Angle of internal friction

c= Cohesion

The modulus of elasticity employed in the model was reduced by a factor of 6 from the laboratory results (Su 1991). The behavior of the gob was simulated by GAP elements and was assumed to form with an initial bulking factor of 1.5. The GAP elements were assumed to have an initial modulus of approximately 1050 psi and to acquire 42000 psi after a compaction of approximately 22%, thus experiencing strain-hardening (Su 1991).

The results obtained by Su's model cover (Su 1991):

- Predicted fracture zone above the longwall
- Predicted overburden deformation
- Associated shearing along planes of weakness
- Predicted surface subsidence

The model by Su has a 195-m-wide panel at a depth of 216 m, and an extraction thickness of 1.83 m. The results show that the predicted fractured height is observed near the edges and has a magnitude of 50 m. His study also estimates shear forces in the longitudinal direction of the panel obtained through Time Domain Reflectometry (TDR). The study uses a total of 28 planes of weakness, which are planes separating rock layers with a large contrast in stiffness magnitudes (Su 1991).

An interpretation of results provided by Su in regard to the role of planes of weakness is that they reduce the overburden strata from a large beam to many thin beams resulting in a much less stiff system, therefore producing realistic deformations (Su 1991). The model with planes of weakness and nonlinear material predicts a maximum subsidence five times greater than the one obtained from the same model without the planes of weakness. Su found that the role of planes of weakness is by far more important than that of material nonlinearity. He found that the difference in the predicted maximum subsidence between two models both having planes of weakness, one with elastic material and the other one with elastoplastic material, was only 2% (Su 1991).

2.2.5 Finite Difference Method models

Researchers have worked with Finite Difference Method-based software packages such as FLAC (Itasca) to simulate mining situations. Subsidence prediction has also been attempted using these methods. Since the inputs required for these methods are similar to those that apply to FEM, two studies are briefly described in this review that shed light on the current status of the task of numerical subsidence prediction.

2.2.5.1 A comparison between linear elastic and some non-linear approaches

The first study to be described here comes from the United Kingdom (Mohammad, Lloyd et al. 1997). These authors used FLAC. They used the Rock Mass Classification System (RMR) in order to derive in situ rock mass properties. For calibration and validation purposes, these authors used the Subsidence Engineer's Handbook (SEH) of the National Coal Board (NCB) of the United Kingdom (NCB 1975), which has been regarded as a reliable tool for subsidence prediction in the Midland coalfields of England (Alejano, Ramírez-Oyanguren et al. 1999).

The aim of the study here described was to model a 200 m wide panel at different depths, with an extraction thickness of 2 m. The model extended from 100 m to 800 m in depth and had a width of 800 m. Roller boundaries were used at the bottom and sides of the model. The horizontal stresses were determined as:

$$\sigma_h = \left[\frac{v}{1-v}\right]\sigma_v \qquad \textbf{2-26}$$

where:

σ_h = Horizontal stress

σ_v = Vertical stress

$v =$ Poisson ratio

The elastic properties are given by the bulk modulus and the shear modulus:

$$K = \frac{E}{3(1-2v)} \qquad \textbf{2-27}$$

$$G = \frac{E}{2(1+v)} \qquad \textbf{2-28}$$

The authors of this study recognized the need to scale down laboratory mechanical properties (Mohammad, Lloyd et al. 1997). They mention two methods to account for the rock mass mechanical properties. The first method is to reduce the laboratory rock modulus by some factor that considers the scale effect and the presence of discontinuities. The second one is to use rock mass classification techniques and use empirical expressions from a wide range of data to determine rock mass modulus (Mohammad, Lloyd et al. 1997). They used a rock mass modulus of 1200 MPa, an unconfined compressive strength in an amount of 1/300 the rock mass modulus, and an unconfined tensile strength in an amount 1/10 the unconfined compressive strength (Mohammad, Lloyd et al. 1997). From typical laboratory modulus results it can be estimated that this modulus magnitude has been obtained by multiplying a modulus of intact rock approximately by 1/25. The authors then use five different constitutive models embedded in FLAC, namely:

- Elastic, isotropic
- Elastic, transversely isotropic
- Non-linear, Mohr-Coulomb model
- Non-linear, ubiquitous joint model
- Non-linear, strain softening model

They concluded that none of the constitutive models in FLAC was adequate for modeling subsidence. These authors carried out an extensive literature research of ways in which numerical modelers have modified laboratory mechanical properties in order to obtain rock mass properties (Mohammad, Lloyd et al. 1997). In that literature review, it was found that 60% of the authors did not mention any specific methodologies to do so. They finally chose to work with an expression developed by Serafim and Pereira published in 1983, although they modified it slightly. The expression is based on Beniawski's Rock Mass Rating (RMR):

$$E = 10^{\frac{RMR-10}{40}} - 0.562 \qquad \textbf{2-29}$$

The authors subtracted 0.562 to eliminate the anomaly that at $RMR=0$ the original expression returned a significant magnitude for E. For the behavior of the caving zone, they propose the use of a strain stiffening behavior with reduced mechanical properties (Mohammad, Lloyd et al. 1997). They adopted a model that allowed the roof and floor strata to converge. The introduction of post-failure parameters was based upon yield and failure of the elements within the model. The authors found a reduction factor of 10 for the rock modulus for varying degrees of yield and plasticity (Mohammad, Lloyd et al. 1997).

For the mechanic behavior the authors used elasto-plasticity. In FLAC, the strain-softening (SS) model was employed (Mohammad, Lloyd et al. 1997).

FLAC SS model takes Mohr-Coulomb failure criterion into account. This criterion typically considers that cohesion, friction angle, and dilation are constants. The SS model, however, considers that after the onset of plastic yield, these parameters change as a function of plastic strain (Mohammad, Lloyd et al. 1997). The basic steps of the calculation are:

1. The material behaves elastically until the failure criterion is exceeded, $f < 0$.
2. If $f < 0$ is detected, plastic flow is allowed in order to bring f back to zero.

3. Values of strength parameters are modified as a function of plastic strain.

The authors found that low constant RMR values through the whole model depth predicted shallow subsidence profiles well while they failed to predict deeper ones, and high constant RMR values did well on deep excavations while poorly on shallow ones. They thus consider variation of stiffness as a function of depth or stress. As a result, they tuned the model with varying values of RMR across the depth of the overburden (Mohammad, Lloyd et al. 1997). Their model predicted a convergence of the roof of 92% and 8% for the floor. Vertical displacements were highest in the highly fractured zone and decreased with height until they reached a final subsidence of 0.55 m (Mohammad, Lloyd et al. 1997).

The expression proposed in the described work to relate RMR and depth, D (in meters) is:

$$RMR = 27.213 ln(D) - 121.65 \qquad \textbf{2-30}$$

These authors explored subsidence sensitivity to extraction thickness and panel width. They found that the model was insufficiently sensitive and considered necessary to manually modify the caving or yielding zone in order to arrive at a universal model (Mohammad, Lloyd et al. 1997). Their departure model or reference for sensitivity analysis has a depth of 400 m, width of 200 m and an extraction thickness of 2 m. $W/H=0.5$ and is therefore well within the subcritical range of deformation. In order to get matching predicted and measured subsidence magnitudes, they found the variation of the ratio Y/X (extent of yield and failure zone over seam extraction thickness) with respect to both extraction thickness and width, to increase (Mohammad, Lloyd et al. 1997). They obtained a very good agreement in what has been introduced in this dissertation as S^*/M versus W/H, which is a single curve for the case of SEH.

2.2.5.2 An elastoplastic FDM model

The second subsidence prediction model described here comes from Spain (Alejano, Ramírez-Oyanguren et al. 1999). That study was carried out using the FDM code FLAC (Itasca).

The authors chose to work with FDM code FLAC arguing that highly non-linear problems are best handled by codes using an explicit solution technique, which is a feature associated to that code (Alejano, Ramírez-Oyanguren et al. 1999). They also stress out the fact that the Lagrangian calculation scheme permits materials to yield and flow and the model grid to deform in large strain mode and move with the material (Alejano, Ramírez-Oyanguren et al. 1999).

The validation of the model is carried out using cases of the Midlands coalfields of England, on which a large subsidence database was based that led to the NCB empirical prediction model (NCB 1975). The two main reasons that led the authors to validate their model using that empirical model were, first, that there is an extensive amount of testing data for the Midlands coalfields, and second, that the empirical model works well for this area (Alejano, Ramírez-Oyanguren et al. 1999).

Regarding the material behavior, that study used an elastoplastic material behavior that exhibits the following features (Alejano, Ramírez-Oyanguren et al. 1999):

1. Transversely isotropic elastic pre-failure behavior.
2. Anisotropic yield surface, since yield may occur by stratification (joints) or across the material itself.
3. Isotropic elastic post-failure behavior, assuming that the material is of the backfill-type, with large individual fragments, exhibits stress-dependence and is isotropic elastic.

The authors use GSI quality rating for the rocks, which are mudstone and siltstone for the area of the Midlands coalfields. This quality index is based on unconfined compressive strength, RQD (Rock Quality Designation), joint spacing, joint conditions, and water. They correlate the uniaxial compressive strength to the triaxial compressive strength and determine the values of the parameters (UCS, m, s, UTS) for the Hoek-Brown yield criterion in two sets, one for the intact rock, and one for the broken rock. The rock joints are characterized by Mohr-Coulomb criterion parameters cohesion and friction (Alejano, Ramírez-Oyanguren et al. 1999).

For the pre-failure deformability parameters, the authors estimate the Young's modulus of the rock mass as a function of the laboratory Young's modulus and the RMR (Rock Mass Rating).

For rocks with horizontal stratification, they use:

$$E_{RM} = E_R e^{(0.0217RMR-2.17)} \qquad \textbf{2-31}$$

For inclined stratification of 30 to 45 degrees, they use:

$$E_{RM} = E_R e^{(0.0564RMR-5.64)} \qquad \textbf{2-32}$$

With the values of the laboratory elastic modulus and the values of RMR, they obtained a wide range of values of E_{RM} from 2545 MPa (based on laboratory modulus of 5500 MPa and a RMR of 64.5) to 740 MPa. After tuning their model with the SEH (NCB) model, they obtained a modulus value of 775 MPa. For the horizontal modulus, they multiplied the vertical modulus by 1.72. The shear modulus was tuned to 33 MPa (Alejano, Ramírez-Oyanguren et al. 1999).

For the post-failure deformability parameters, three different attempts to find suitable values of Young's modulus were proposed for the broken material. They first tried two backfill models (Alejano, Ramírez-Oyanguren et al. 1999):

$$E = \left(a^2 + 4b\sigma\right)^{1/2} \qquad \textbf{2-33}$$

$$E = 490\sigma_m^{0.7} \text{ [kPa]} \qquad \textbf{2-34}$$

Using the expressions above for ranges of depth between 100 and 700 m, they obtained Young's moduli from 100 MPa to 500 Mpa (Alejano, Ramírez-Oyanguren et al. 1999). A second attempt was considered by using the same expressions as for the intact rock, however employing a value of RMR of 32. With this approach they obtained a range of values of Young's modulus between 120 MPa and 1250 MPa (Alejano, Ramírez-Oyanguren et al. 1999). The third approach, which they selected, is based upon tuning parameters considering maximum and rib subsidence, and limit angle as calibrating references, and was run for different values of overburden depth. They obtained various values of Young's modulus for various depths, ranging from 150 MPa at 150 m to 245 MPa at 500 m and 700 m (Alejano, Ramírez-Oyanguren et al. 1999).

As far as modeling technique is concerned, these authors used FLAC 2D arguing that the problem of longwall subsidence may be analyzed as a plane-strain problem (Alejano, Ramírez-Oyanguren et al. 1999). For the stress initialization, they used an isotropic stress field that resembles the site conditions. After preliminary runs of the problem, they arrived at a discretization area 500 m wide, 375 m high, and a coal seam 200 m long. They modeled half of the problem and used rollers on all three constrained sides. They refined the mesh in the region surrounding the excavation (Alejano, Ramírez-Oyanguren et al. 1999).

Modeling was carried out in two stages. In a first stage, the failure criterion needed to be applied. Since this was only possible on an isotropic elastic behavior, they assigned this behavior to the whole model and ran it in order to predict the height of the plastified or fractured zone (Alejano, Ramírez-Oyanguren et al. 1999). In the second stage, they kept the isotropic behavior for the fractured zone and modified the upper zone with transversely isotropic elastic behavior. They claim that anisotropic deformability features control the behavior of this region, which has been also reported elsewhere (Tajdus 2009).

In general, the results compare well with the empirical results. However, divergence was found to be an issue on horizontal displacement. In general, this parameter was underestimated for subcritical cases and overestimated for supercritical ones. They attribute this to the elastic modeling of soil (Alejano, Ramírez-Oyanguren et al. 1999).

3.0 DATA DESCRIPTION

The present chapter deals with the data upon which this dissertation is based. The data were collected by the Pennsylvania Department of Transportation (PennDOT) along segments of the Interstate Route I-79 that ran above undermined areas. The project "A study of highway subsidence due to Longwall Mining using Data collected from I-79" (Gutiérrez, Vallejo et al. 2010), part of the PennDOT / University of Pittsburgh Intergovernmental Agreement, is based on these data. The highway segments that were instrumented and surveyed are located south of Waynesburg, PA, in Greene County. Data were collected before, during, and after the mine face passed underneath the points of interest. Panels were extracted from the Cumberland mine and the Emerald mine, operated by Alpha Natural Resources, Inc.

3.1 GEOLOGY OF SITE

Figure 3-1 shows the location of the Emerald and Cumberland mines southeast of Waynesburg, Pennsylvania, underneath interstate I-79.

Figure 3-1. Location of Emerald and Cumberland mines below I-79

(Steve Thomas/Post-Gazette, source: Consol)

The following paragraphs on the description of the geology of the Greene County quote extensively from Stone (Stone 1932). These descriptions are consistent with stratigraphic columns provided elsewhere (Edmunds 1999; Edmunds, Skema et al. 1999) shown in Figure 3-2 and Figure 3-3.

Green County is hilly with few broad flat areas either in valley bottoms or on hilltops. It is all slope and for the most part rather steep slopes.

The rocks in Greene County are all in layers or beds ranging from a fraction of an inch to many feet thick and for the most part lying nearly horizontal. The surface rocks in Greene County belong to the Upper Carboniferous system. There are four main groups, the Conemaugh, Monongahela, Washington, and Greene.

The Conemaugh group lies underneath the Pittsburgh Coal, the first 50 to 80 feet usually being shale with thin beds of limestone.

The Monongahela group extends from the base of the Pittsburgh coal to the top of the Waynesburg coal. The group ranges in thickness in this county from 279 feet to 405 feet, according to the record of wells that passed through it. An average for the county is about 330 feet, and the range for Whiteley Township is: Least 313 ft, greatest 363 ft, and average 332 ft. The Monongahela group differs from the Conemaugh group below and the Washington group above it in having much more coal and limestone. It contains over 100 ft of limestone, some heavy beds of sandstone, shales, and five persistent coal beds. The Pittsburgh coal, which is at the base of the group, is the thickest bed, probably the least variable, and has the shortest outcrop line of all the workable coals in the county.

The Washington group underlies much of the surface of the county east of Waynesburg. The Washington group is composed of shales, sandstones, and thin beds of limestone and coal.

The Greene group has a maximum thickness of 700 to 800 feet. The Greene group is composed of such soft rocks that good exposures of more than a few feet of strata are rare. In the eastern half of the county the beds are so variable and so poorly exposed that the sequence of strata can scarcely more than be guessed at. In most places it consists of shales and shaly sandstones. A few of the sandstones are massive but not persistently so. Thin beds of red shale, several thin limestones and coal beds are interspersed throughout the group.

Table 3-1 contains a layered representation of the description above for 750 feet of overburden on top of the Pittsburgh coal bed.

Table 3-1. Tabular summary of the first 750 feet down to Pittsburgh coal bed

Layer No.	Min. Thickness [ft]	Max. Thickness [ft]	Hardrock	Rock Type
1		118		Shale and sandstone
2		3	x	Limestone
3		18	x	Sandstone
4		3		Shale
5		3.5	x	Lower Washington limestone
6		6		Shale
7		2.5		Washington Coal Bed
8		18	x	Clay and sandstone
9		20	x	Sandstone
10		1		Waynesburg "B" Coal Bed
11		18		Sandstone and shale
12		1		Waynesburg "A" Coal Bed
13		10		Shale
14		30	x	Limestone
15	6	11		Washington Coal Bed
16		70	x	Washington Sandstone
17	0	12		Shale
18		6		Waynesburg Main Coal Bed
19		3		Clay
20		20	x	Sandstone
21		5	x	Limestone
22		60		Sandstone and shale
23	1	3		Uniontown Coal Bed
24		18	x	Upper Great Limestone
25		60		Sandstone and shale
26		55	x	Lower Great Limestone
27		40		Sandy shale
28	1	6		Sewickley Coal Bed

Table 3-1 (continued)

29		10	x	Sandstone
30		18	x	Fishpot limestone
31		25		Sandstone and shale
32	1	4		Redstone Coal Bed
33		10	x	Limestone
34		40	x	Pittsburgh Upper Sandstone
35	0	10		Shale
36	5	12		Pittsburgh Coal Bed
Total Depth [ft]		750		
Hardrock percentage by thickness		45%		

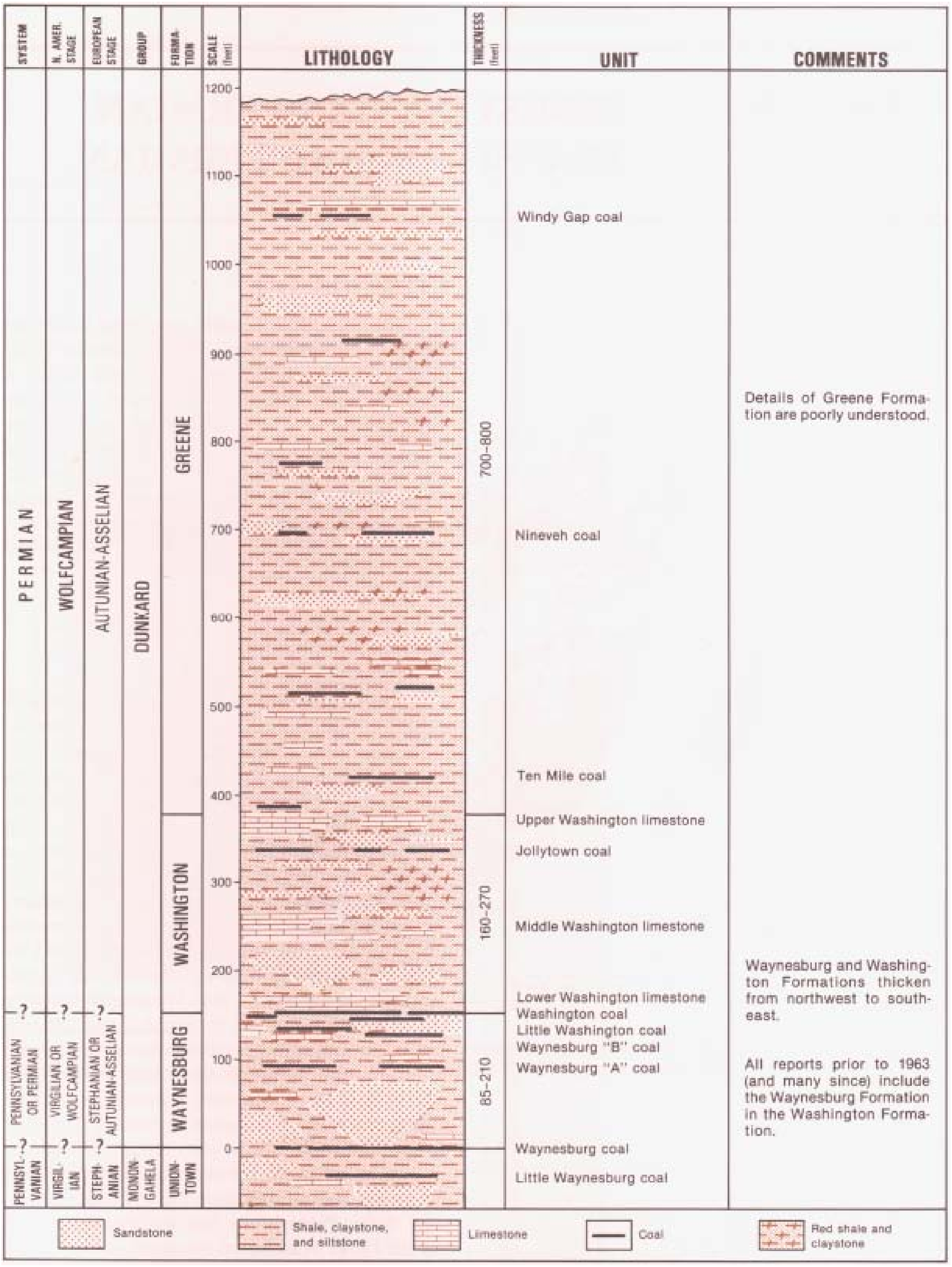

Figure 3-2. Stratigraphy of the Pennsylvanian-Permian and Permian sequence

(Edmunds 1999)

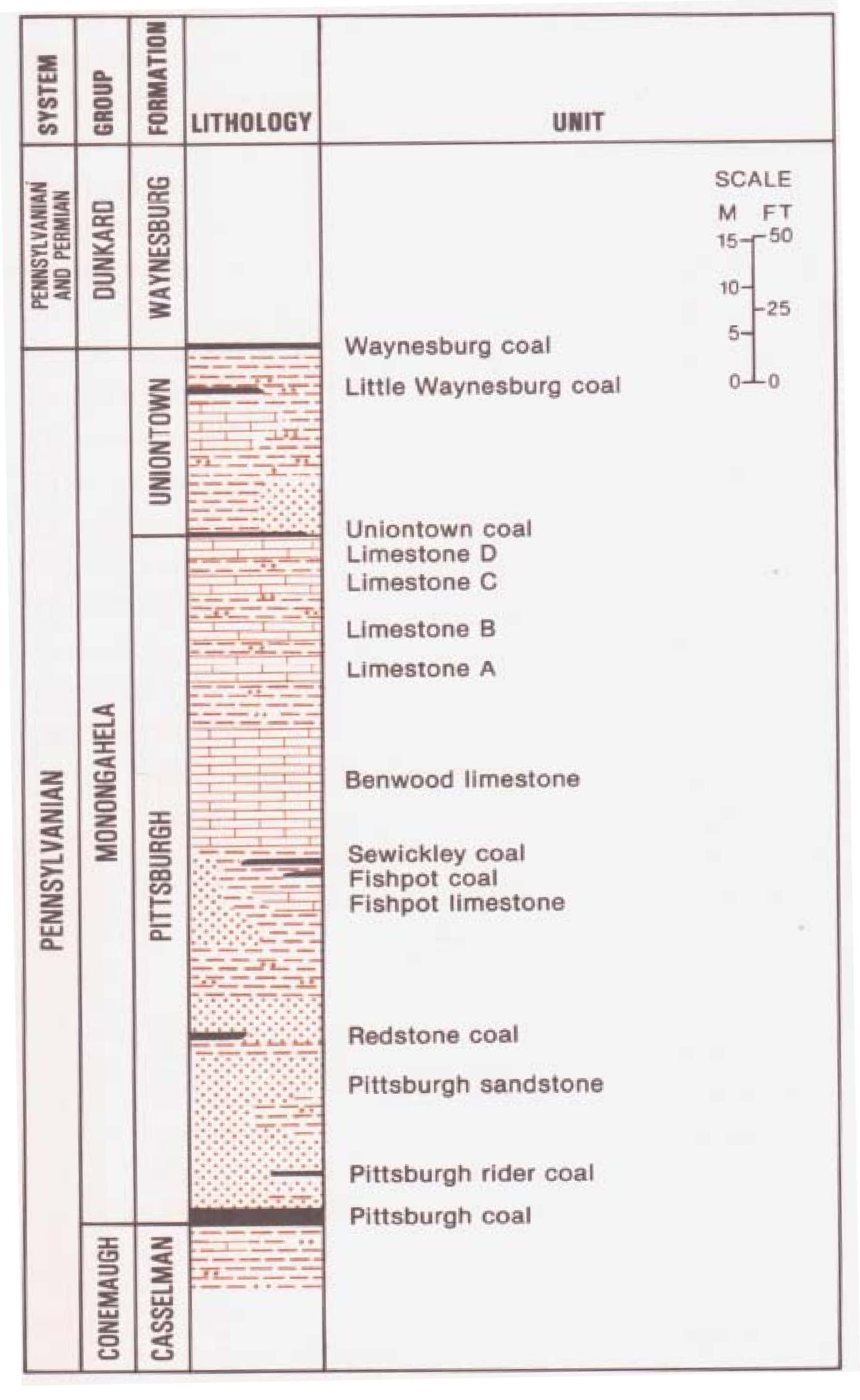

Figure 3-3. Stratigraphic column of the Monongahela Group of Western Pennsylvania

(Edmunds 1999)

Jeran and Adamek (Jeran and Adamek 1988) provide two columnar diagrams of core test holes of the Pittsburgh Coalbed in southwestern Pennsylvania (Figure 3-4). The similarity between the two diagrams is apparent. These two diagrams are the most detailed stratigraphic data available from the region where the Cumberland and Emerald mines are located. Table 3-2 and Table 3-3 show the approximate thickness readings taken from Figure 3-4.

A detailed stratigraphy of the roof and first few layers above a longwall panel in Southwestern Pennsylvania up to 5.5 meters is also available in the literature (Oyler, Mark et al. 2004). For most layers they provide the Rock Quality Designation (RQD) percentage and the unconfined compressive strength (Figure 3-5).

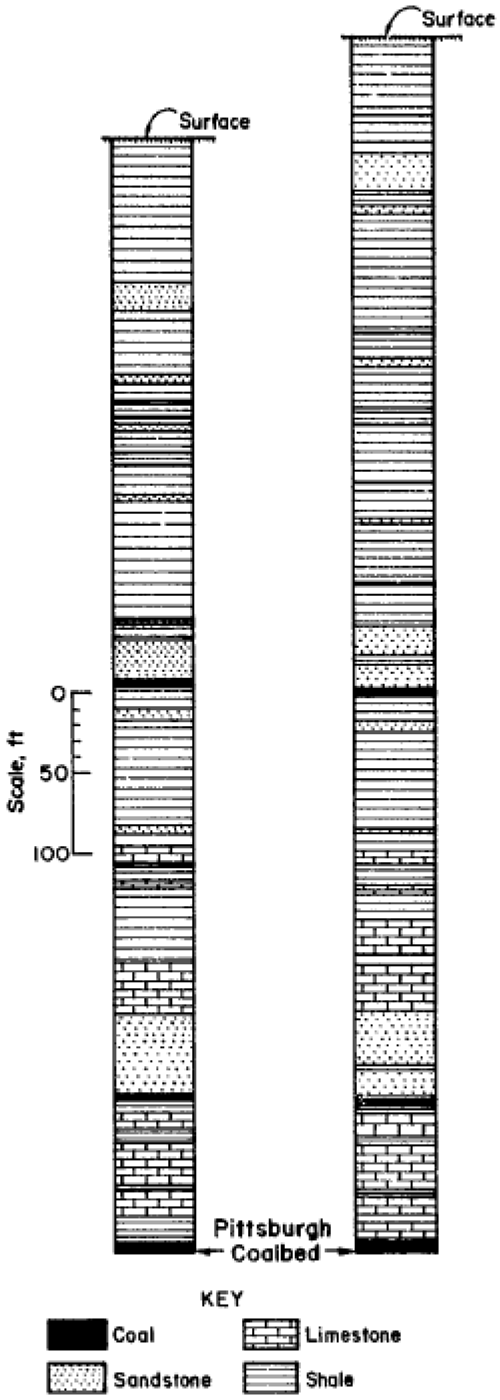

Figure 3-4. Columnar diagrams of two core test holes in southwestern Pennsylvania

(Jeran and Adamek 1988)

Table 3-2. Typical layer thickness read from core test hole No. 1

Layer No.	Aprox. Layer Thickness [ft]	Rock type
1	90	Shale
2	17	Sandstone
3	35	Shale
4	5	Sandstone
5	10	Shale
6	3	Coal
7	10	Shale
8	2	Coal
9	3	Shale
10	5	Sandstone
11	10	Shale
12	2	Coal
13	8	Shale
14	2	Coal
15	17	Shale
16	5	Sandstone
17	70	Shale
18	4	Coal
19	2	Sandstone
20	10	Shale
21	2	Coal
22	25	Sandstone
23	5	Coal
24	10	Shale
25	10	Sandstone
26	67	Shale
27	7	Sandstone
28	7	Shale
29	10	Limestone
30	2	Coal
31	7	Shale
32	5	Sandstone
33	50	Shale
34	33	Limestone
35	50	Sandstone
36	5	Coal
37	8	Shale
38	10	Limestone
39	10	Shale
40	30	Limestone
41	3	Shale
42	20	Limestone
43	20	Shale

Table 3-2 (continued)

44	8	Coal
Total Overburden Thickness	714	
Hardrock Cumulative Thickness	234	
Percent Hardrock	33%	

Table 3-3. Typical layer thickness read from core test hole No. 2

Layer No.	Aprox. Layer Thickness [ft]	Rock type
1	75	Shale
2	25	Sandstone
3	10	Shale
4	7	Sandstone
5	80	Shale
6	3	Sandstone
7	15	Shale
8	5	Sandstone
9	25	Shale
10	3	Sandstone
11	3	Shale
12	3	Sandstone
13	60	Shale
14	3	Sandstone
15	40	Shale
16	3	Coal
17	20	Shale
18	20	Sandstone
19	5	Shale
20	15	Sandstone
21	8	Coal
22	15	Shale
23	8	Sandstone
24	37	Shale
25	3	Sandstone
26	10	Shale
27	10	Limestone
28	10	Shale
29	10	Limestone
30	15	Shale
31	20	Limestone
32	5	Shale

Table 3-3 (continued)

33	30	Limestone
34	40	Sandstone
35	5	Shale
36	15	Sandstone
37	8	Coal
38	15	Limestone
39	5	Sandstone
40	35	Limestone
41	5	Sandstone
42	25	Limestone
43	8	Coal
Total Overburden Thickness	762	
Hardrock (limestone and sandstone) Cumulative Thickness	305	
Percent Hardrock	40%	

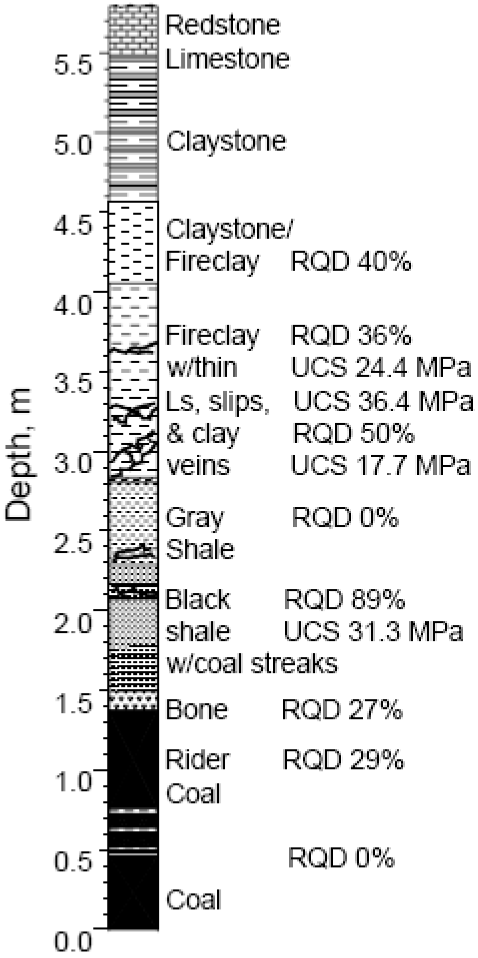

Figure 3-5. Composite core log from a study site in southwestern Pennsylvania

(Oyler, Mark et al. 2004)

3.2 LONGWALL PANEL OVERVIEW

The Emerald and Cumberland mine panels and highway I-79 are depicted in Figure 3-6 and Figure 3-7. Among the panels shown, a few are useful as far as the development of subsidence prediction tools is concerned. Some panels are partially documented and provide useful information as well.

Table 3-4 contains basic data from the panels.

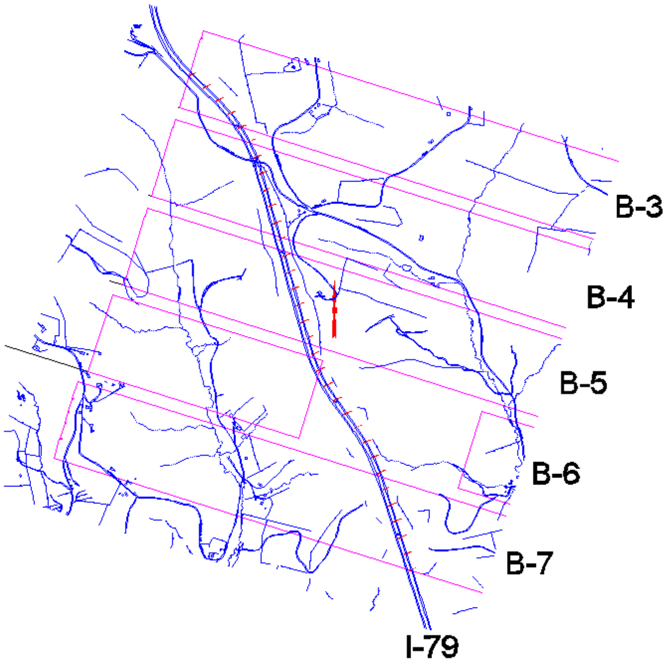

Figure 3-6 Emerald mine panels overview

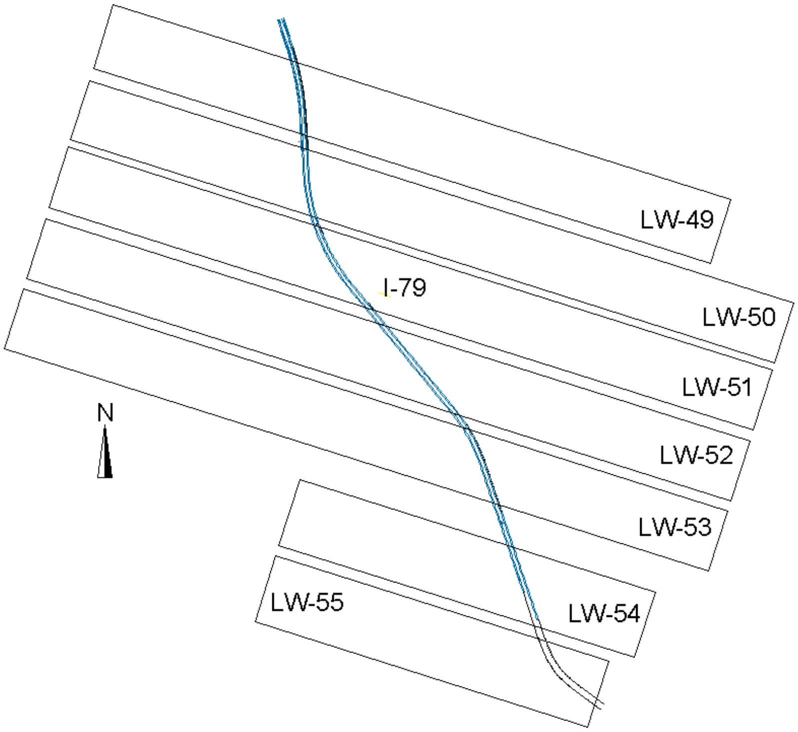

Figure 3-7 Cumberland mine panels overview

Table 3-4 Panel basic geometric parameters and maximum measured subsidence

Panel	S* [m]	M[m]	S*/M	H [m]	Width [m]	W/H
B-4	1.20	1.93	0.62	234	443	1.9
LW-49	1.40	2.26	0.62	240	378	1.6
LW-50	1.39	2.26	0.61	244	375	1.5
B-3	1.43	2.00	0.72	220	436	2.0
LW-52	1.50	2.26	0.67	233	378	1.6
LW-53	1.62	2.35	0.69	224	376	1.7
LW-51	1.43	2.26	0.63	233	378	1.6
LW-55	1.66	2.35	0.71	195	411	2.1

3.3 NATURE OF SURVEYING DATA

Empirical models, such as profile function and influence function methods, consist of two main stages, as described in chapter 2.0 :

1. Estimation of maximum subsidence, here represented by S^*.
2. Construction of a subsidence 2D profile (3D trough) based on S^* and other parameters.

For the purpose of 3D subsidence prediction to be proposed here, the proper data are the surveying data collected during the time when the panel mine face approached, passed underneath, and left the projected I-79 highway segments for each of the documented panels.

A series of stations running parallel to the highway direction were surveyed (Easting, Northing, and Elevation) on various dates with respect to a predetermined coordinate system covering the time span during which the mining operation took place. Stations were surveyed along the northbound and southbound sides of the highway and for some panels along the central axis of the highway as well. Below is an example of raw data for panel LW-51 for three consecutive stations.

Table 3-5 Surveying raw data sample for three consecutive stations

Station		East [m]	North [m]	Elevation [m]		East [m]	North [m]	Elevation [m]
		Baseline				3/25/2006		
481+0NB		398252.98	57563.06	359.25		398252.98	57563.06	359.29
481+50NB		398243.28	57574.83	359.16		398243.28	57574.83	359.22
482+0NB		398233.58	57586.59	359.07		398233.58	57586.59	359.14

Table 3-5 shows the raw surveying data for three consecutive stations. The baseline coordinates were obtained from AutoCAD files of the highway at the panel sites obtained long before mining. For a top view of a typical panel with mine face positions at different dates, refer to Figure 3-24, which shows an overview of panel LW-51. Using the raw data that are only partially shown in Table 3-5, the deformation experienced by the three stations with respect to the baseline on March 25 2006 were calculated as the difference between the elevation column of the baseline and the elevation column on 03/25/2006, and so on. Sections 3.4 and 3.5 give a general description of the raw data; section 3.6 describes the significance of supercritical conditions in the case of longwall mining, and section 3.7 presents a proposed data transformation upon which an empirical subsidence prediction model shall be based.

3.4 EMERALD MINE

3.4.1 PANEL B-3

Emerald mine panel B-3 is the only panel that is crossed by the highway near one of its corners. As a result, projected profiles in this area do not reach maximum potential subsidence, as shown in Figure 3-9. The farthest points from the panel corner are located at distances from the edges where critical or supercritical profiles may be expected. However, from the limited surveying data, which contains data until February 28, 2006, critical or supercritical profiles could not be observed. Figure 3-10 shows the location of 8 tiltmeters along I-79. Since tiltmeter data provide elevation differences and tiltmeter data are available from dates after the panel was completely mined out, these were checked and it could not be concluded that B-3 reached maximum potential subsidence.

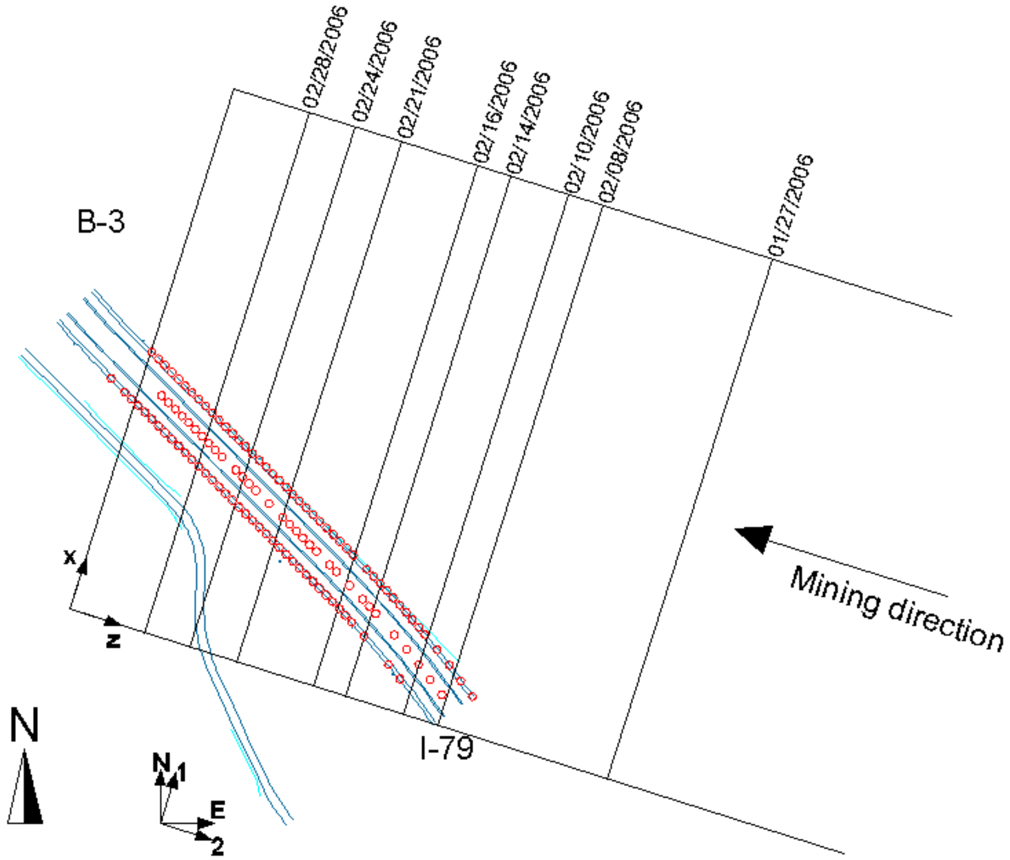

Figure 3-8 Overview of the west end of Emerald mine panel B-3 intersecting I-79

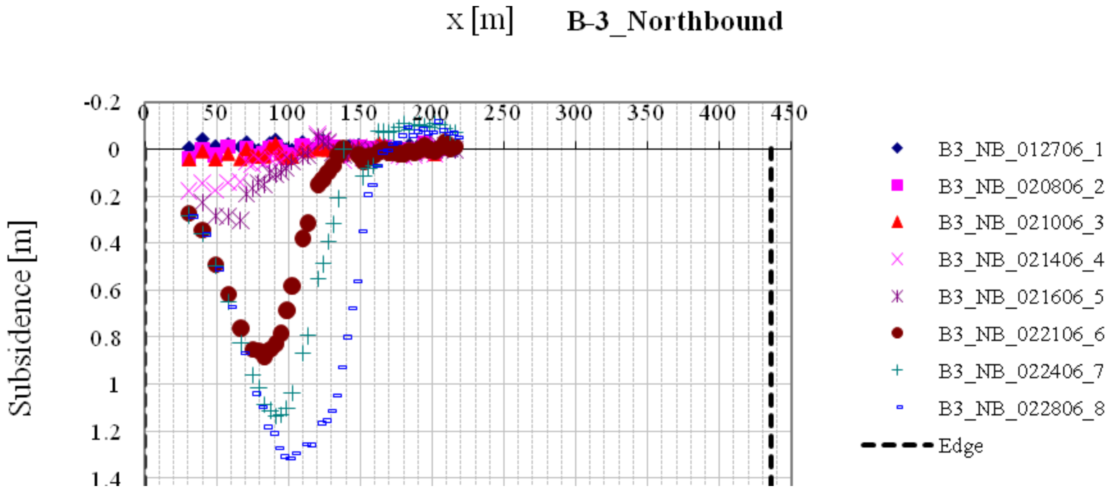

Figure 3-9 Emerald B-3 z-plane (transversal) projection of northbound station surveying data

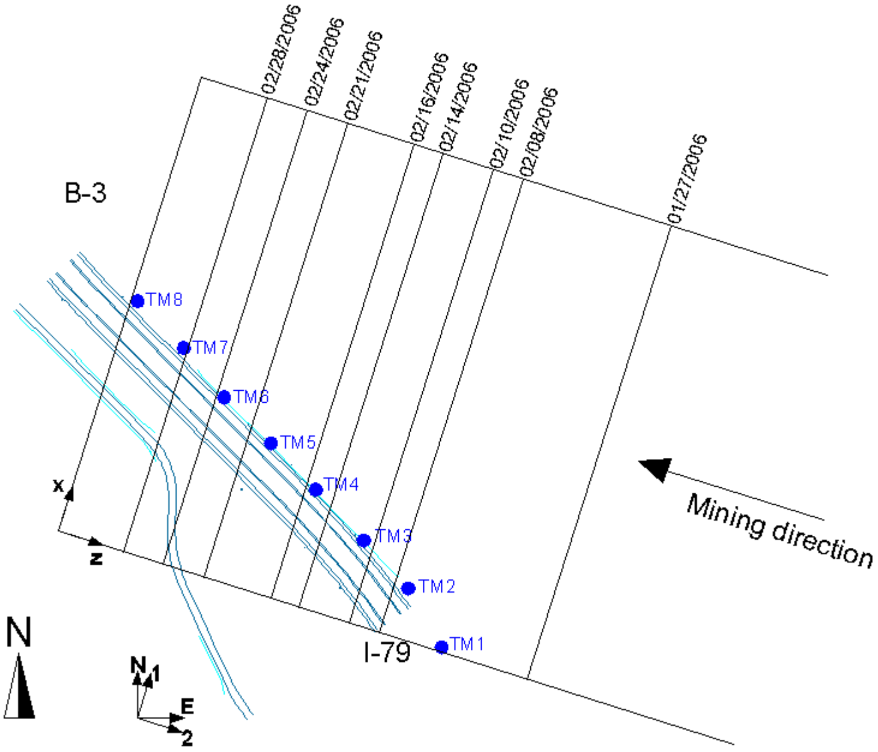

Figure 3-10 Tiltmeter location at Emerald mine panel B-3

3.4.2 PANEL B-4

Emerald B-4 panel is located next to B-3 panel to the South. The highway intersects this panel in a region where the final longitudinal and transversal subsidence profiles are supercritical. Figure 3-11 shows the panel, the highway and the data points along the northbound side of the highway. The southbound data points could not be plotted due to a lack of Northing data. Another factor that limits the amount of data for B-4 is the fact that only 4 surveying dates are available. Figure 3-12 shows the location of tiltmeters. Figure 3-14 shows a transversal projection of all surveying data sorted by surveying date. It is important to note that these data correspond to a projection of the highway points on a plane normal to the *z*-axis. In other words, what the chart depicts is the highway deformation, for the given dates, projected on a transversal plane. From this plot of B-4, a few important and unusual characteristics of subsidence evolution can be readily observed:

- The heave recorded in areas adjacent to panel edges and ahead of the mine face, reaches a magnitude of roughly 0.30 m with an affecting distance up to 400 m from the mine face.
- The subsidence profile was lower for 11/21/2006 than it was for 12/06/2006 by a magnitude of roughly 0.15 m.
- Three low points are observed on the right portion of the graph. These three points lie on bridge structures that were removed ahead of the advance of the longwall face, according to the October 2006 report on panel B-4 presented to PennDOT by Earth Inc (Earth 2006).

The highway gradient of the segment crossed by the longwall panel is given in Figure 3-13. Figure 3-15 gives a general topographic map with zones of fill and cut. The numbers in fill zones are approximate elevation differences between the highway and the embankment toe elevations. The final horizontal displacements are given in Figure 3-16. Subsidence magnitudes were double-checked with the tiltmeter elevation data which are plotted in Figure 3-17. Tiltmeter 3 had problems during surveying and data for this tiltmeter is missing, which resulted in a gap in the plot. From the figure, it is apparent that tiltmeters followed a supercritical profile. The magnitude of subsidence read from the tiltmeters is higher than that obtained from the surveying data by roughly 0.09 m.

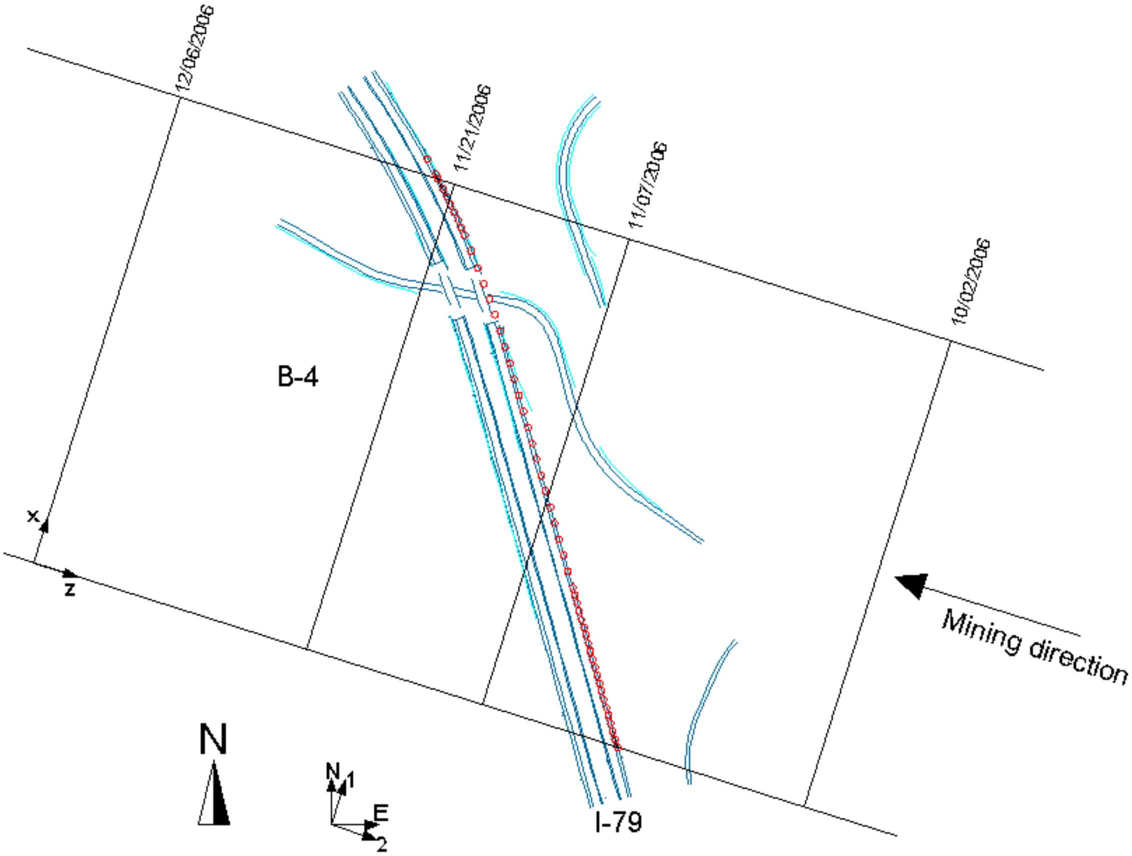

Figure 3-11 Overview of Emerald mine panel B-4 intersecting I-79

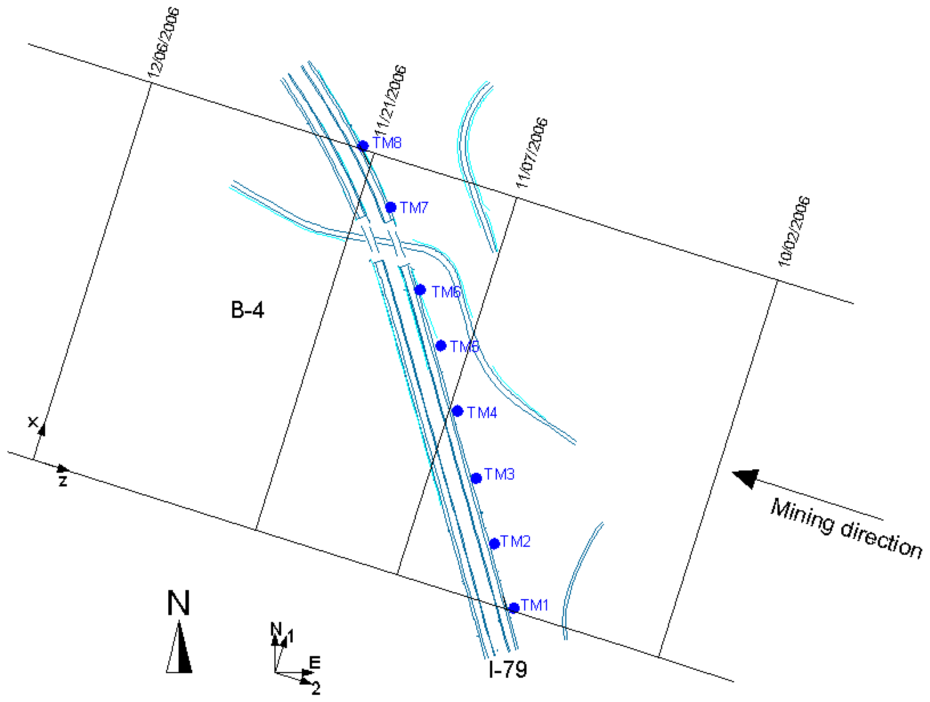

Figure 3-12 Tiltmeter location at Emerald mine panel B-4

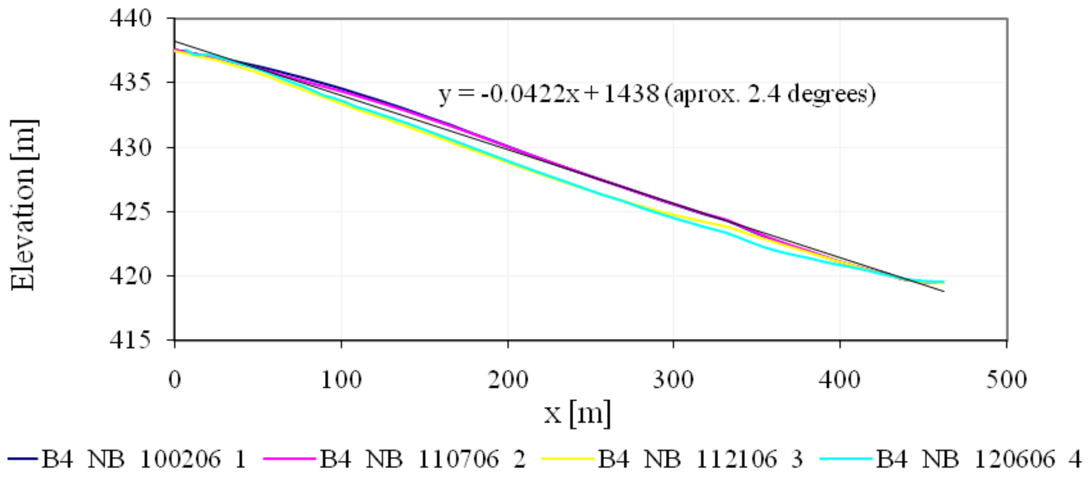

Figure 3-13 Highway elevation in the *z*-plane projection

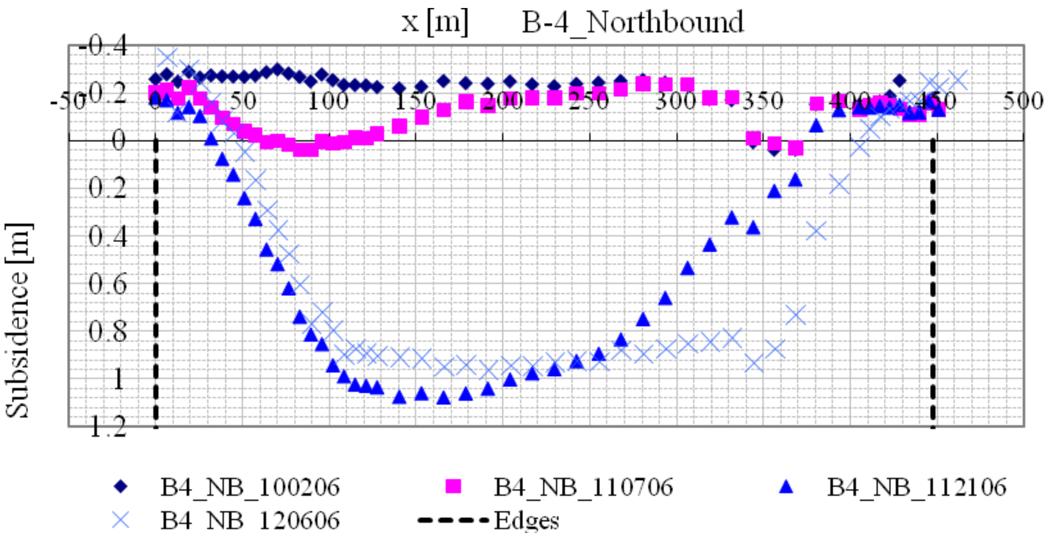

Figure 3-14 Emerald B-4 *z*-plane (transversal) projection of surveying data

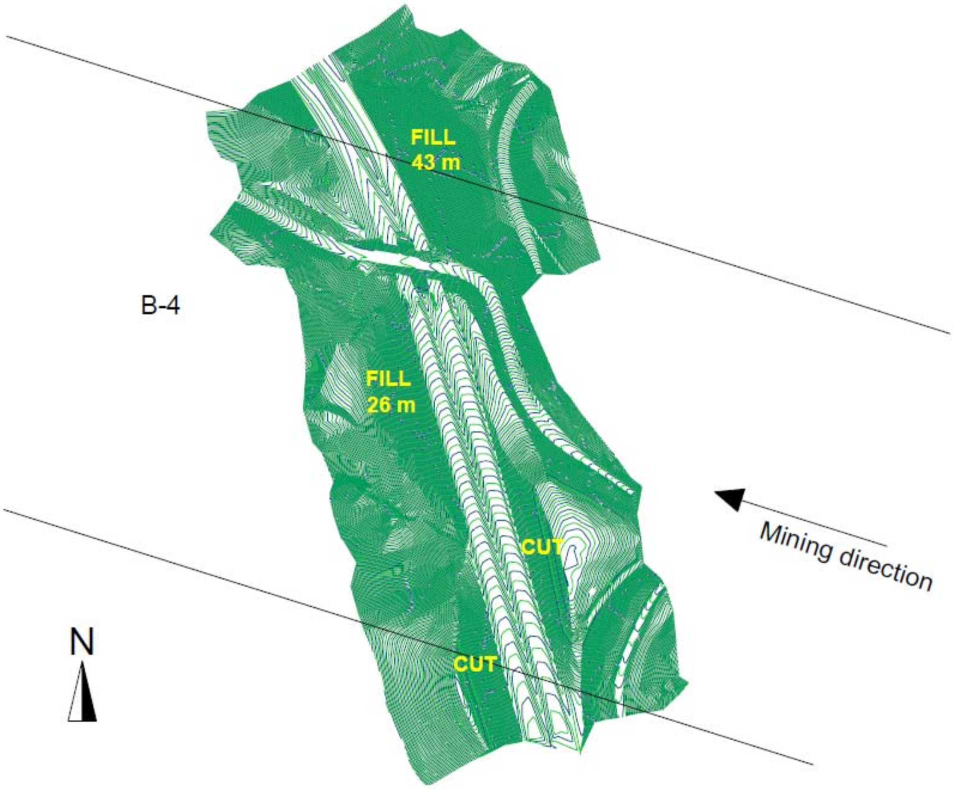

Figure 3-15 Emerald mine panel B-4 cut and fill zones

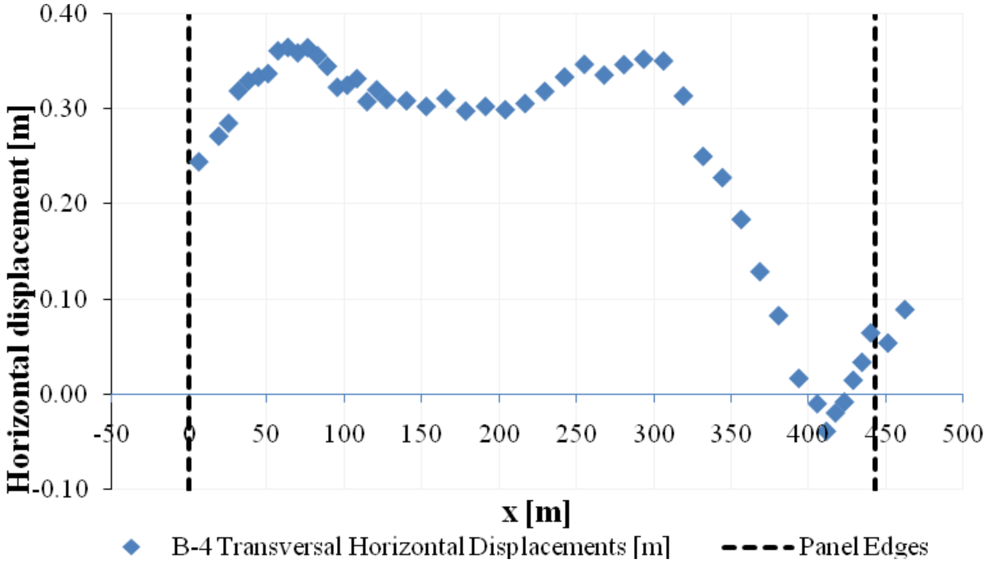

Figure 3-16 Emerald B-4 *z*-plane projection of northbound horizontal displacements

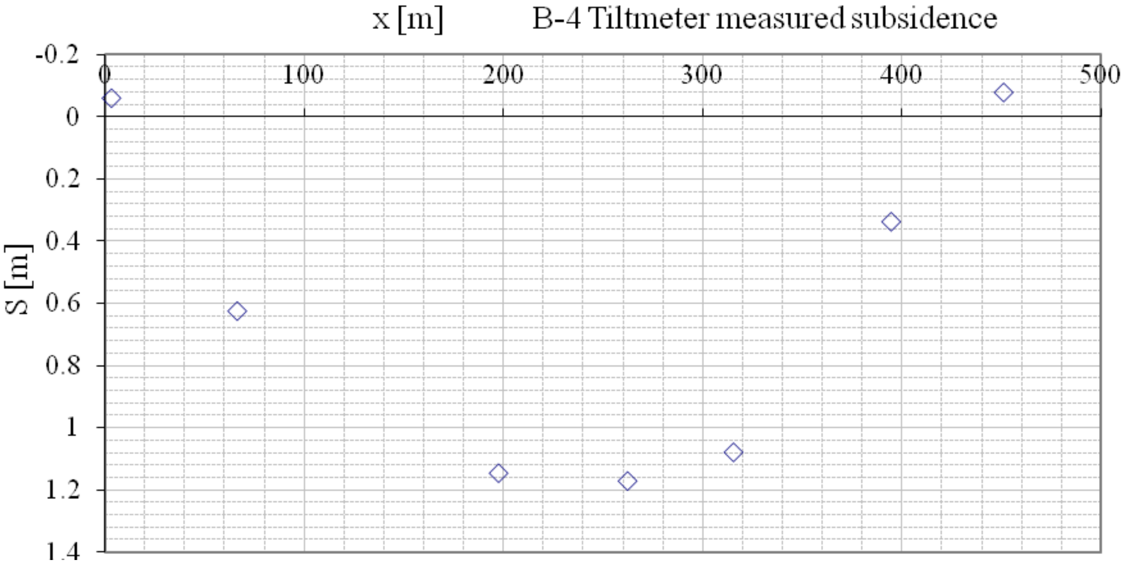

Figure 3-17 B-4 Tiltmeter subsidence readings

3.5 CUMBERLAND MINE

3.5.1 PANEL LW-49

The segment of I-79 above panel LW-49 began to be surveyed after the mine face had passed underneath it, as observed in Figure 3-18. Figure 3-19 gives the highway elevation in the transverse projection. Figure 3-20 and Figure 3-21 show transversal projection of subsidence data for different dates. Figure 3-22 gives a general topographic map with fill and cut zones. Figure 3-23 depicts the final horizontal displacements.

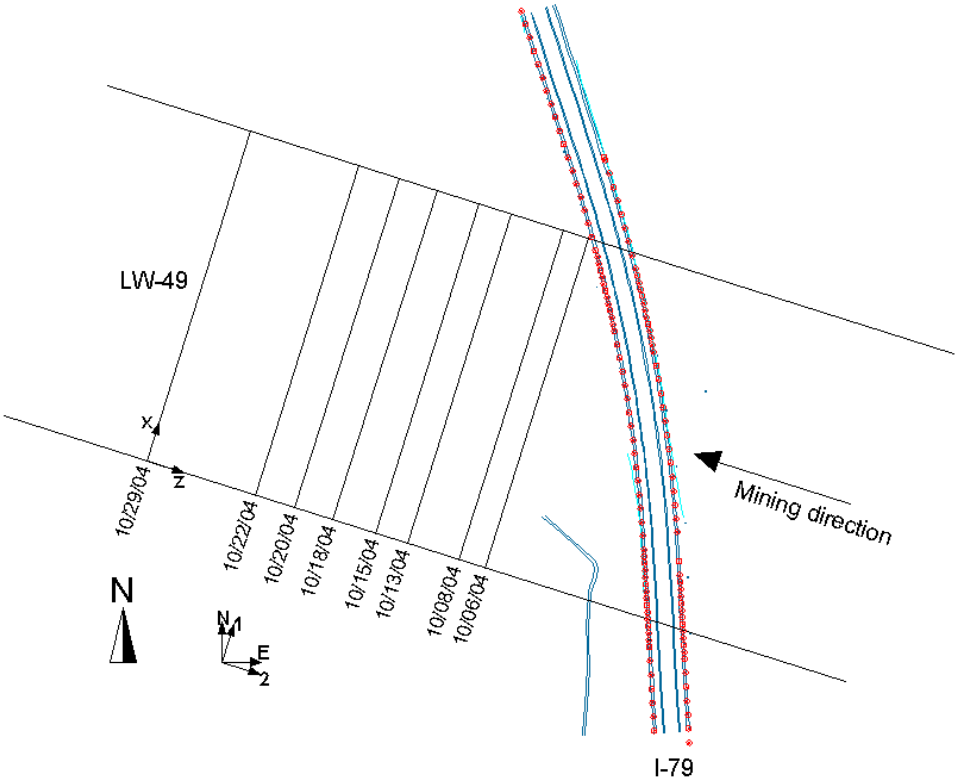

Figure 3-18 Overview of Cumberland mine panel LW-49 intersecting I-79

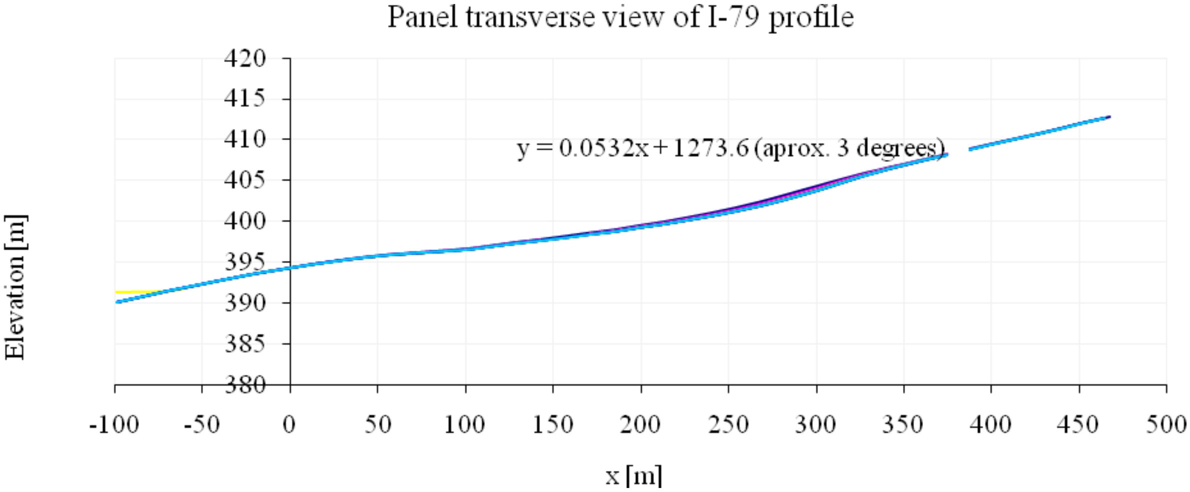

Figure 3-19 Highway northbound elevation in the *z*-plane projection

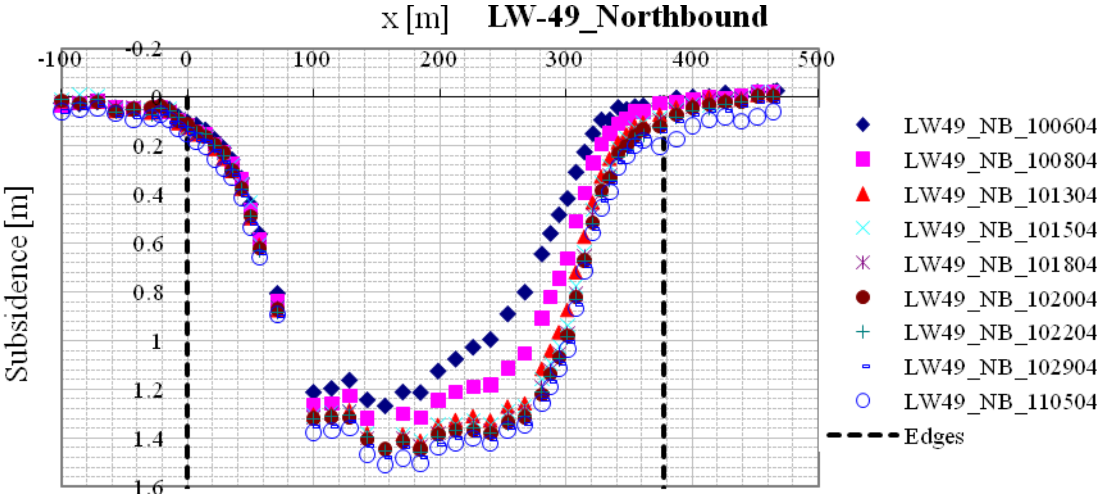

Figure 3-20 Cumberland LW-49 *z*-plane (transv.) projection of northbound surveying data

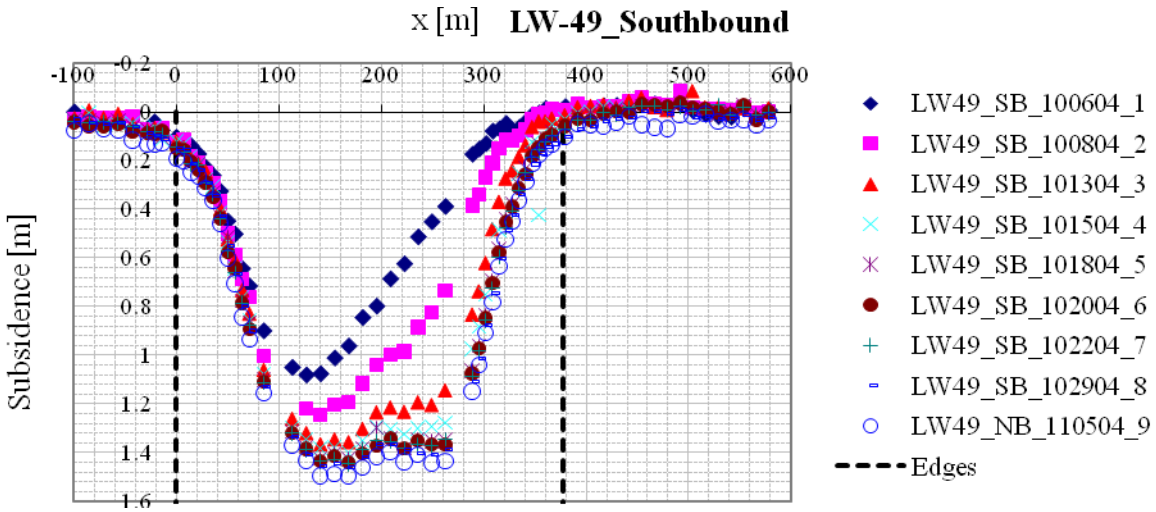

Figure 3-21 Cumberland LW-49 *z*-plane (transv.) projection of southbound surveying data

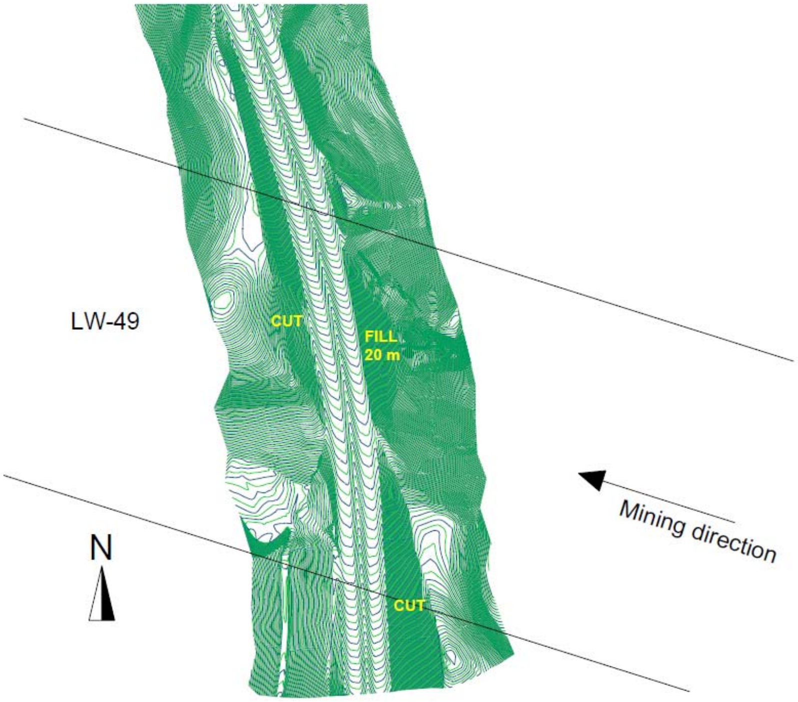

Figure 3-22 Cumberland mine panel LW-49 cut and fill zones

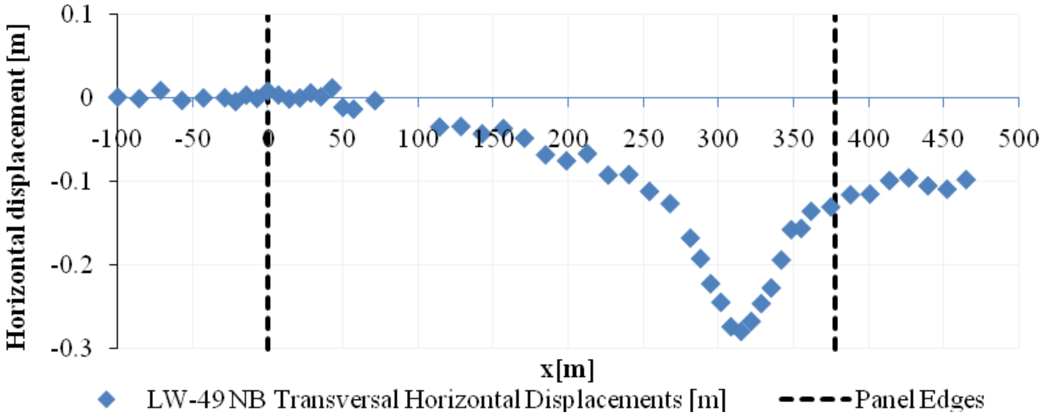

Figure 3-23 Cumberland LW-49 *z*-plane projection of northbound horizontal displacements

3.5.2 PANEL LW-51

Panel LW-51 is one of the best documented panels of this study. This fact is apparent from Figure 3-26 and Figure 3-27, showing a total 9 different surveying dates, well spaced and corresponding to mine face positions before the highway is reached, at locations underneath the highway, and passed it, as illustrated in Figure 3-24. Figure 3-25 provides the highway elevation. The southbound data corresponding to 05/04/2006 seems to differ from the general smooth pattern. The data showed some abrupt change in the surface elevation as observed in Figure 3-27. This could very well be a result of deformation of highway fills. Figure 3-28 provides a general topographic map with cut and fill zones. Figure 3-29 gives the final horizontal displacements.

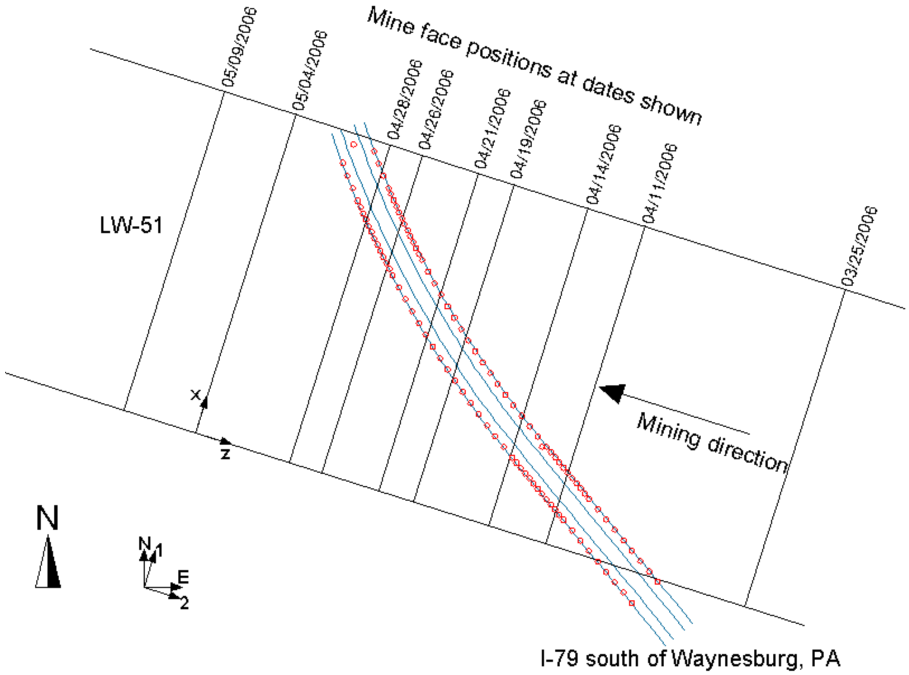

Figure 3-24 Overview of I-79 intersecting the projected Cumberland panel LW-51

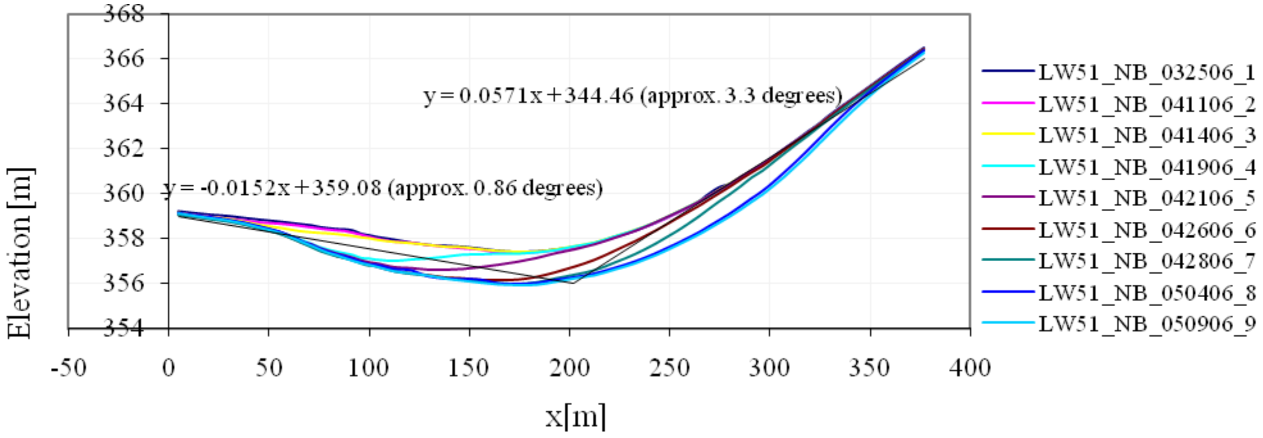

Figure 3-25 Highway northbound elevation in the *z*-plane projection

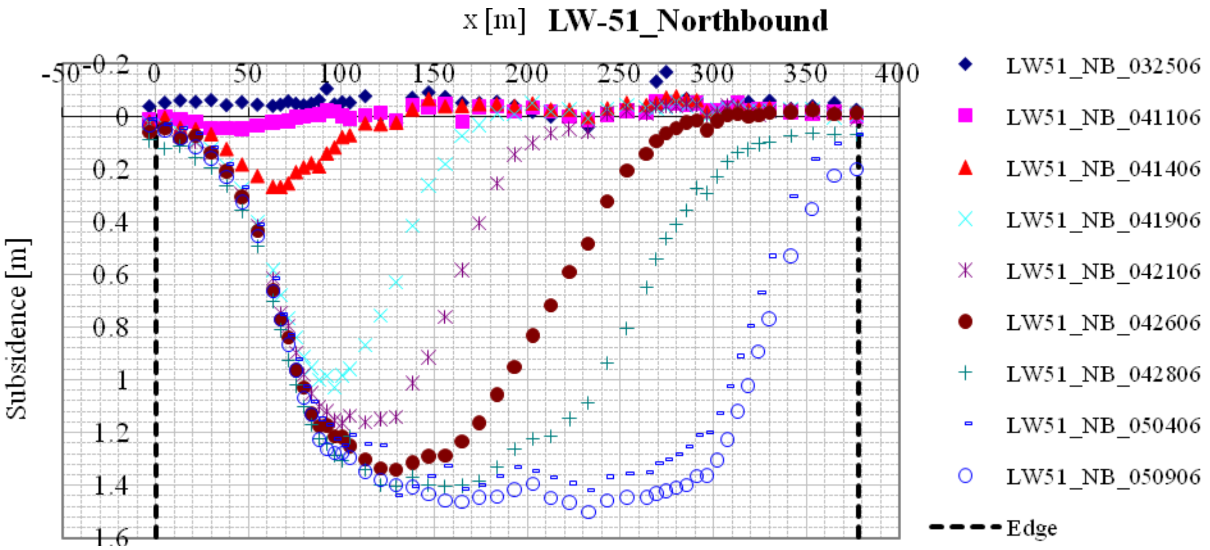

Figure 3-26 Cumberland LW-51 *z*-plane (transv.) projection of northbound surveying data

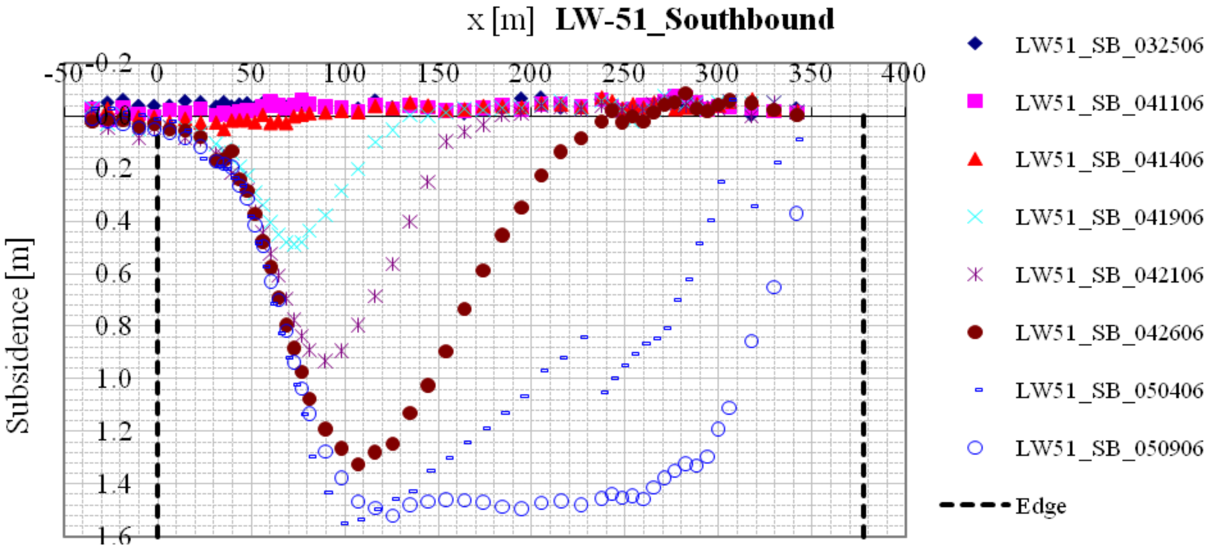

Figure 3-27 Cumberland LW-51 *z*-plane (transv.) projection of southbound surveying data

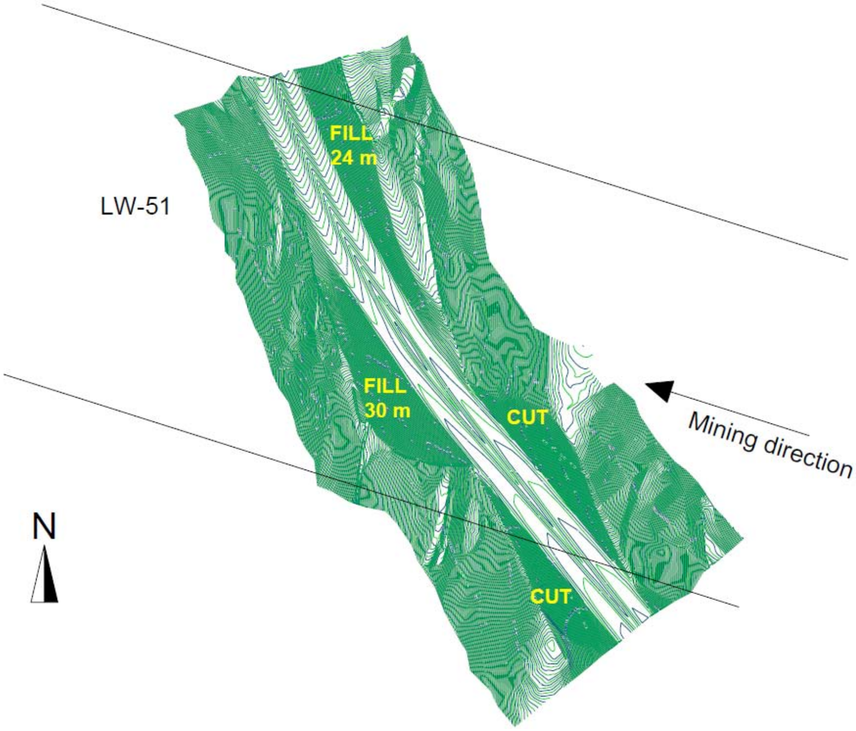

Figure 3-28 Cumberland mine panel LW-51 cut and fill zones

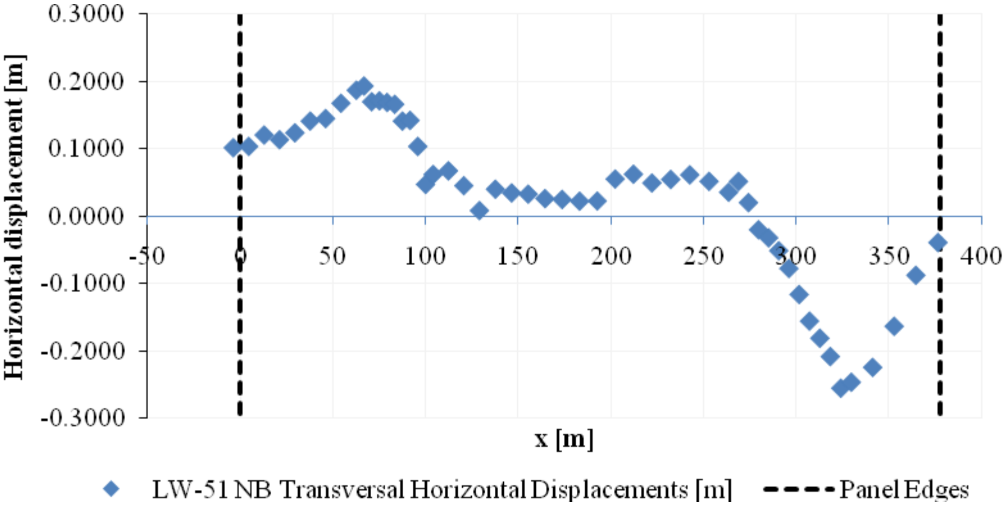

Figure 3-29 Cumberland LW-51 *z*-plane projection of northbound horizontal displacements

3.5.3 PANEL LW-52

Panel LW-52 had a large data gap observed between the last two survey dates (Figure 3-30), which will affect the transformed data as will be seen in section 3.7. Figure 3-31 provides the highway elevation. Figure 3-32 and Figure 3-33 depict profiles from different dates on the northbound and southbound of I-79. Substantial differences in maximum subsidence are apparent in Figure 3-33 if the last profile is compared to that of the northbound. The shape of the final transversal profile for the southbound does not resemble a typical supercritical profile, which would be presumed to be more or less flat in the central region along the panel width. Instead, on the right side of the panel a sharp rise in subsidence occurred giving an unusually high maximum subsidence equal to 1.68 m. This behavior could very well be influenced by zones of highway fills, similar to panel LW-51. Figure 3-34 gives a general topographic map with cut and fill zones. Figure 3-35 depicts the final horizontal displacements.

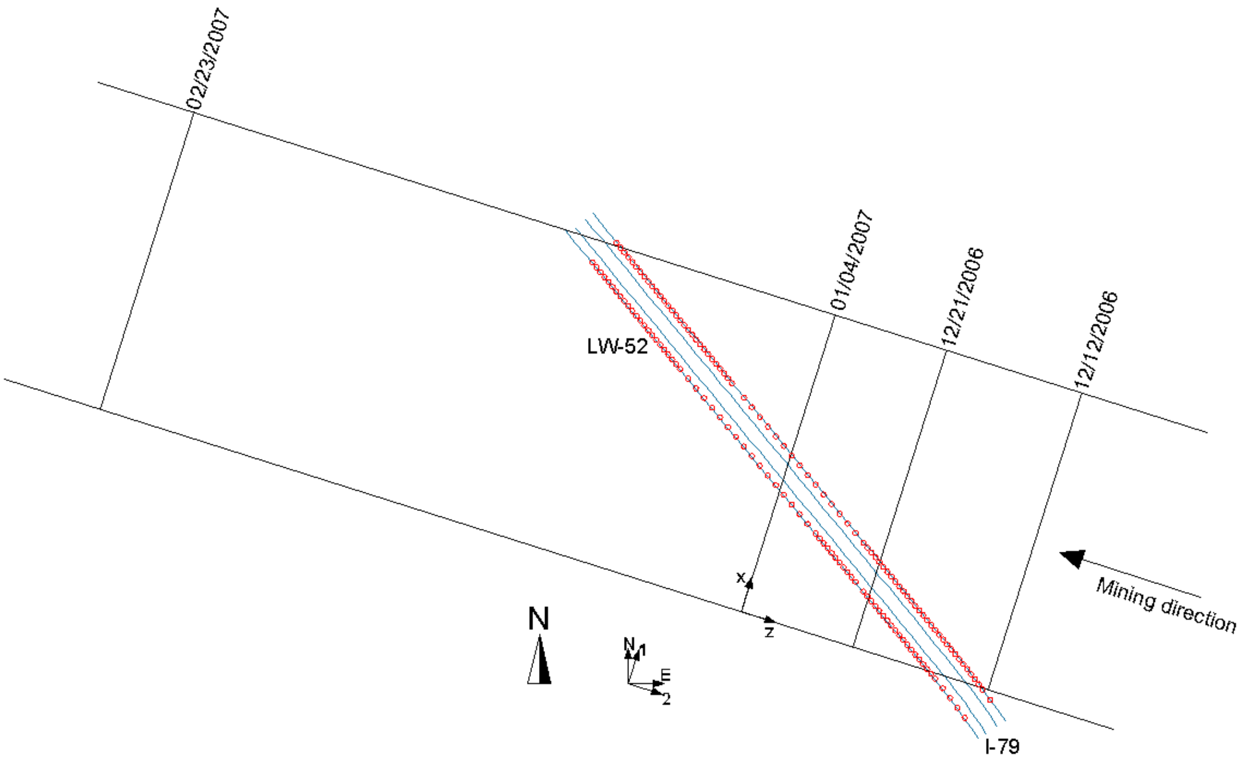

Figure 3-30 Overview of Cumberland mine panel LW-52 intersecting I-79

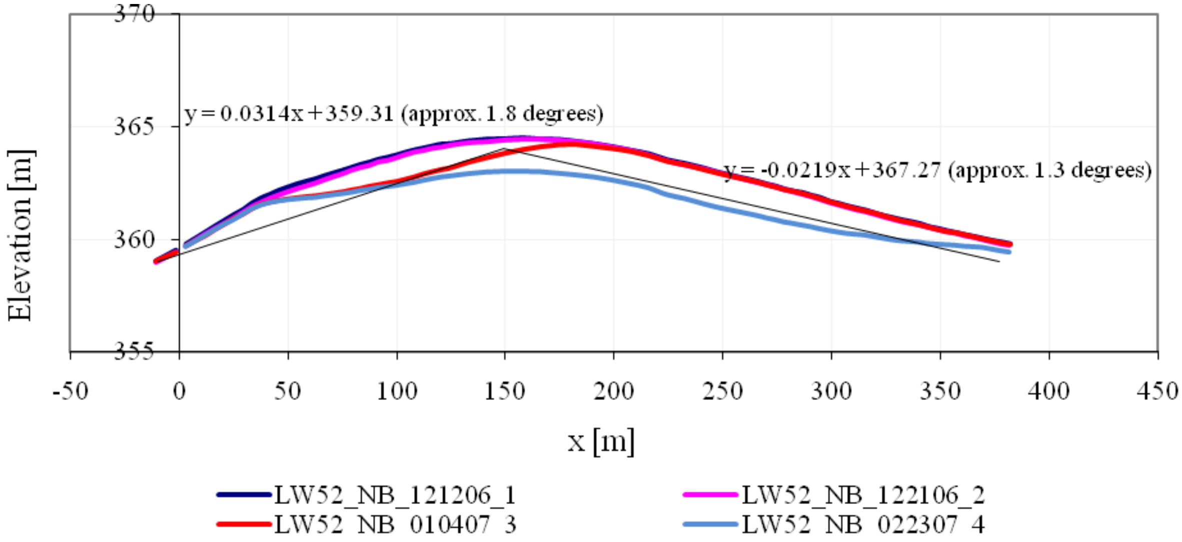

Figure 3-31 Highway northbound elevation in the *z*-plane projection

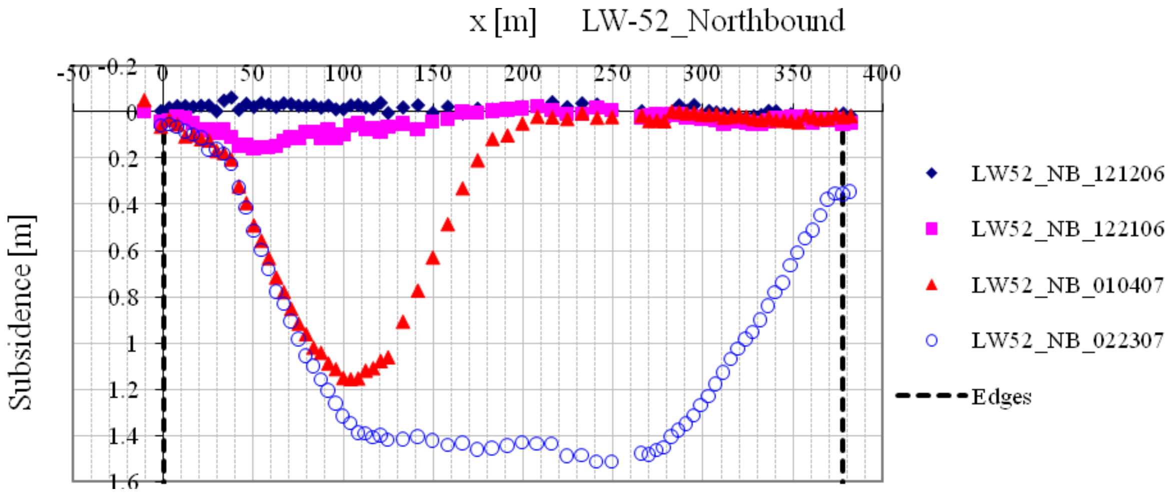

Figure 3-32 Cumberland LW-52 *z*-plane (transv.) projection of northbound surveying data

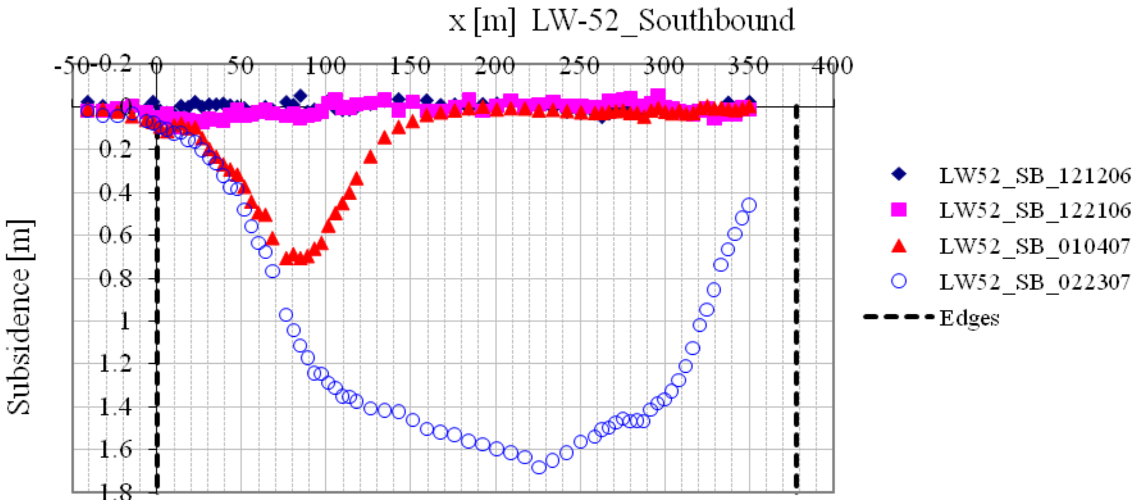

Figure 3-33 Cumberland LW-52 *z*-plane (transv.) projection of southbound surveying data

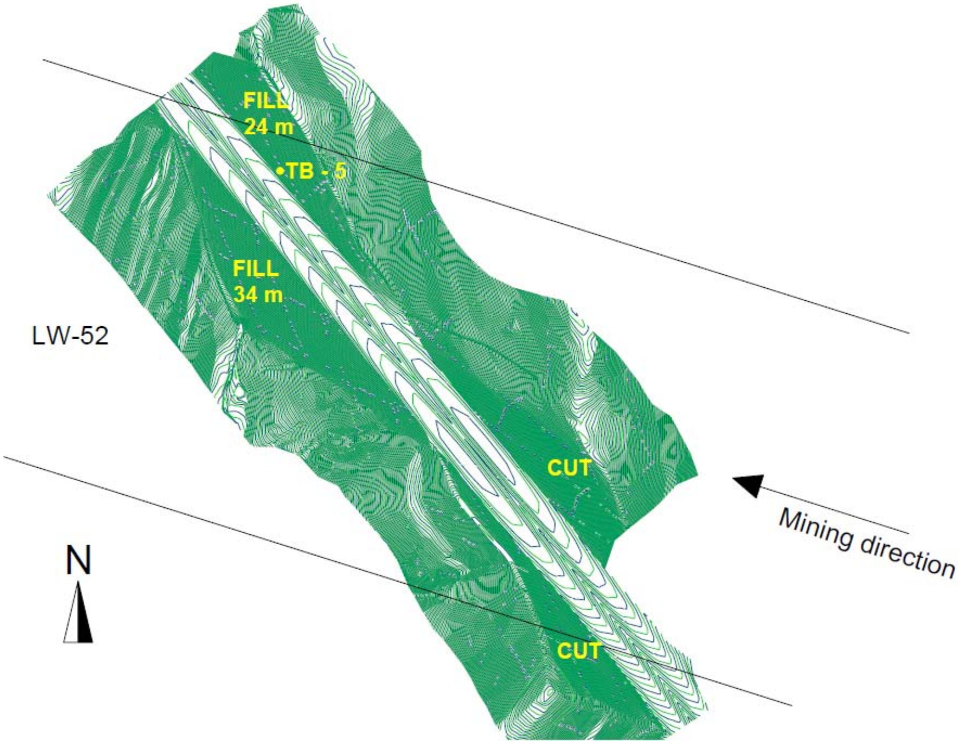

Figure 3-34 Cumberland mine panel LW-52 cut and fill zones

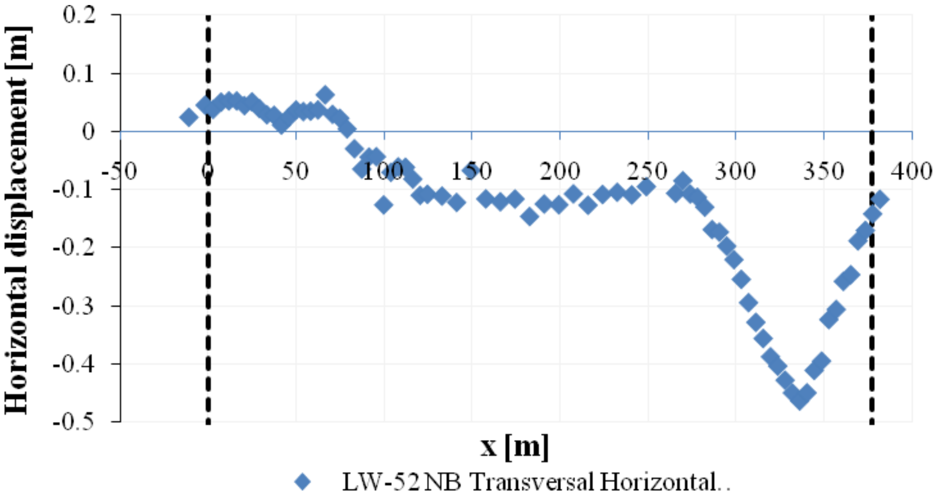

Figure 3-35 Cumberland LW-52 *z*-plane projection of northbound horizontal displacements

3.5.4 PANEL LW-55

Panel LW-55 was added to the above mentioned PennDOT project as data became available during and after mining, on the month of October 2008. This panel is unique in that it starts right at the area of concern. Transformation of this data for supercritical-based prediction is not relevant because a complete history until profiles became supercritical may not be obtained. One reason is that the highway does not completely cross the panel and crosses close to a corner. Another reason is the limitation of data, which were only measured until October 27 2008, as shown in Figure 3-36. However, a small region of supercritical deformation may be observed in Figure 3-37 and Figure 3-39, thus providing a valuable maximum subsidence magnitude. Figure 3-39 and Figure 3-40 show excessive heave taking place from 10/03/08 to 10/06/08 for the southbound. A double-check of tiltmeter data seems to show no such drastic changes in elevation, as depicted in Figure 3-42 and Figure 3-43.

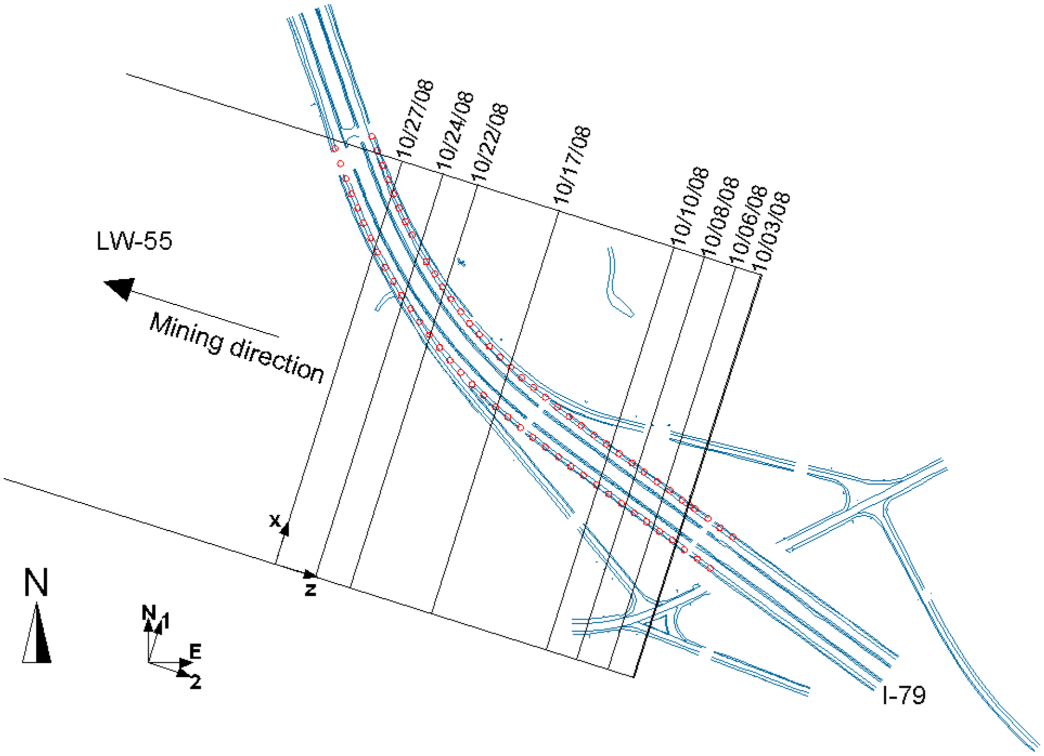

Figure 3-36 Overview of Cumberland mine panel LW-55

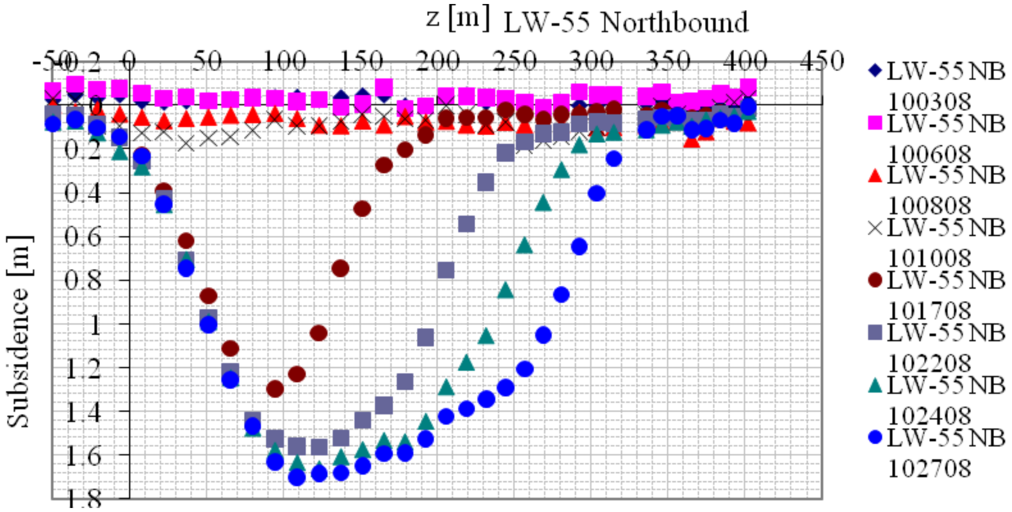

Figure 3-37 Cumberland LW-55 *x*-plane (long.) projection of northbound surveying data

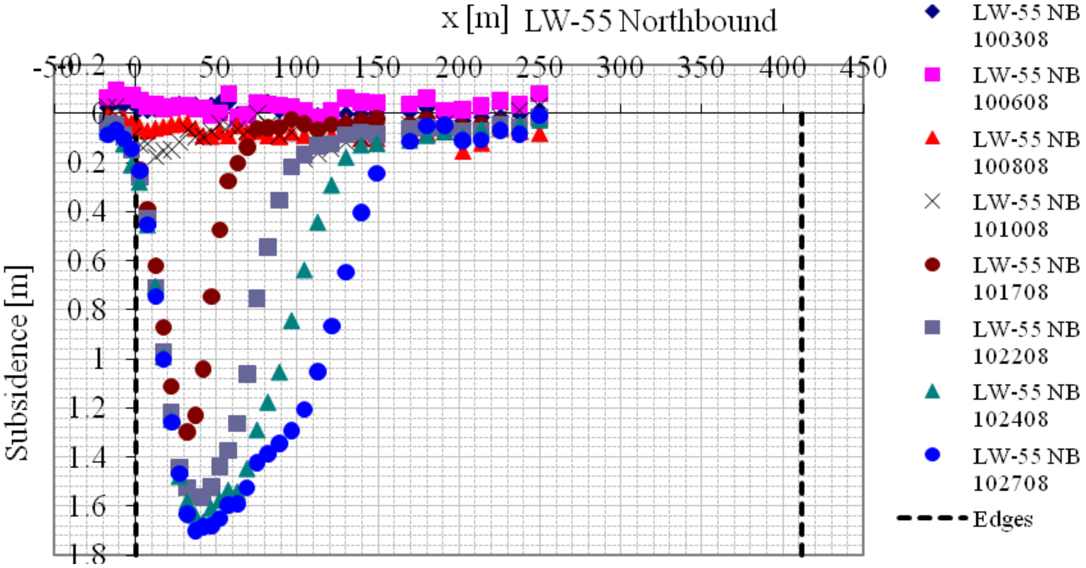

Figure 3-38 Cumberland LW-55 *z*-plane (transv.) projection of northbound surveying data

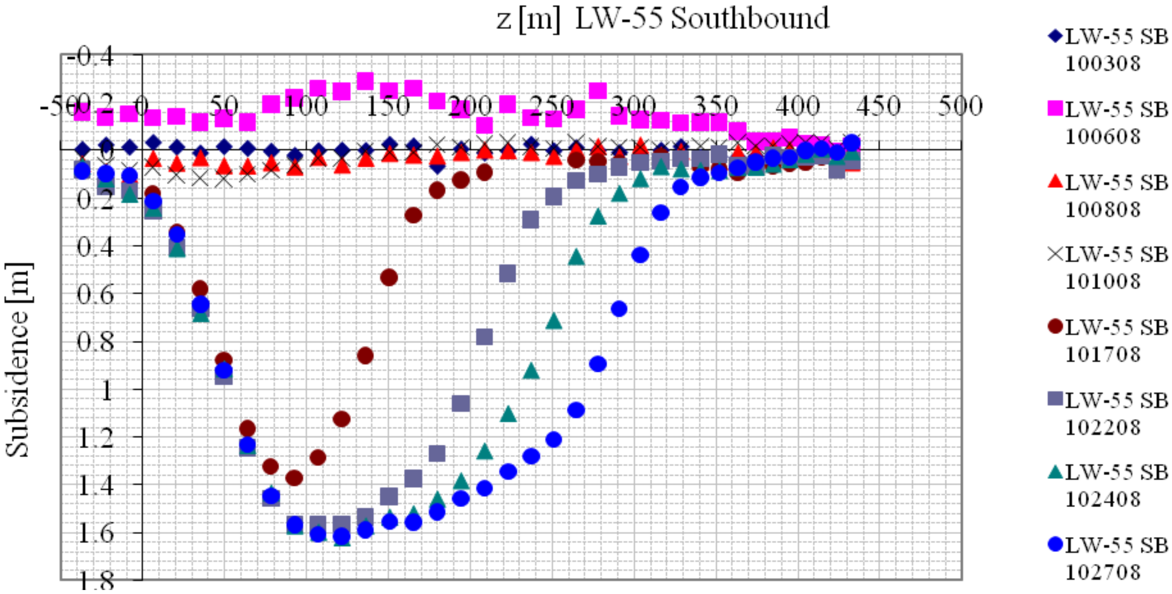

Figure 3-39 Cumberland LW-55 *x*-plane (long.) projection of southbound surveying data

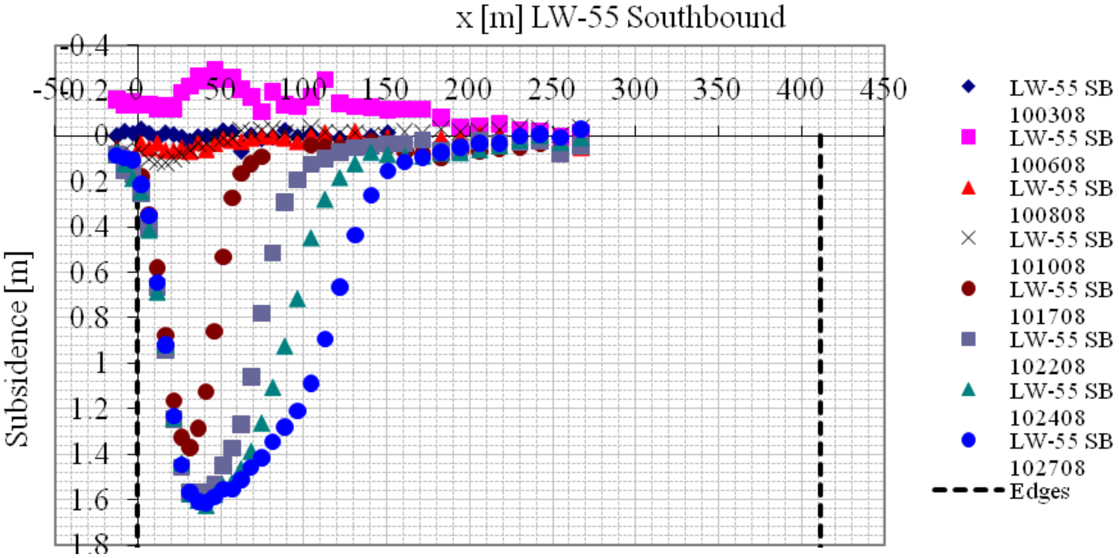

Figure 3-40 Cumberland LW-55 *z*-plane (transv.) projection of southbound surveying data

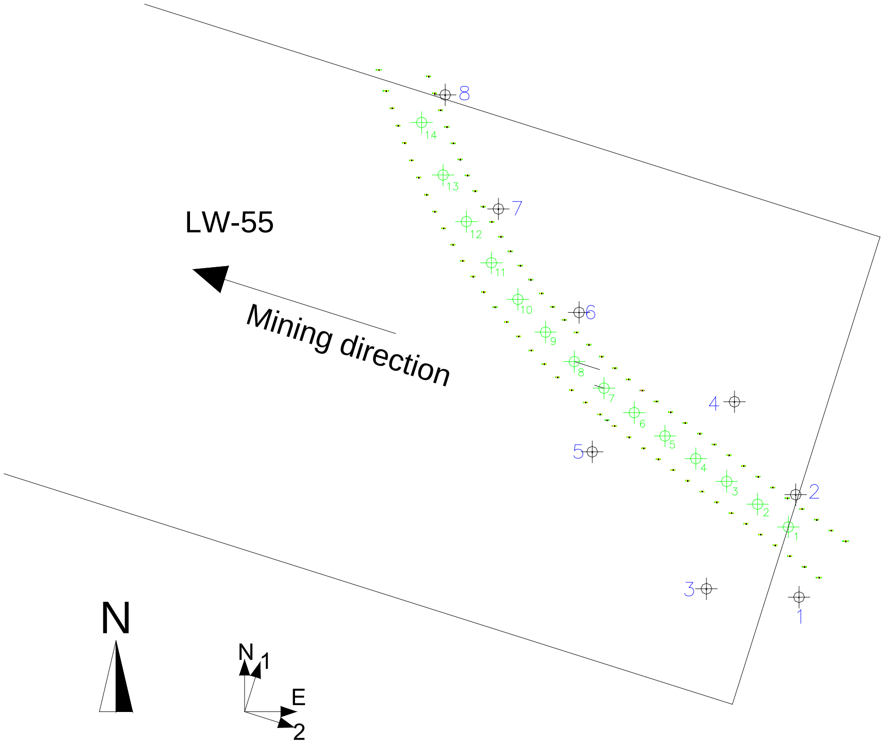

Figure 3-41 Overview of LW-55 tiltmeters

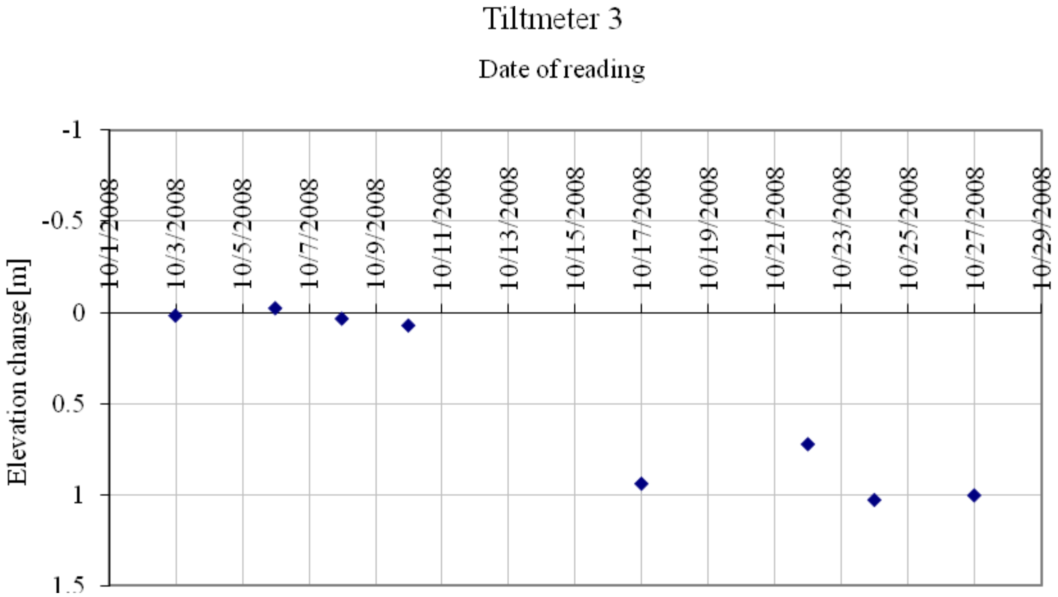

Figure 3-42 Cumberland mine panel LW-55 tiltmeter 3 elevation change readings

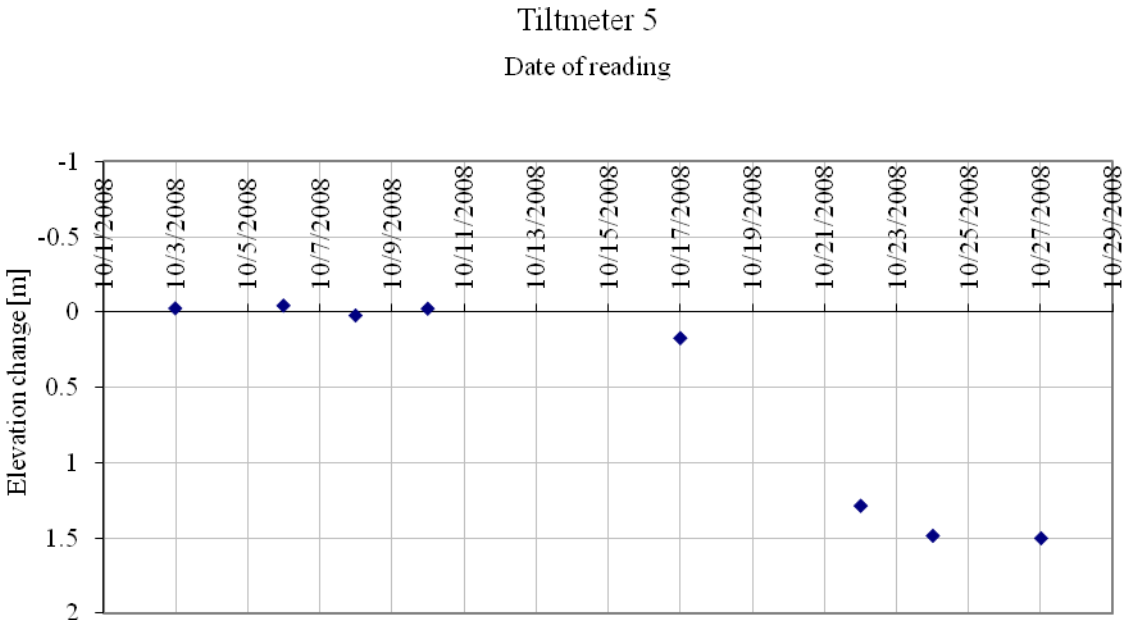

Figure 3-43 Cumberland mine panel LW-55 tiltmeter 5 elevation change readings

3.5.5 PANELS LW-50 AND LW-53

From panels LW-50 and LW-53 only the maximum subsidence could be estimated from elevation changes, since no East, North coordinates were available. The subsidence magnitude is contained in Table 3-4.

3.6 SIGNIFICANCE OF SUPERCRITICAL SUBSIDENCE TROUGHS

From the geometry illustrated in Figure 3-6 and Figure 3-7 and the last column of Table 3-4, it is clear that supercritical conditions are expected to take place due to the extraction of all panels. Except for cases in which the highway crossed the projected area of panels at corners or close to the panel ends, most of the data exhibited supercritical conditions.

To illustrate the role of the supercritical conditions in the construction of the subsidence trough, a drawing is presented in Figure 3-44.

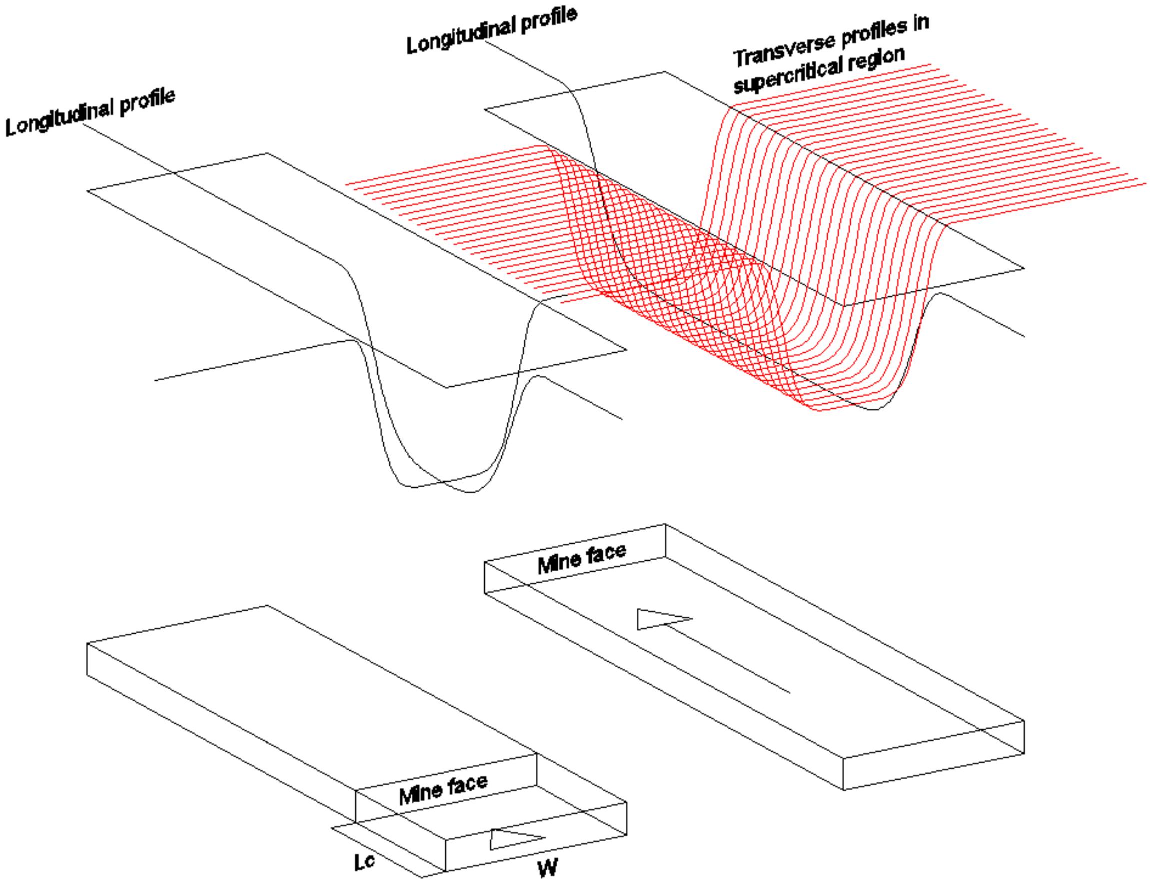

Figure 3-44 Supercritical trough above a longwall panel

After the mining operation reaches the critical dimension *Lc* in the longitudinal direction, subsidence experiences supercritical conditions. In all panels used here, this critical dimension is also reached in the transversal (width) direction. Once this critical length is surpassed, and provided that the rate of advance of the mine face is constant, the trough front that is formed propagates like a wave in the direction of mining preserving its shape and advancing at roughly the same rate at which the mine face progresses. This assumes that the overburden is homogeneous and the mining operation remains steady. The reasonableness of the assumption is illustrated in the data analysis.

Figure 3-45 shows two positions 1 and 2, representing two mine face positions with Position 2 farther advanced than Position 1. Both positions were reached after the critical dimension had been surpassed. The assumption of the unchanged trough front advance is reflected in the shift of the front.

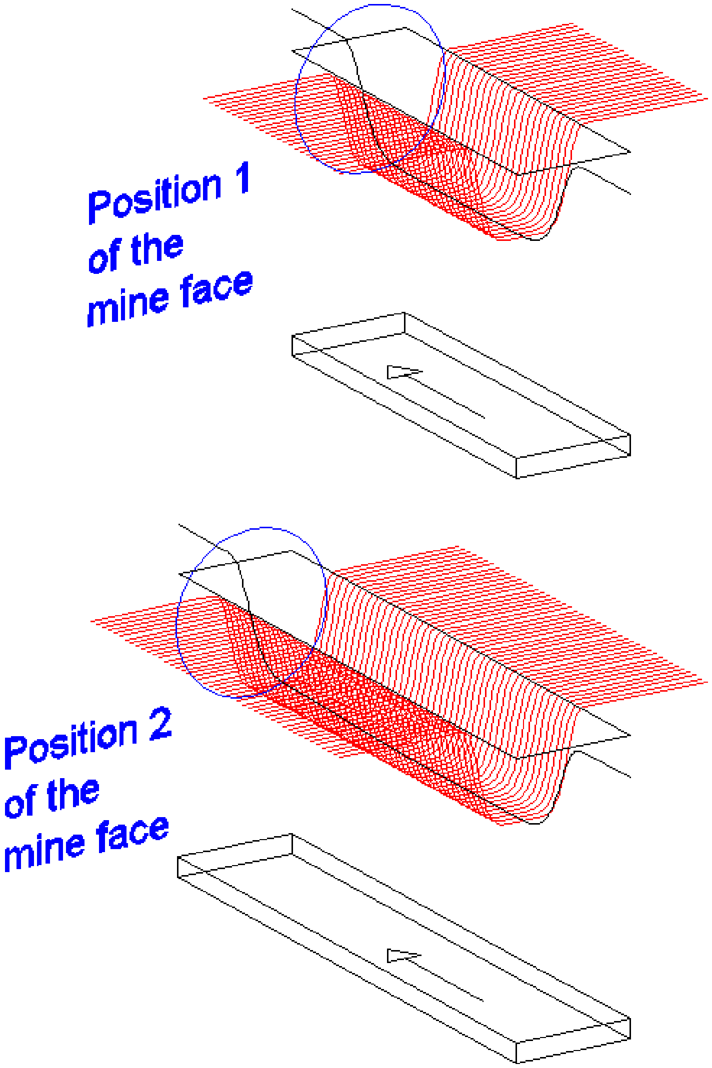

Figure 3-45 The trough front in supercritical conditions

3.7 PROPOSED DATA TRANSFORMATION

After all subsidence values were obtained for each and every single station and coupled with the position of the mine face for each surveying date, a transformation of the data was performed on each panel that provided a sufficient amount of data. A step-by-step description of the process is given here:

1. For every single station and every single date of surveying, subsidence, *S*, was computed by subtracting the elevation from the baseline elevation.
2. For every single date, the position of the mine face was noted.
3. From the East, North, Elevation coordinate system, data was transformed into a rotated coordinate system whose axes are parallel and perpendicular, respectively, to the panel longitudinal direction (see Figure 3-24). The origin of this coordinate system is the same as the East, North, Elevation, since the transformation involves only rotation (clockwise at an angle of 17°32’53”). This coordinate system has axes 1, 2, as shown in Figure 3-24.
4. In order to express point position locally for each panel in a convenient way, a local coordinate system *x*, *z*, *S*, whose origin is located at the left end of the mine face projected to the ground surface, was used for all stations available for each surveying date (see Figure 3-46). The local *x*, *z*, *S* system moves as the mine face advances. For the troughs that were within the supercritical region in the longitudinal direction, with the adoption of homogeneous assumption, all these data were combined in a 3D single *x*, *z*, *S* set.

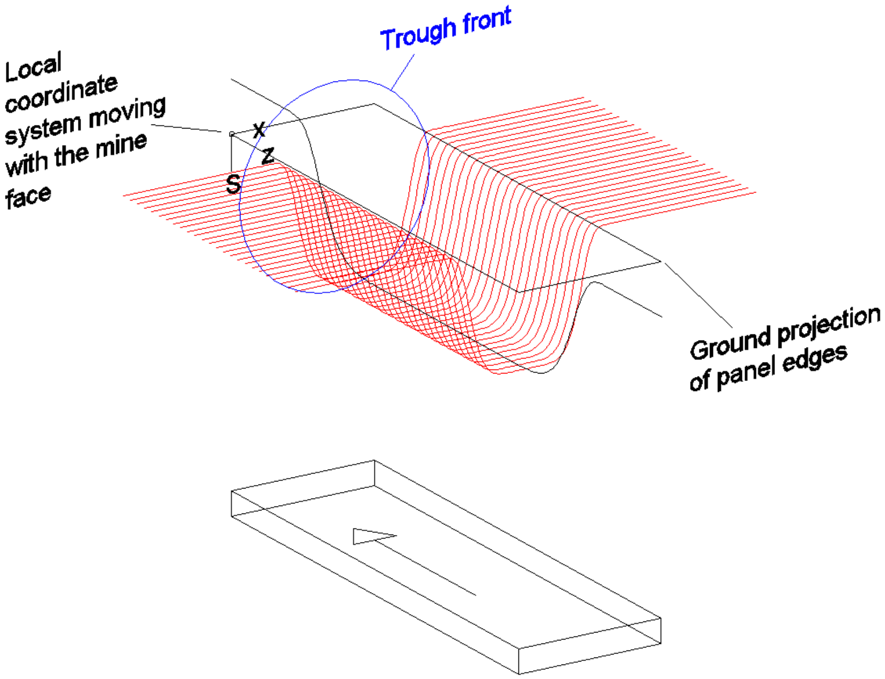

Figure 3-46 Local coordinate system moving at the same rate as the mine face

Figure 3-47 through Figure 3-58 show transformed data for panel LW-51. Only a few positions with respect to the mine face are shown, illustrating that a trough may be obtained. The farther away from the mine face, the higher the magnitude of subsidence. It can be appreciated in Figure 3-58 that subsidence remains constant at the maximum potential magnitude after a certain distance. This can also be seen in the longitudinal profiles obtained at the center of the panels, shown in Figure 3-59 through Figure 3-62.

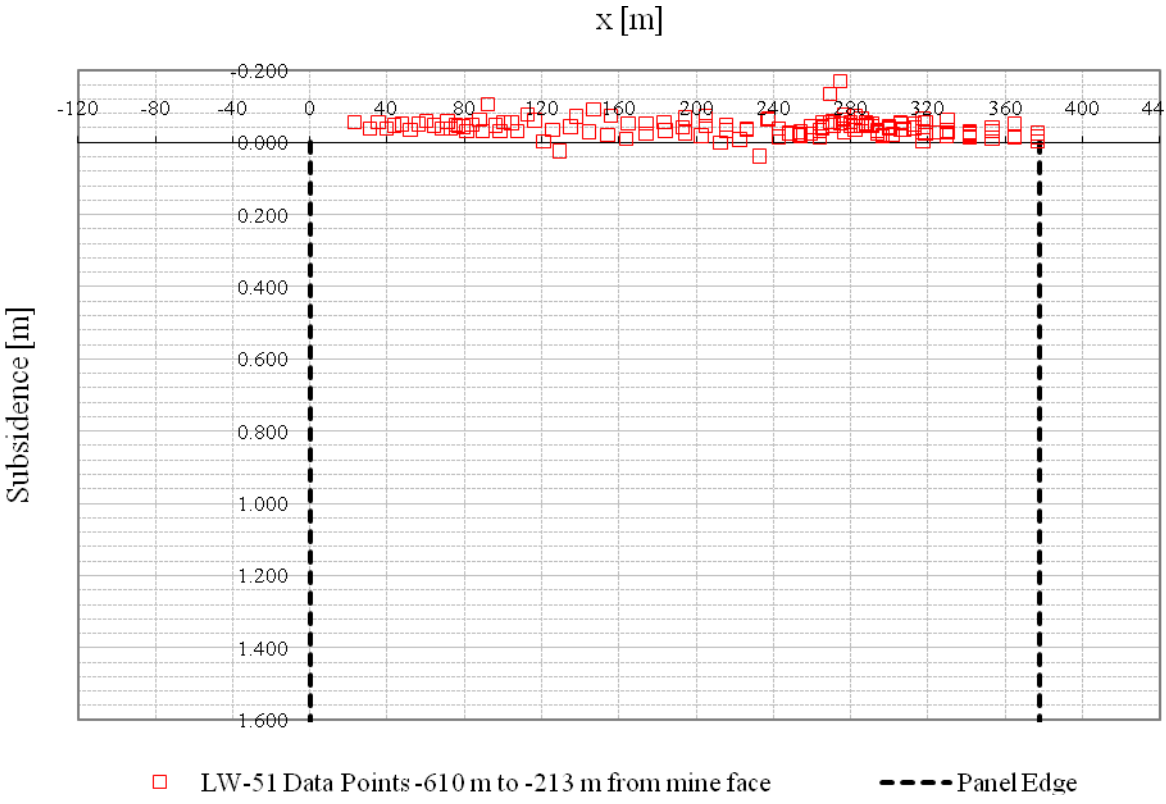

Figure 3-47 LW-51 transformed data between -610 m and -213 m from mine face

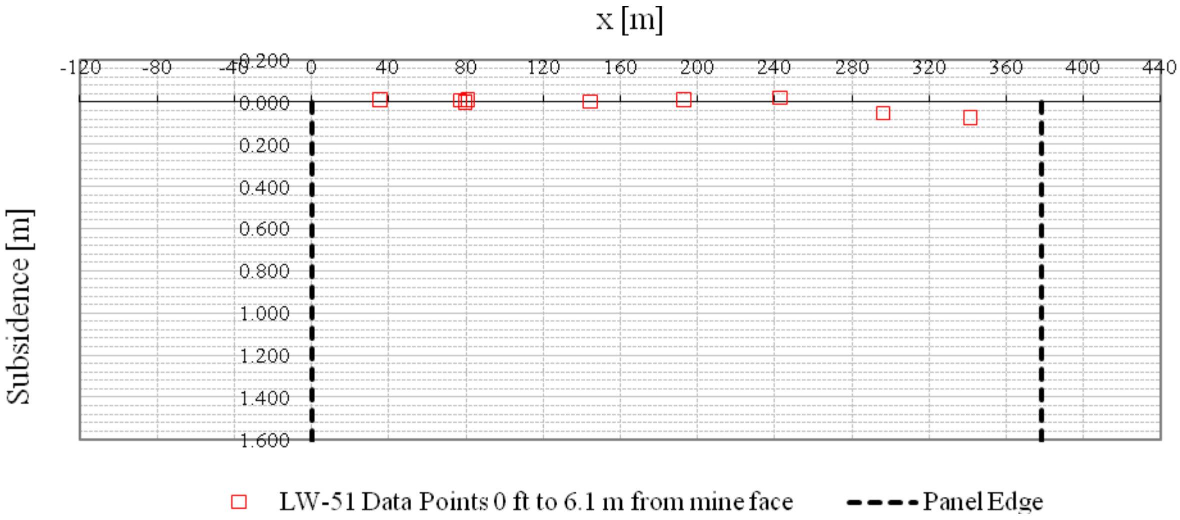

Figure 3-48 LW-51 transformed data between 0 m and 6.1 m from mine face

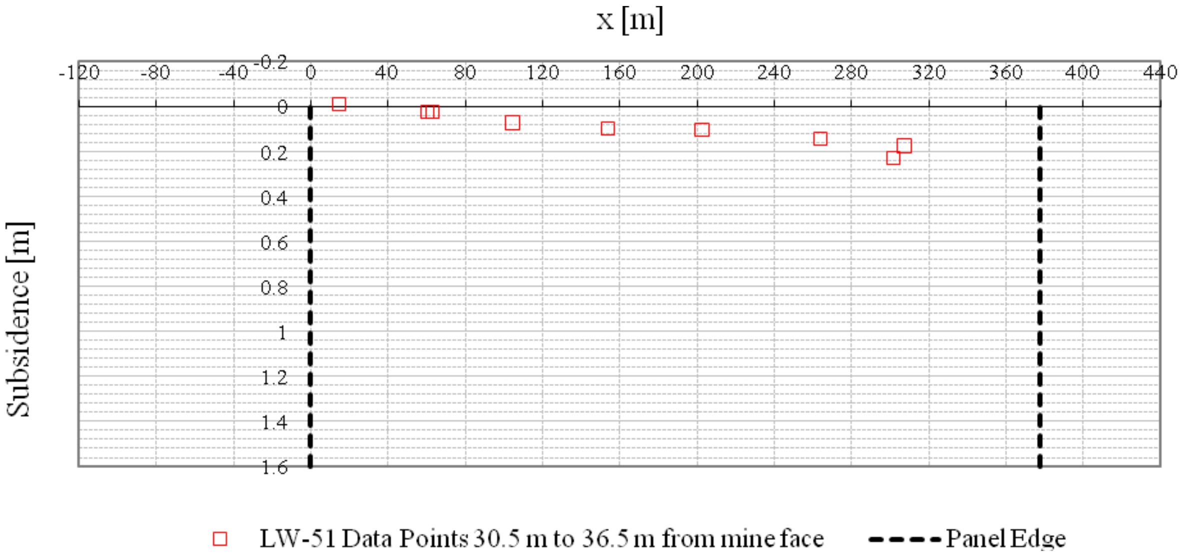

Figure 3-49 LW-51 transformed data between 30.5 m and 36.5 m from mine face

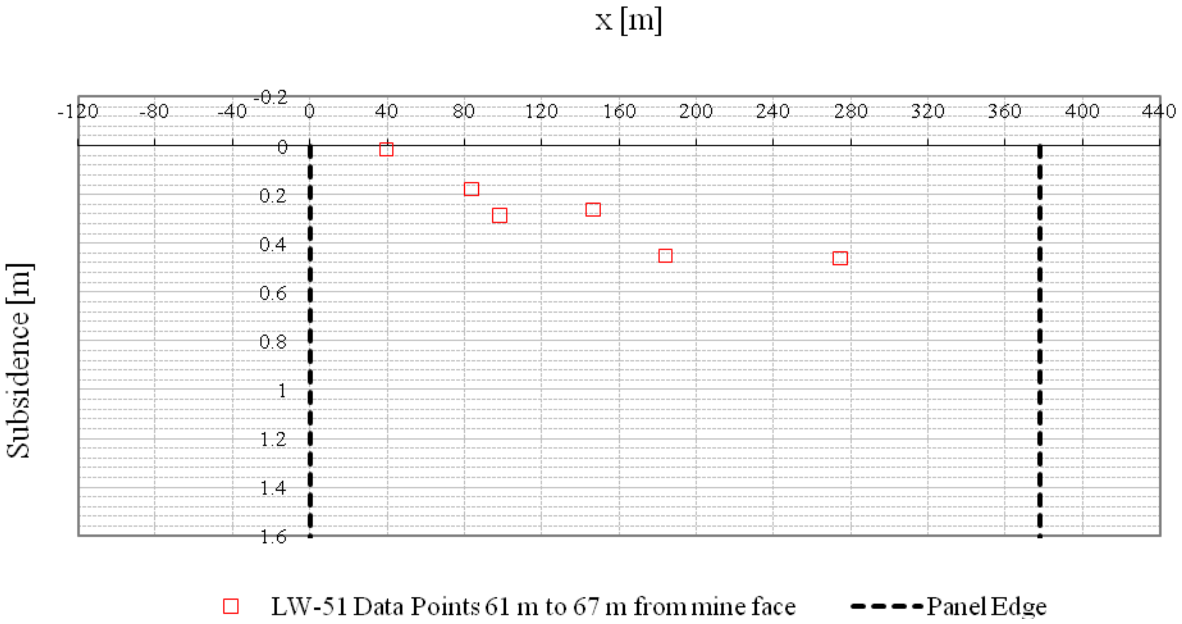

Figure 3-50 LW-51 transformed data between 61 m and 67 m from mine face

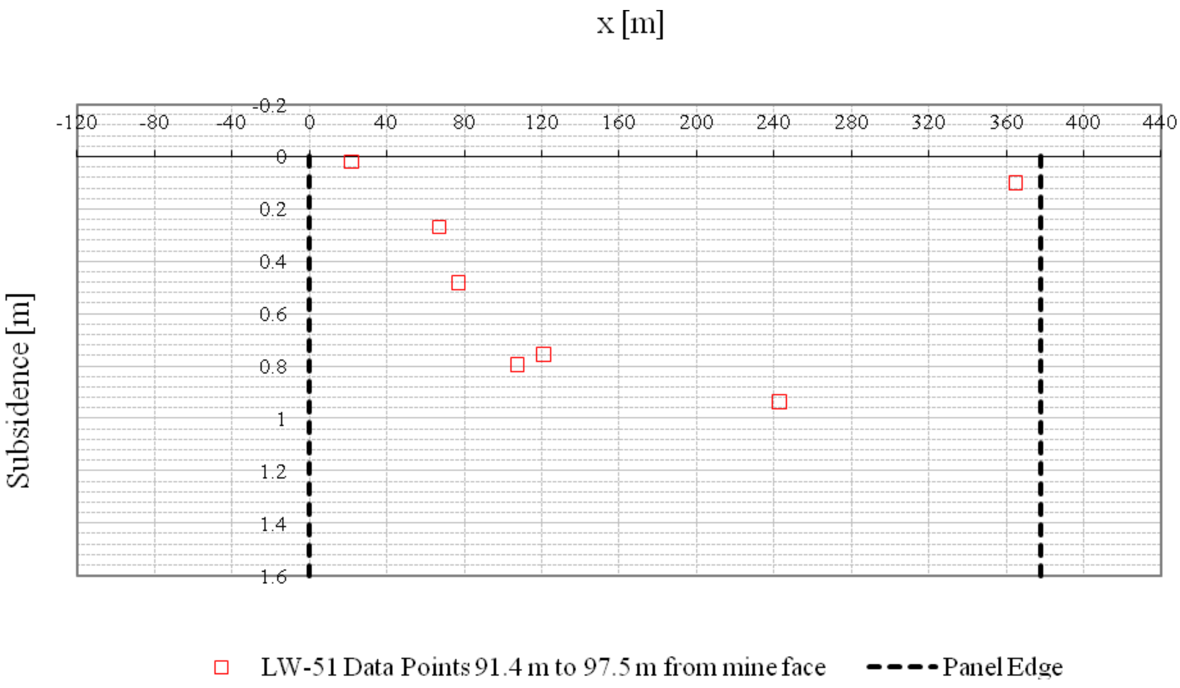

Figure 3-51 LW-51 transformed data between 91.4 m and 97.5 m from mine face

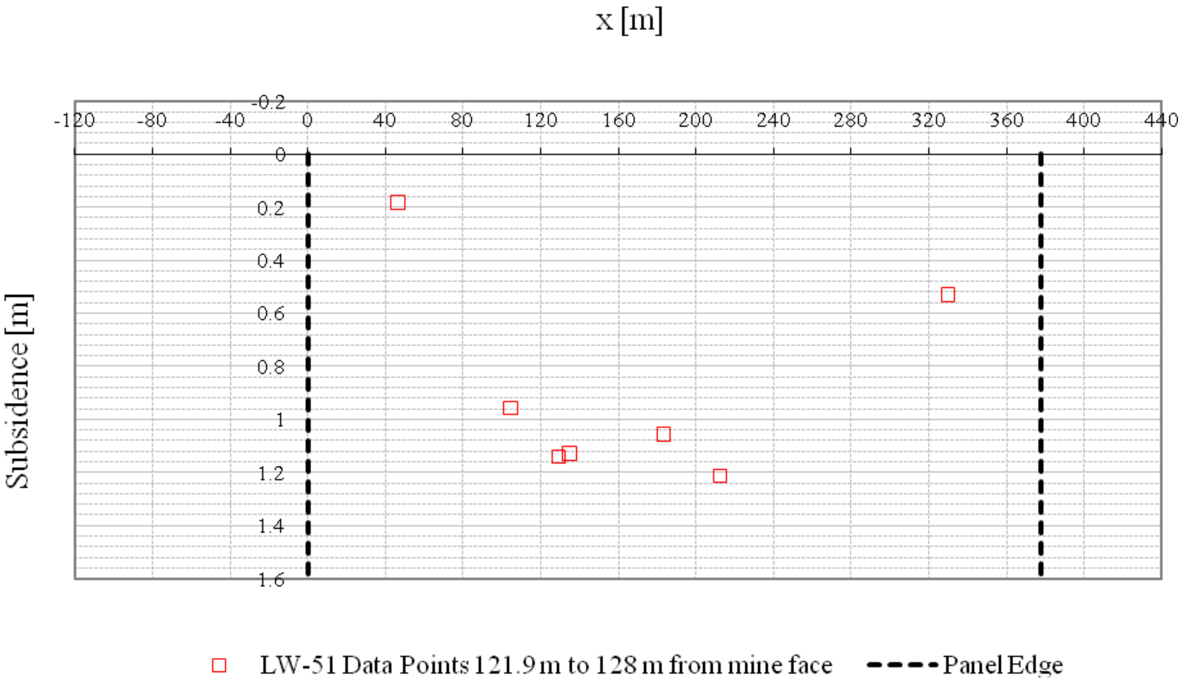

Figure 3-52 LW-51 transformed data between 121.9 m and 128 m from mine face

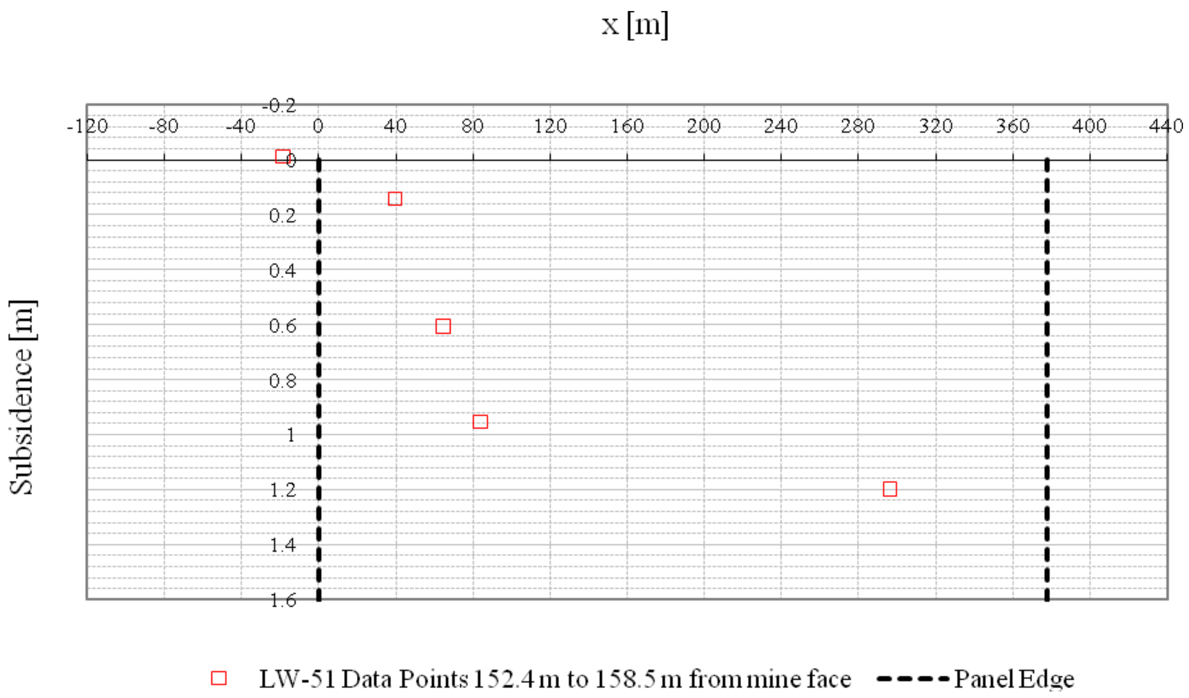

Figure 3-53 LW-51 transformed data between 152.4 m and 158.5 m from mine face

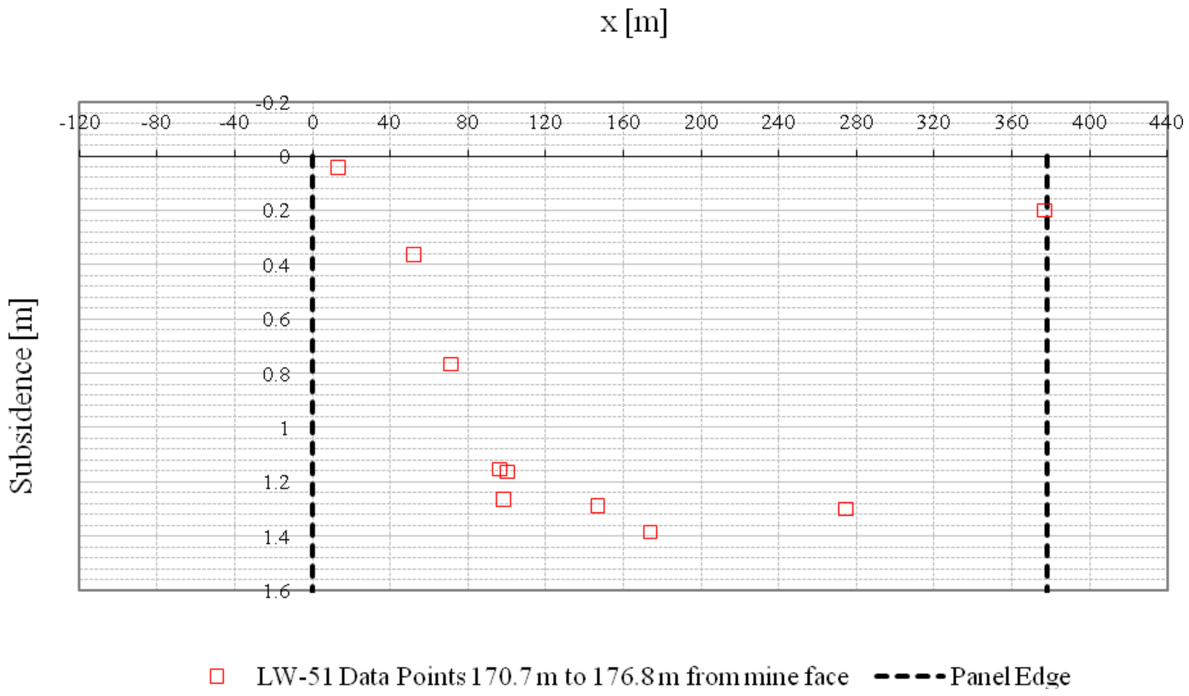

Figure 3-54 LW-51 transformed data between 170.7 m and 176.8 m from mine face

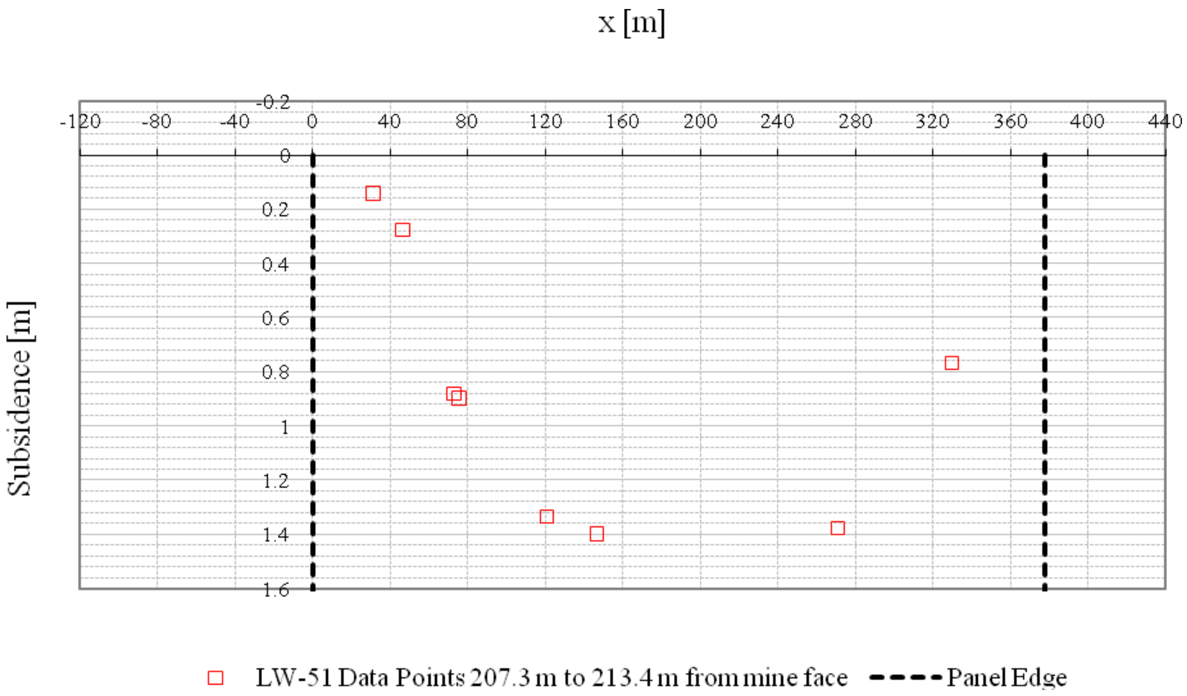

Figure 3-55 LW-51 transformed data between 207.3 m and 213.4 m from mine face

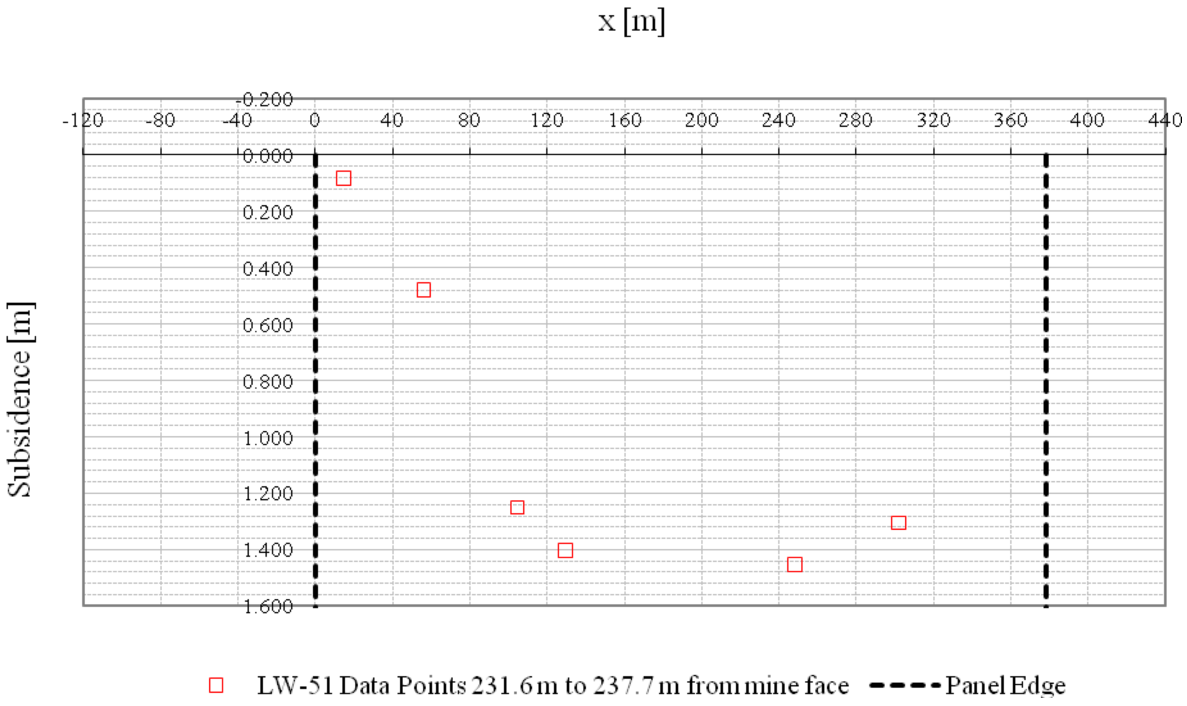

Figure 3-56 LW-51 transformed data between 231.6 m and 237.7 m from mine face

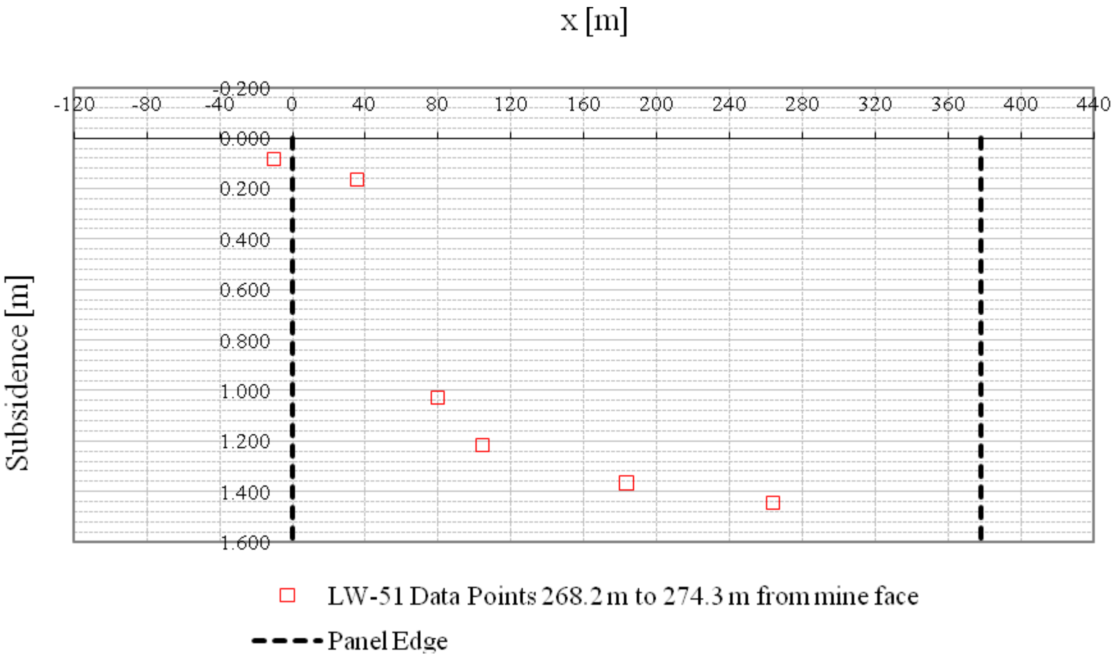

Figure 3-57 LW-51 transformed data between 268.2 m and 274.3 m from mine face

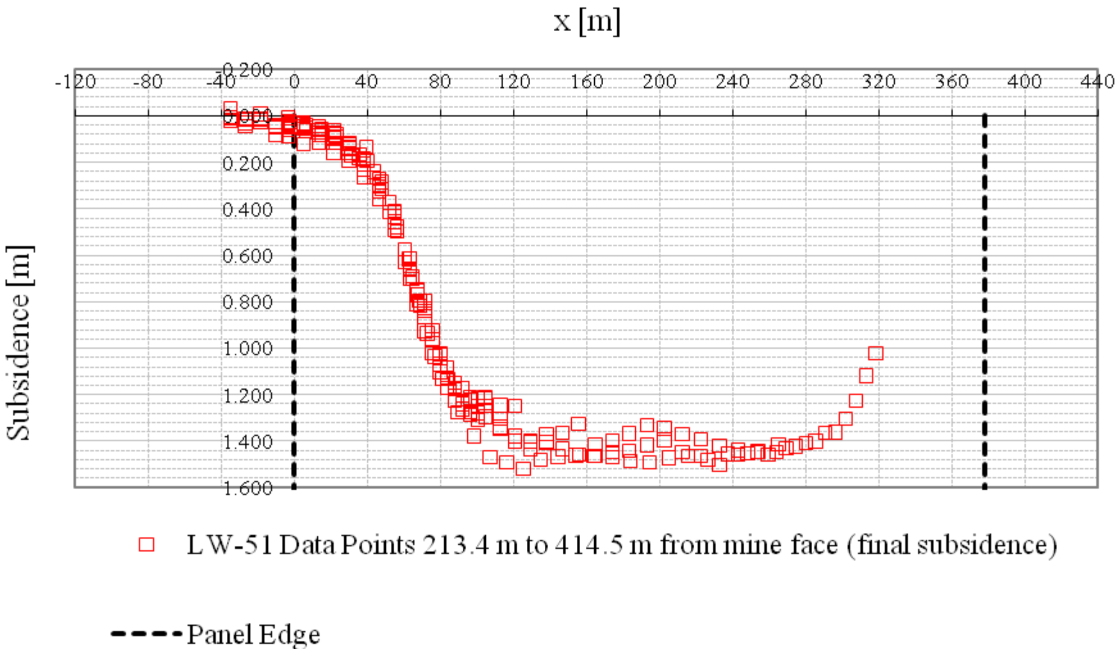

Figure 3-58 LW-51 transformed data between 213.4 m and 414.5 m from mine face

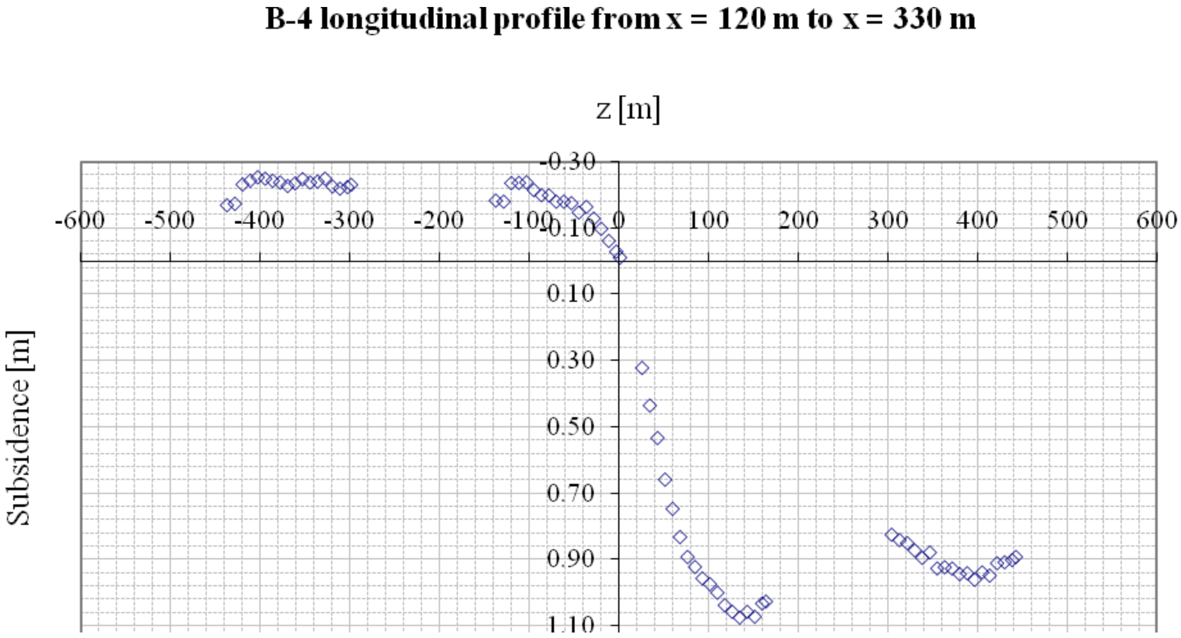

Figure 3-59 B-4 longitudinal subsidence profile in the central 210 m

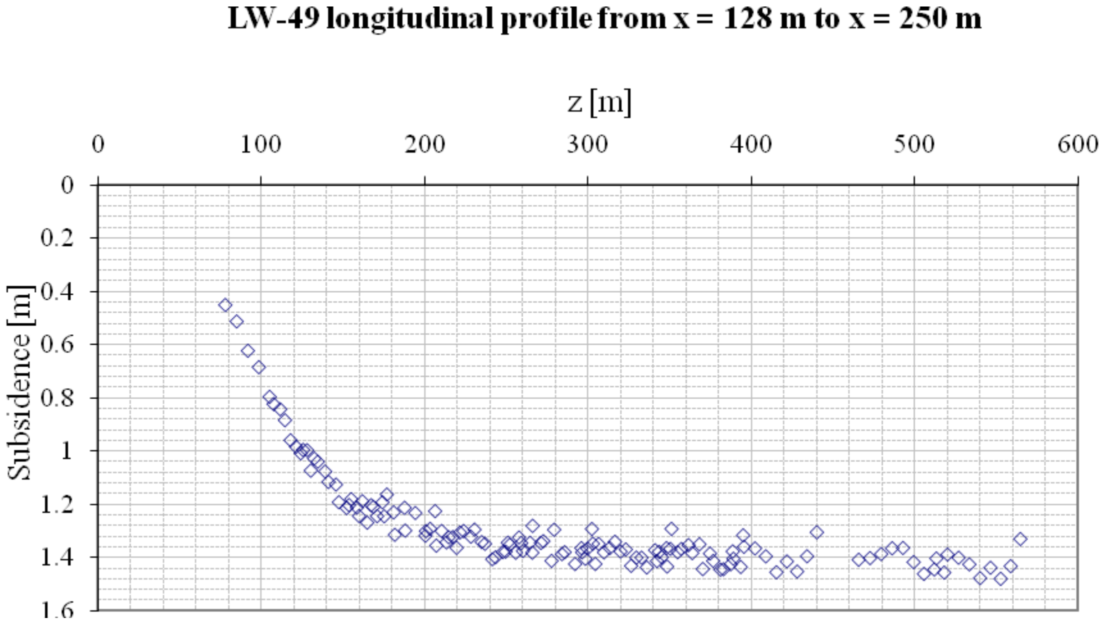

Figure 3-60 Cumberland mine panel LW-49 longitudinal profile for the central 120 m

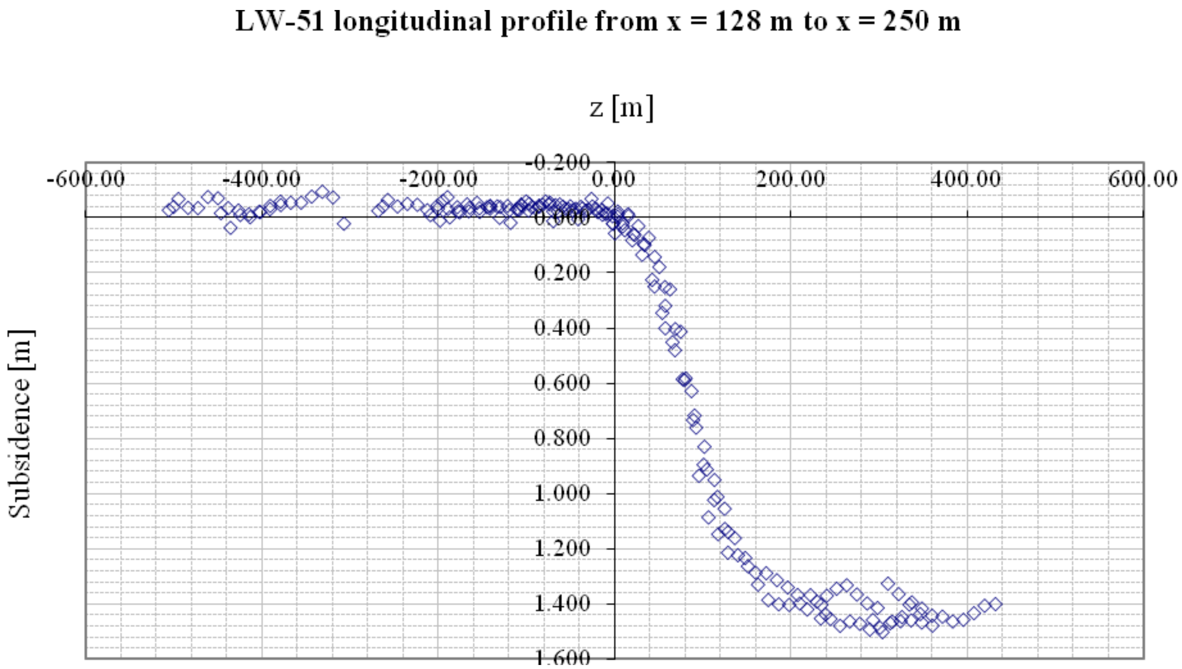

Figure 3-61 Cumberland mine panel LW-51 longitudinal profile for the central 120 m

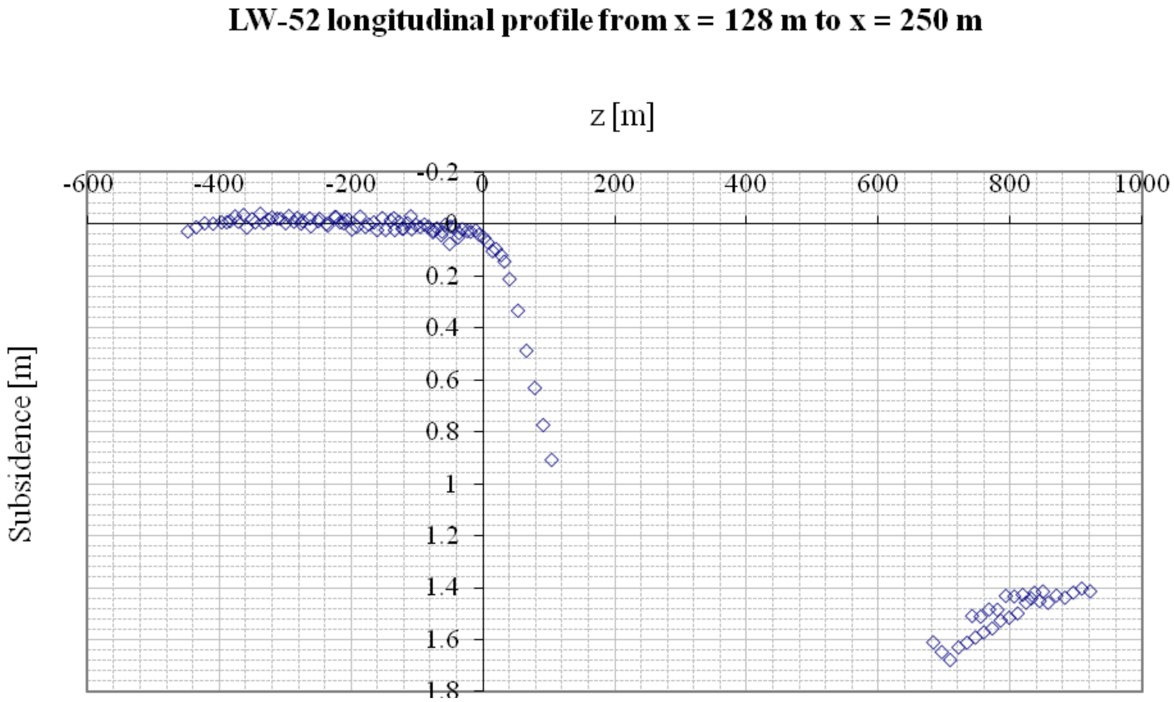

Figure 3-62 Cumberland mine panel LW-52 longitudinal profile for the central 120 m

4.0 DEVELOPING AN EMPIRICAL SUBSIDENCE PREDICTION MODEL

The previous chapter provided a general description of surveying data and a description of a transformation process that allows expressing the subsidence trough as a spatial function in supercritical subsidence deformation regions along the longwall panel.

The representation of the subsidence trough of a given longwall panel in terms of point coordinates and subsidence magnitude is a very useful result. Its deformation magnitudes are geology dependent and tied to the geometric characteristics of the given panel, such as width of the panel, extraction thickness, and overburden thickness.

The present chapter introduces the proposed methodology to empirically obtain any supercritical subsidence trough by taking the overburden thickness, extraction thickness, and panel width into consideration. It is important to emphasize at this point that any empirical model based upon data of a given geology shall serve as a prediction tool for the same geology from which the data were obtained.

The proposed methodology considers two main stages as described in section 3.3. The first stage consists of a maximum subsidence model. The second stage consists of a normalized subsidence distribution model.

4.1 MAXIMUM SUBSIDENCE PREDICTION

In this dissertation, all panels reached supercritical subsidence conditions, which implies that maximum potential subsidence fully develops. Researchers report that the subsidence factor, *a*, as defined in chapter 2.0 , reaches a constant value for the case of supercritical conditions, given the geology doesn't change (NCB 1975; Whittaker and Reddish 1989; Agioutantis and Karmis 2009). Peng, however, provides an inverse relationship between maximum potential subsidence factor and overburden depth based upon several Appalachian sites (Peng 1992), suggesting that the depth of the mine has a direct influence on the magnitude of subsidence. An accompanying explanation by Peng on this relationship claims that as depth increases, the area of influence of the extraction increases, producing milder subsidence and also decreased deformation indices that result along with subsidence. The relationship found in this study supports the findings by Peng.

Figure 4-1 gives the relationship between subsidence factor and overburden thickness, based on the data from Table 3-1.

The model illustrates that the ultimate absolute magnitude of maximum potential subsidence is a function of overburden thickness and extraction thickness. This relationship alone is a very useful predictive tool as far as the maximum subsidence magnitude is concerned. The two parameters it is based on are generally available.

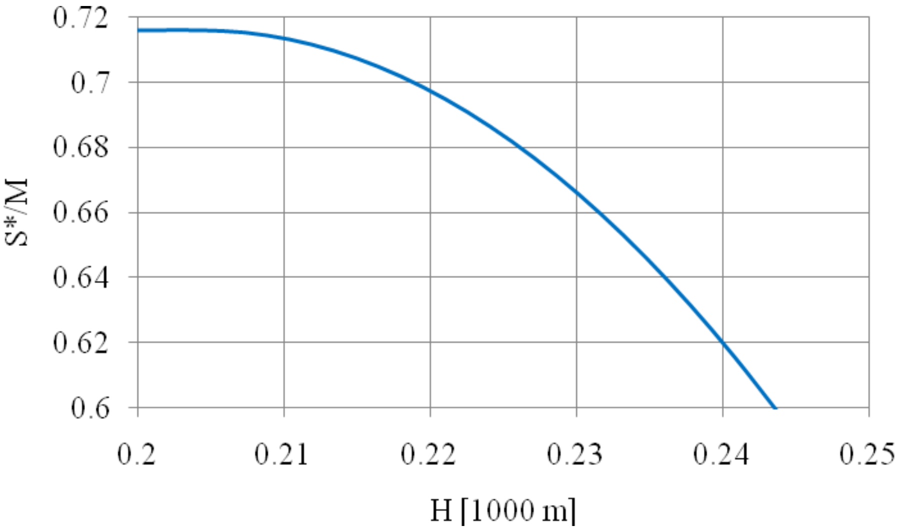

Figure 4-1 Highway maximum subsidence model in Greene County

4.2 NORMALIZED SUBSIDENCE DISTRIBUTION MODEL

The previous section described a model to obtain maximum potential subsidence. Even though it is a very simple and useful model for practical applications, it is not capable of providing information such as the distribution of subsidence near the edges, and the consequent deformation indices that are required to be quantified for proper prediction and control.

In order to achieve the final stage of subsidence trough prediction, surface distribution of normalized subsidence is required. In order to obtain a generic distribution, both the magnitude of subsidence at a point and its surface location need to be normalized.

4.2.1 Subsidence normalization

Given a distribution of absolute subsidence readings like that obtained after data transformation and illustrated in Figure 3-47 through Figure 3-58, all readings may be normalized with respect to the maximum subsidence, S^*, obtained from the maximum subsidence model described in section 4.1.

4.2.2 Lateral position normalization or edge effect

The lateral normalization or edge effect normalization is obtained by normalizing the lateral distance of every point measured from the panel edges. The parameter by which this lateral normalization is carried out is the overburden depth, H. Performing the normalization of lateral location x, z, with respect to H, is equivalent to considering the edge effect of subsidence deformation. This can be seen for example in the prediction of the location of the inflection point as a function of the ratio W/H in SDPS (Agioutantis and Karmis 2009). Beyond $W/H = 1.2$, d/H becomes constant. This suggests that normalizing the abscissas of our data with respect to the overburden depth, H, would bring all supercritical profiles together in the inflexion point. Figure 4-2 and Figure 4-3 depict the transversal and longitudinal normalized subsidence profiles, respectively.

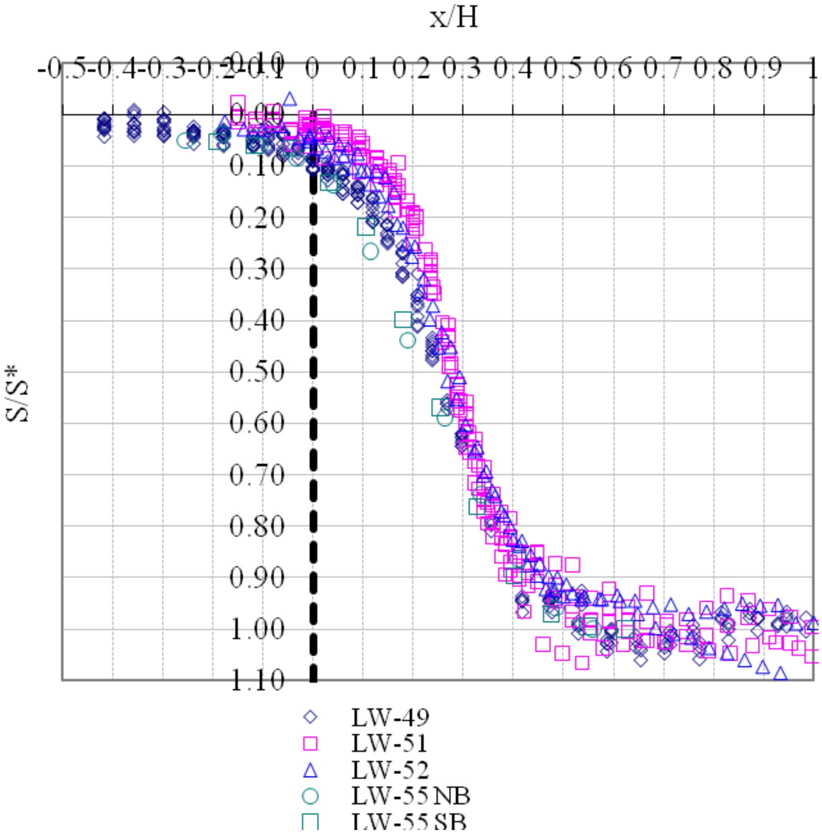

Figure 4-2 Normalized subsidence and normalized location in the transverse direction

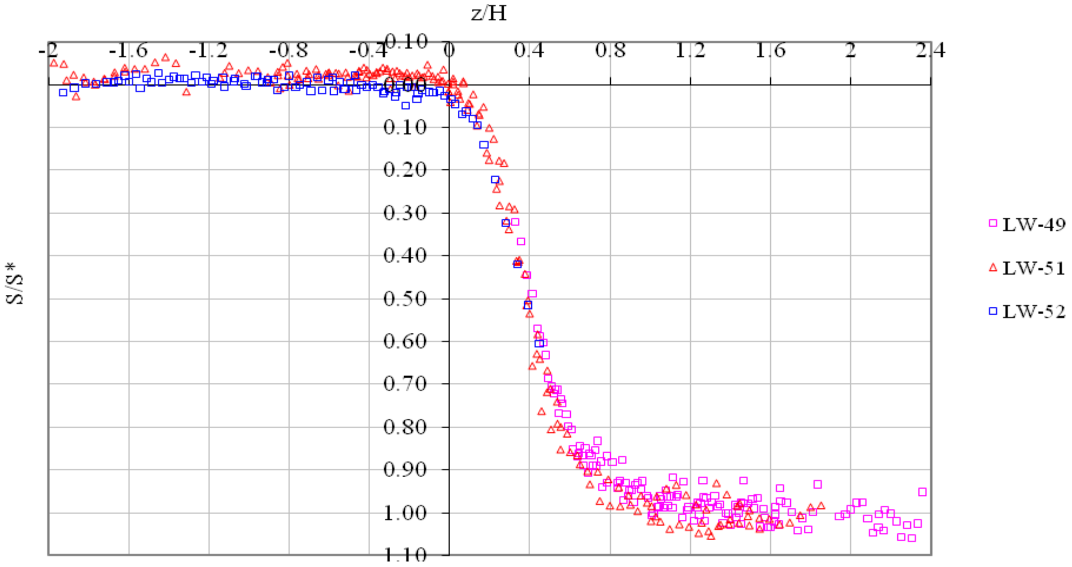

Figure 4-3 Normalized subsidence and normalized location in the longitudinal direction

4.3 FITTING A 3D MODEL

The previous section described how data can be normalized both vertically and horizontally and showed that the data available follow convenient trends when normalized. That is, narrow bounds are formed in normalized data. This leads to the next step, which is fitting a three-dimensional normalized subsidence model to the data.

In order to obtain a 3D model, a transverse 2D model and a longitudinal 2D model will be multiplied. Two-dimensional models are common in the literature. One of them has been described in chapter 2.0 (Agioutantis and Karmis 2009).

A transversal view of 3D data for all panels is shown in Figure 4-4. The view presented is from the mined area toward the mine face. Each point is at a unique distance away from the mine face, and some trends can be observed that stand for data taken on a given date along I-79. The procedure to obtain data in *x*, *z*, *S* (transversal, longitudinal, subsidence) has been explained in section 3.7. In summary, what can be visualized in this figure is the 2D-projected subsidence trough to which a 3D function can be fitted. The function, or model, will have to address the following factors:

- Panels do not have the same width.
- Some panels are symmetric in the case that no adjacent panel has been previously mined out in the immediate neighborhood (e.g. LW-49).
- Some panels exhibit asymmetry, that is, the side adjacent to a mined-out panel is more subsided than the opposite side, etc.

These features, however, are easy to deal with, as long as a good model can be found to describe the complex shape of the typical edge deformations, whether these are adjacent to mined-out or not mined-out panels. The symmetric and asymmetric trends that appear in Figure

4-4 are depicted separately for a symmetric case (LW-49 in Figure 4-5) and an asymmetric case (LW-52 in Figure 4-6). The model proposed here will be capable of predicting either case, unlike any other subsidence prediction tool developed in the past. Figure 4-7 through Figure 4-10 show data according to its use as symmetric side (without mined-out adjacent panel) or asymmetric side (with mined-out panel adjacent).

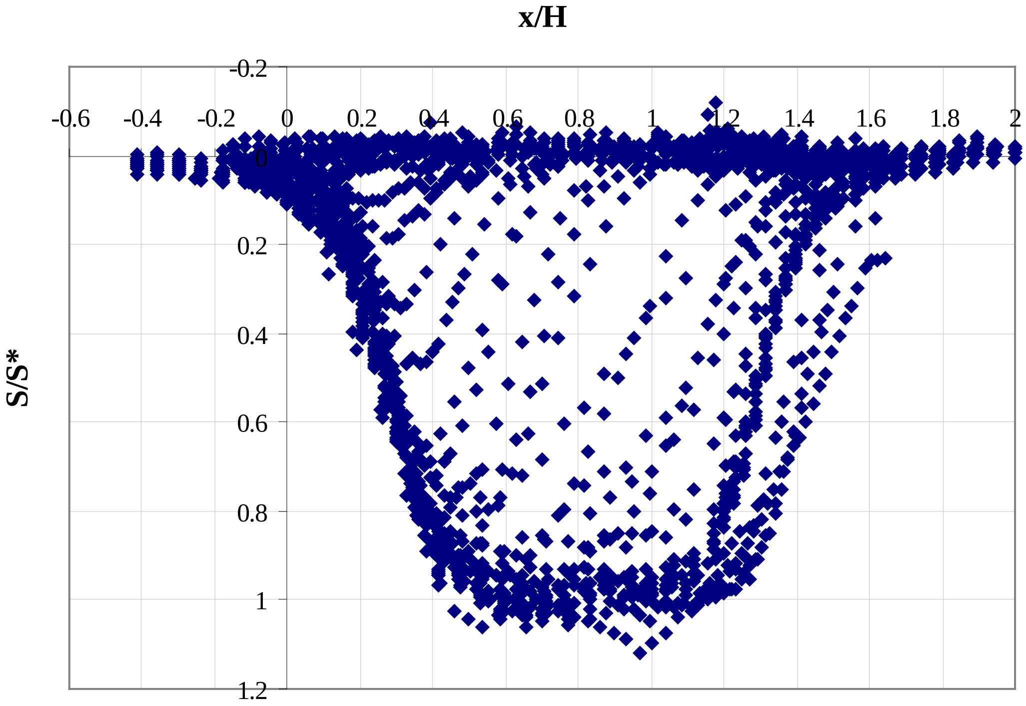

Figure 4-4 Transversal view of data from all panels

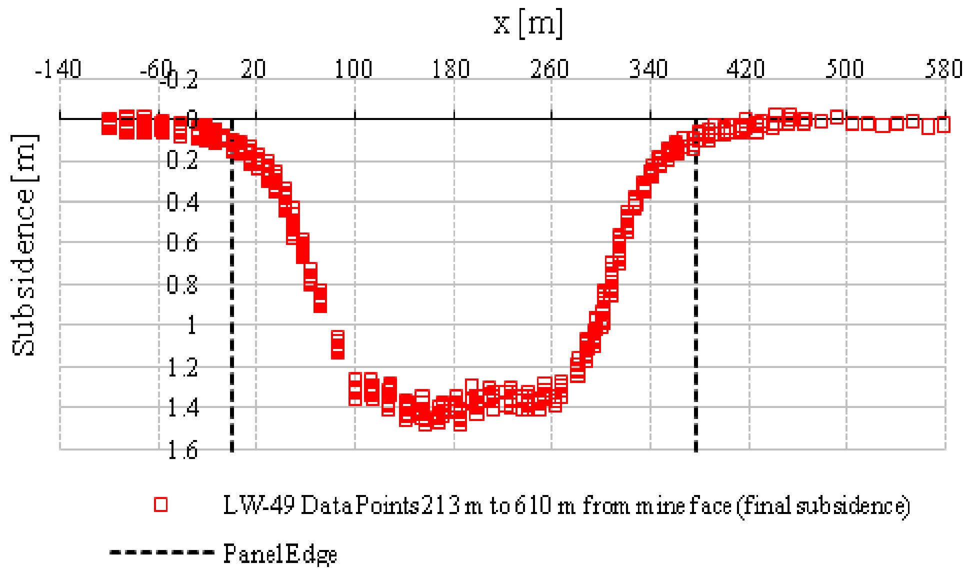

Figure 4-5 Final subsidence for symmetric case LW-49

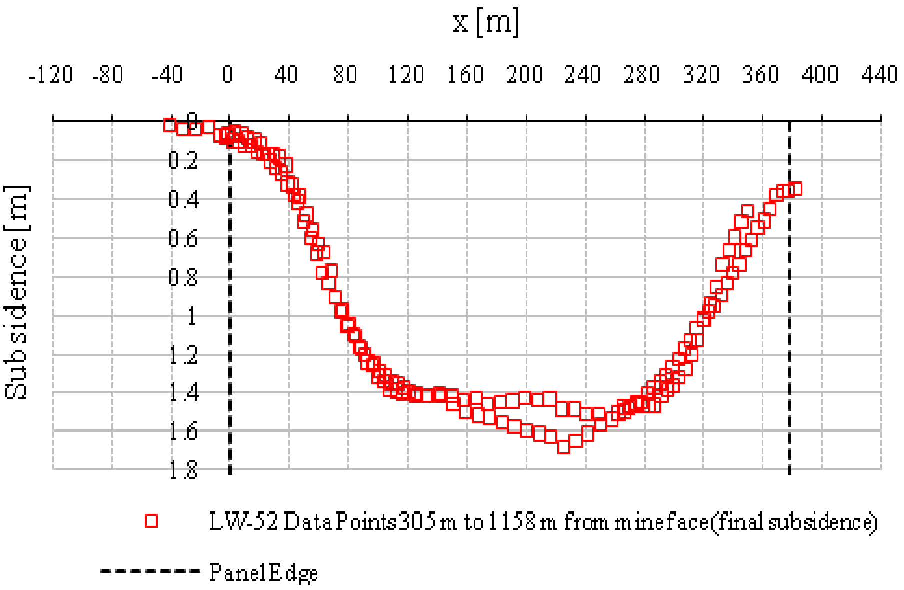

Figure 4-6 Final subsidence for asymmetric case LW-52

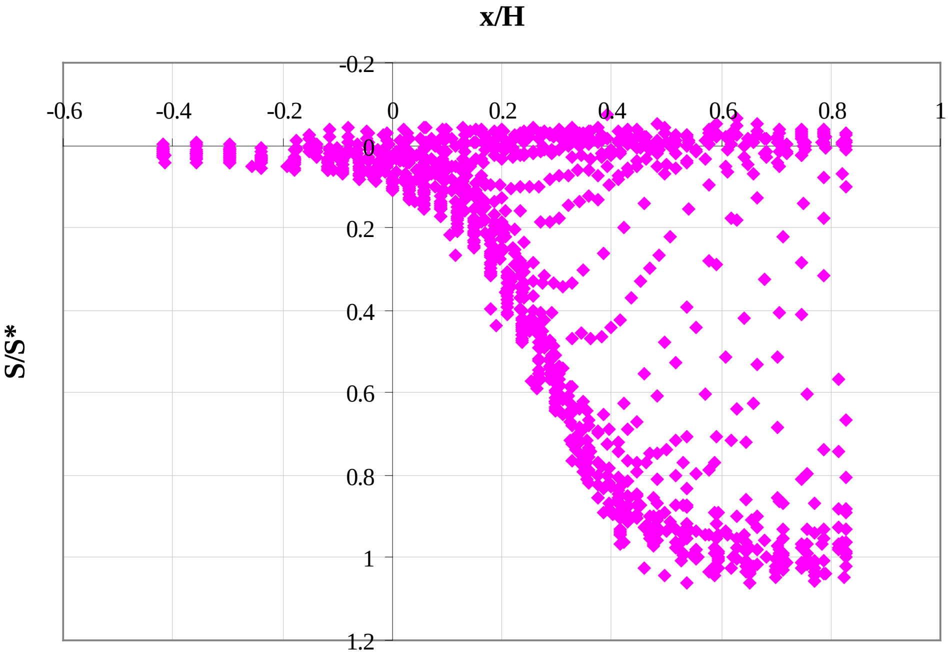

Figure 4-7 Transversal view of panels LW-49, 51, 52 data adjacent to non-mined-out panel

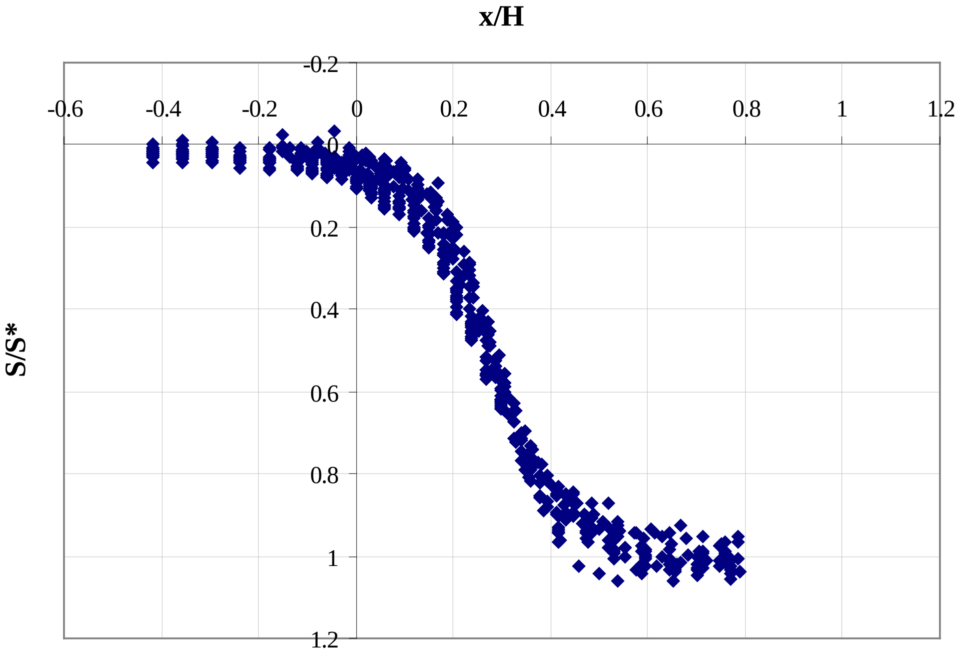

Figure 4-8 LW-49, 51, 52 transversal final deformation adjacent to non-mined-out panel

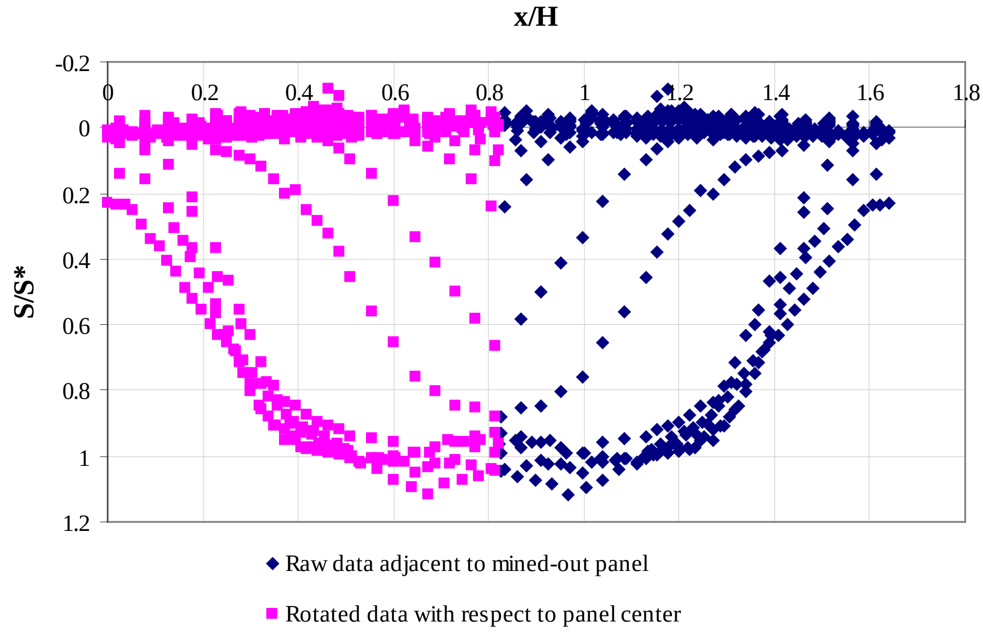

Figure 4-9 LW-51, 52 transversal raw and rotated data adjacent to mined-out panel

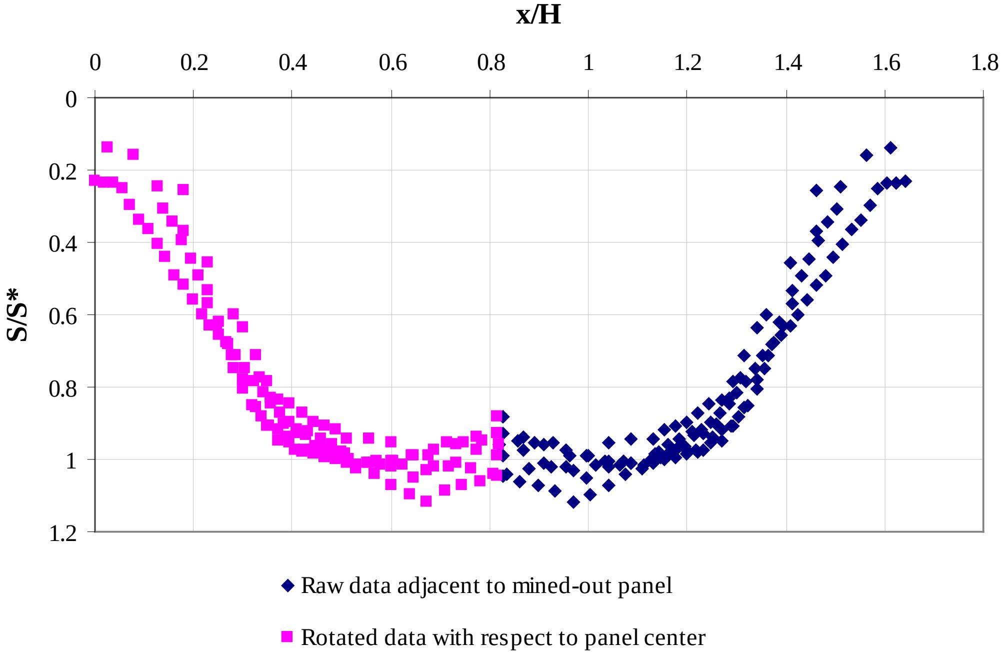

Figure 4-10 LW-51, 52 transversal final deformation data adjacent to mined-out panel

The problem of fitting data with a 3D profile function requires a non-linear regression technique. Since the data trends are clear, the search for functions to fit the data is relatively straightforward. For the non-linear regression, a Genetic Algorithm (GA), which is a robust search technique in determining the parameters of the proposed model, will be used. After specifying a profile function, an objective function, and giving a range of possible parameter values, the GA finds parameter values that provide a global minimum fit according to the objective functions.

For this dissertation, the objective is to find the parameters of the model such that the sum of squared errors between the model and data is minimum. Thus, the objective function is simply a function that defines the sum of squared errors.

Investigations have been made on four different 3-D profile models in this work. The first model has the following form:

$$\frac{S}{S*} = e^{a1\left|a2-\frac{x}{H}\right|^{a3}} e^{a4\left|a5-\frac{z}{H}\right|^{a6}} \qquad \textbf{4-1}$$

The model in 4-1 is similar to the model proposed by Chen and Peng of West Virginia University (OSMRE 1986).

$$\frac{S}{S*} = e^{-e^{-\left(a1+a2\frac{x}{H}\right)}} e^{-e^{-\left(a3+a4\frac{z}{H}\right)}} \qquad \textbf{4-2}$$

The second model (4-2) is called the Gompertz model in its 2D version (Graybill and Iyer 1994) and has not been employed in subsidence prediction before.

$$\frac{S}{S*} = 0.25\left[1-tanh\left(a1+a2\frac{x}{H}\right)\right]\left[1-tanh\left(a3+a4\frac{z}{H}\right)\right] \qquad \textbf{4-3}$$

The third model (4-3) would be the 3D version of the subsidence profile function used by SDPS (Agioutantis and Karmis 2009).

$$\frac{S}{S*}=\frac{1}{\left[1+e^{-\left(a1+a2\frac{x}{H}\right)}\right]^{a3}\left[1+e^{-\left(a4+a5\frac{z}{H}\right)}\right]^{a6}} \qquad \textbf{4-4}$$

The fourth model (4-4) is known as Richard's model (Graybill and Iyer 1994) in its 2D version, and as model 4-2, it has not been used in the past for subsidence prediction either. All these models in their 2D version are capable of dealing with profile fitting in the problem of subsidence. Usually the 2D problem involves estimation of maximum or final subsidence, for which a supercritical final deformed profile is fit usually by taking the transversal coordinate as the horizontal distance. However, the 3D problem that arises from the data depicted in Figure 4-4 through Figure 4-10 imposes the challenge of dealing with both final deformations (large and far from mine face) and dynamic deformations (small and close to mine face) through a single 3D regression model. Runs of the GA algorithm for everyone and each of the above four models show that two of the models, i.e. models 1 and 4, each having 6 model parameters (namely models equation 4-1 and equation 4-4) best fit the data. This is not surprising since dealing with the 3D nature of the data requires a level of detail that the 6 parameter models are much more capable of accounting for than the 4-parameter models. Table 4-1 and Table 4-2 contain the output of parameters for the various regression models, together with the objective function value and standard deviation. Trial function number 4 (4-4) proved to best fit the data.

Table 4-1. Genetic algorithm output for side without adjacent panel

Trial function	a_1	a_2	a_3	a_4	a_5	a_6	Sum of squared error	n	p	Standard Deviation
1	0.00	1.93	16.04	0.00	2.42	9.67	10.2	1264	6	0.090
2	-2.72	2.57	-0.35	-0.19			87.2	1264	4	0.263
3	1.32	-5.58	1.94	-2.81			111.3	1264	4	0.297
4	-2.79	11.60	1.24	-1.94	5.99	1.23	8.5	1264	6	0.082

Table 4-2. Genetic algorithm output for side with adjacent panel

Trial function	a_1	a_2	a_3	a_4	a_5	a_6	Sum of squared error	n	p	Standard Deviation
1	0.00	2.06	13.23	0.00	2.14	10.87	0.89	628	6	0.038
4	-1.83	10.34	1.11	-1.45	6.73	2.23	0.73	628	6	0.034

When the asymmetrical model is used, however, it is still desired that the two model halves match along a central line smoothly. Therefore, the parameters a_4, a_5, a_6 may be set equal to those of the symmetric model (longitudinal, z, parameters), leaving only the transversal parameters a_1, a_2, a_3 as variables. Setting the former constant and equal to -1.94, 5.99, and 1.23, and re-running the genetic algorithm, the results in Table 4-3 are obtained, which are still very good results.

Table 4-3. Genetic algorithm output for side with adjacent panel Trial function 4

Trial function	a_1	a_2	a_3	a_4	a_5	a_6	Sum of squared error	n	p	Std. Dev.
4	-2.77	12	0.73	-1.94	5.99	1.23	0.92	628	6	0.038

4.4 SPATIAL DISTRIBUTION OF SUBSIDENCE

The previous sections of this chapter described the way empirical relationships can serve the purpose of three-dimensional subsidence prediction by using the maximum subsidence model and the non-linear regression proposed for normalized data.

The first stage, which is concerned with the estimation of maximum potential subsidence, is achieved using the maximum subsidence model and obtaining maximum subsidence, *S**, as a function of extraction thickness, *M*, and overburden thickness, *H*.

The second stage is to use the non-linear model, by plugging in the overburden thickness, *H*, and the maximum subsidence, *S**, to obtain the subsidence trough. In step-wise form, spatial distribution of subsidence is obtained following the two steps:

1. *S*/M* is read as a function of *H*. *S** is thus obtained by multiplying *S*/M* by *M*.
2. The non-linear model (e.g. without mined adjacent panel) is evaluated by plugging in *H* and *S**:

$$\frac{S}{S*} = \frac{1}{\left[1+e^{-\left(-2.79+11.60\frac{x}{H}\right)}\right]^{1.24}\left[1+e^{-\left(-1.94+5.99\frac{z}{H}\right)}\right]^{1.23}} \qquad \textbf{4-5}$$

An example of the use of this model is illustrated by its application on panel LW-51 and depicted in Figure 4-11 through Figure 4-22.

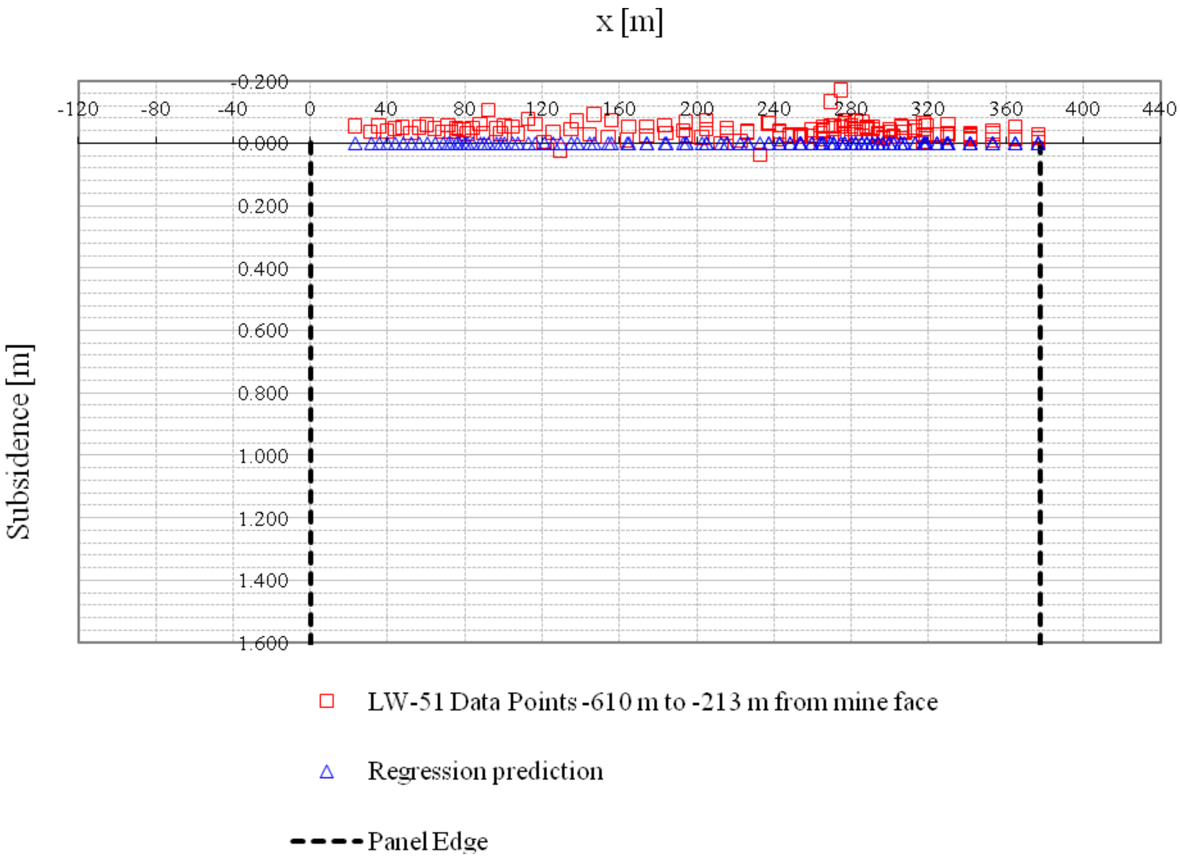

Figure 4-11 LW-51 subsidence prediction between -610 m and -213 m from mine face

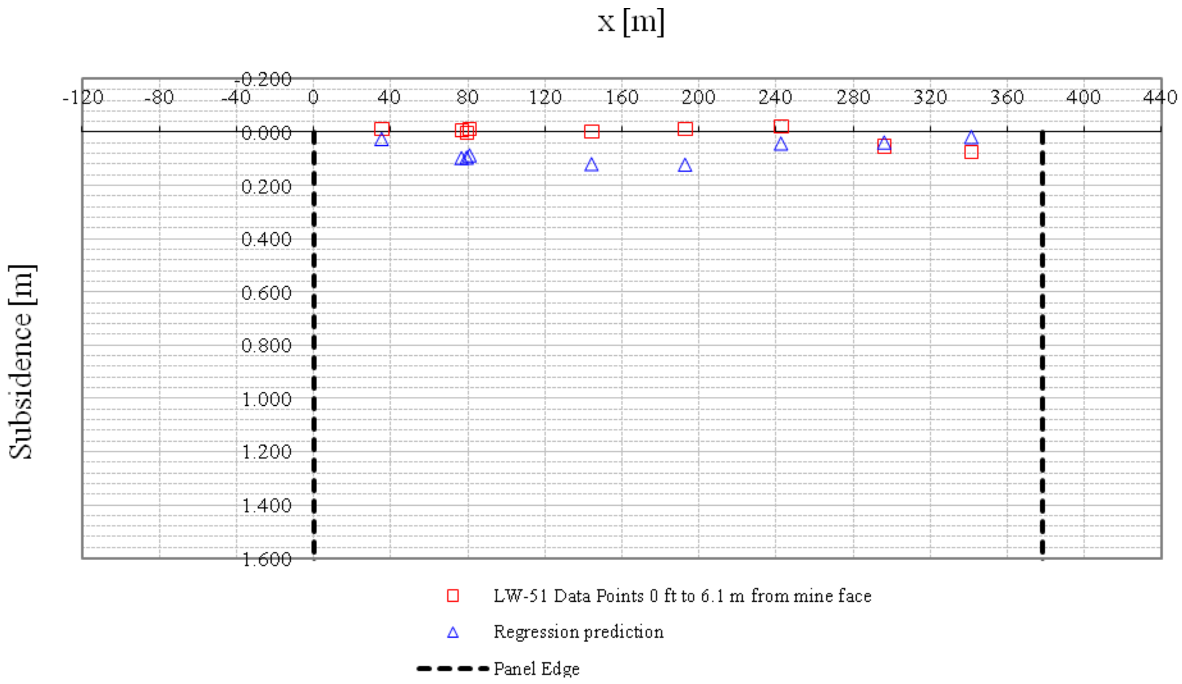

Figure 4-12 LW-51 subsidence prediction between 0 m and 6.1 m from mine face

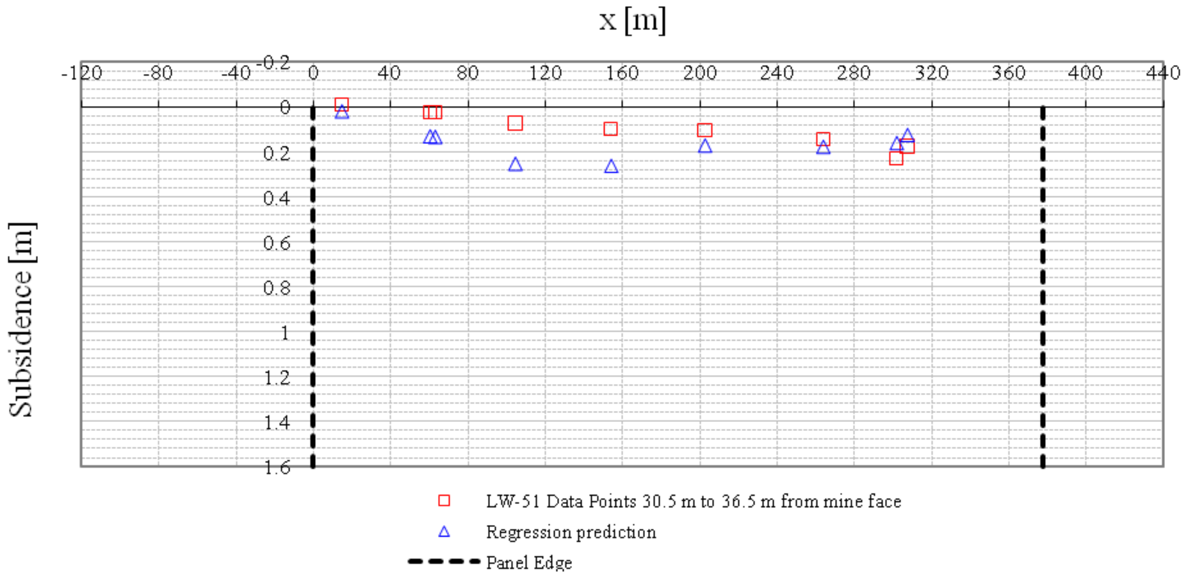

Figure 4-13 LW-51 subsidence prediction between 30.5 m and 36.5 m from mine face

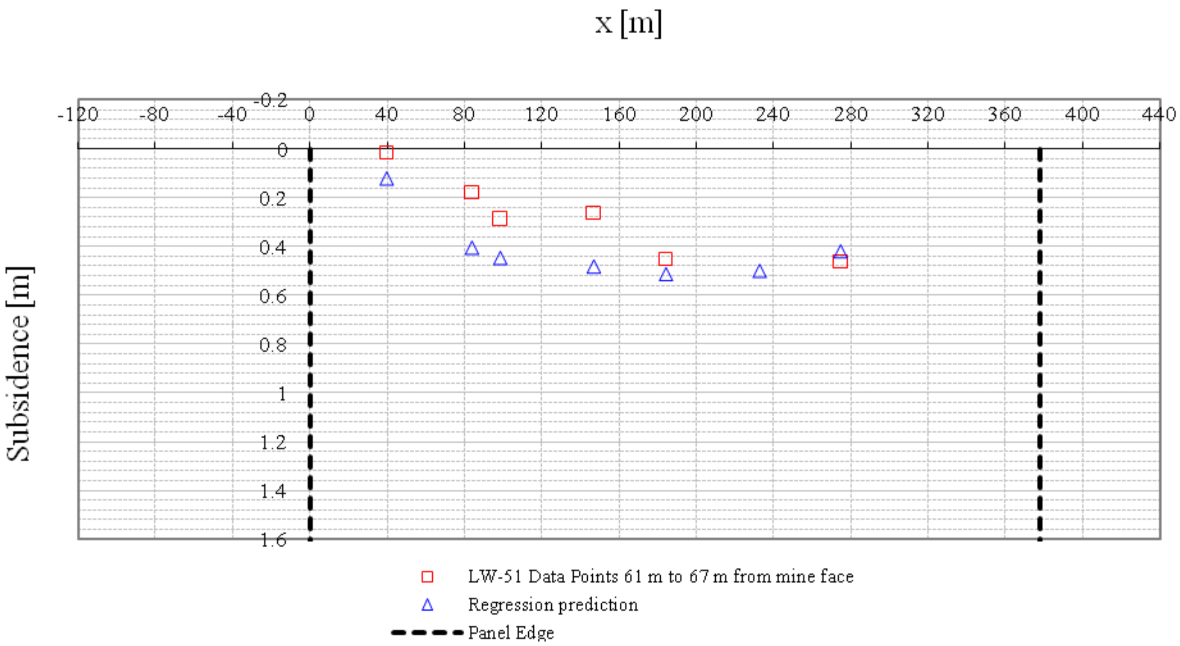

Figure 4-14 LW-51 subsidence prediction between 61 m and 67 m from mine face

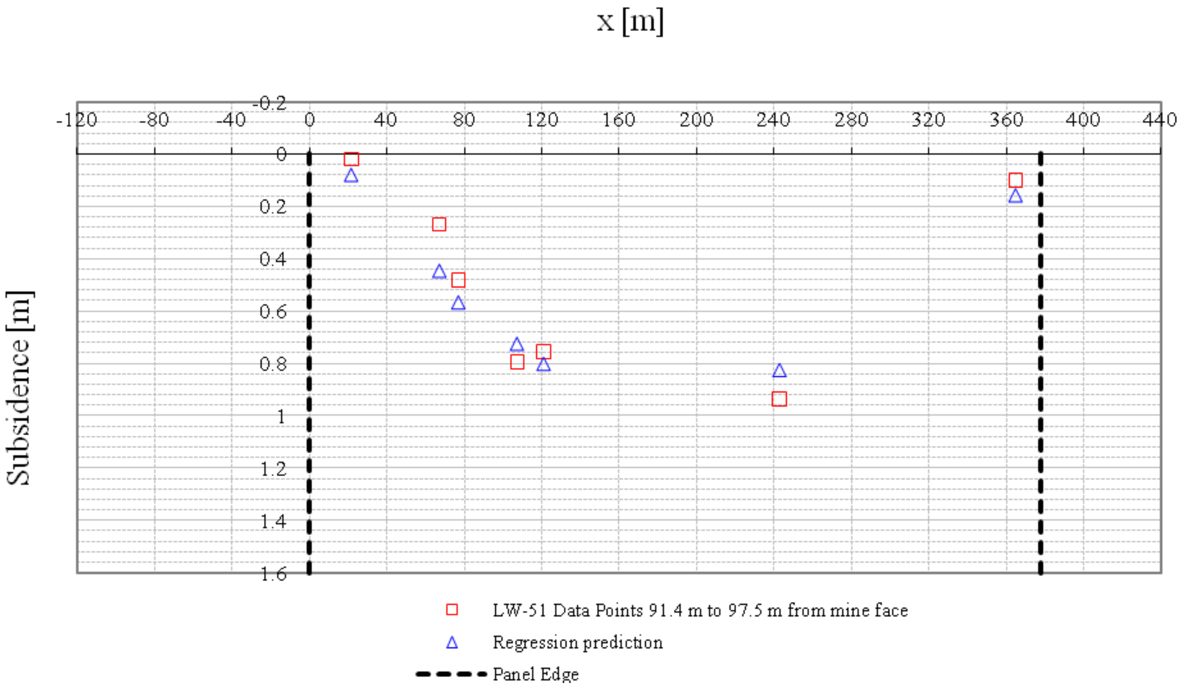

Figure 4-15 LW-51 subsidence prediction between 91.4 m and 97.5 m from mine face

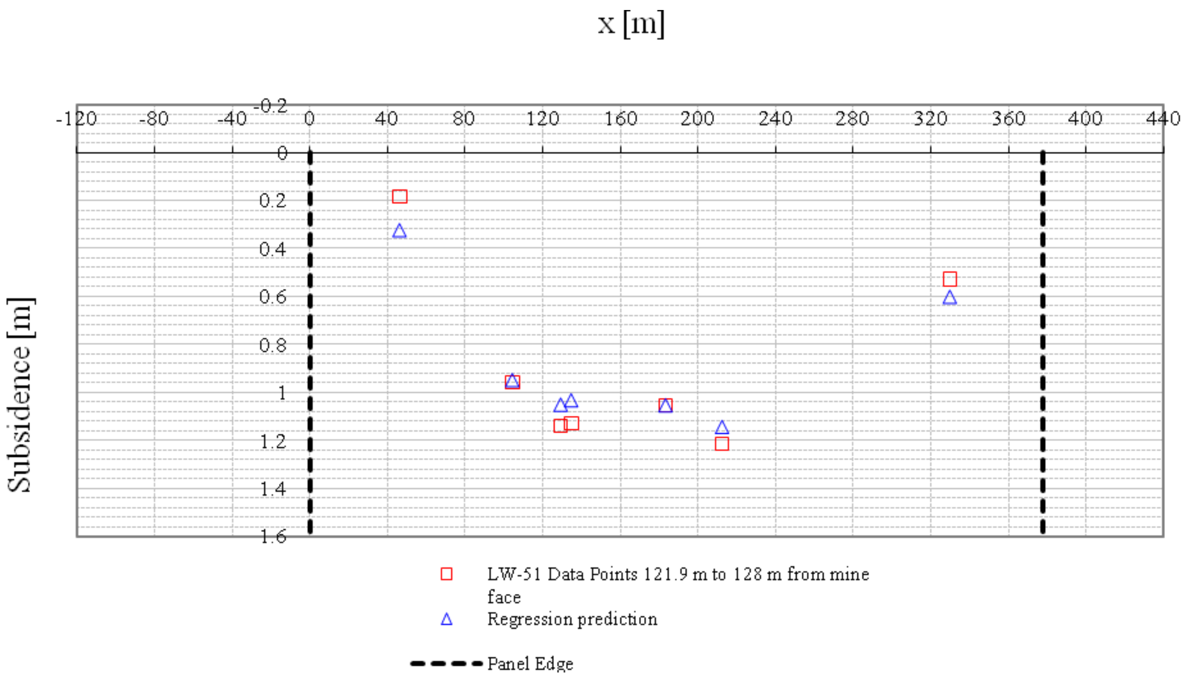

Figure 4-16 LW-51 subsidence prediction between 121.9 m and 128 m from mine face

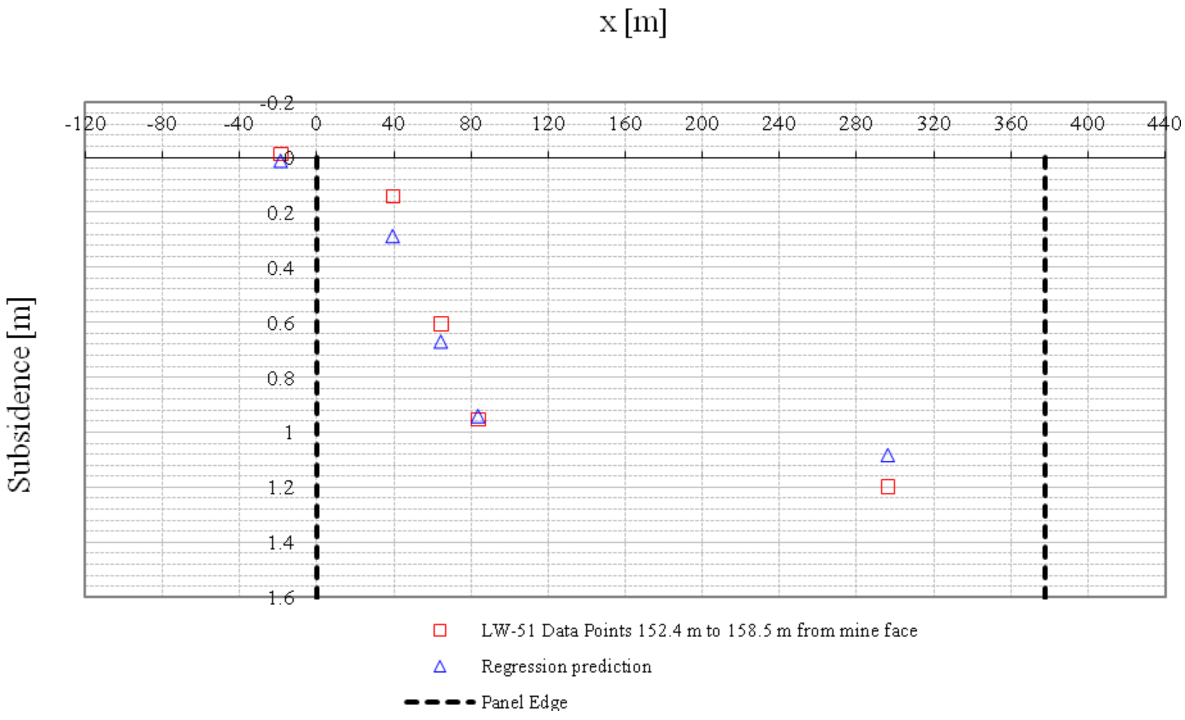

Figure 4-17 LW-51 subsidence prediction between 152.4 m and 158.5 m from mine face

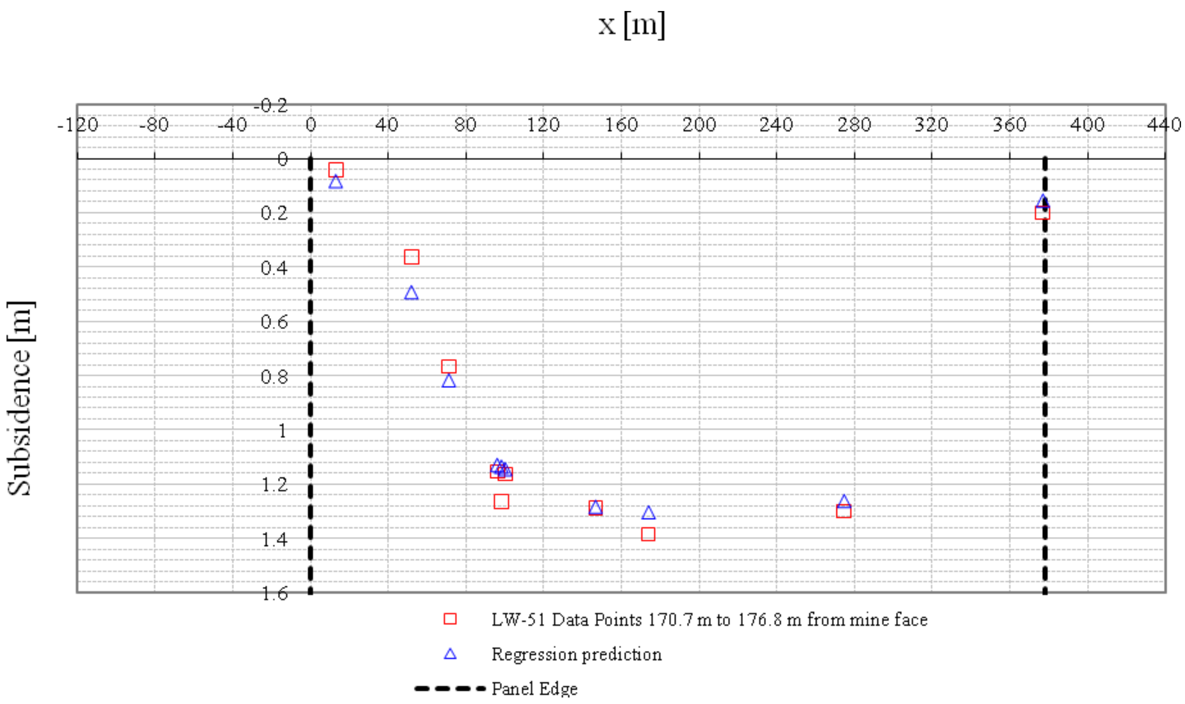

Figure 4-18 LW-51 subsidence prediction between 170.7 m and 176.8 m from mine face

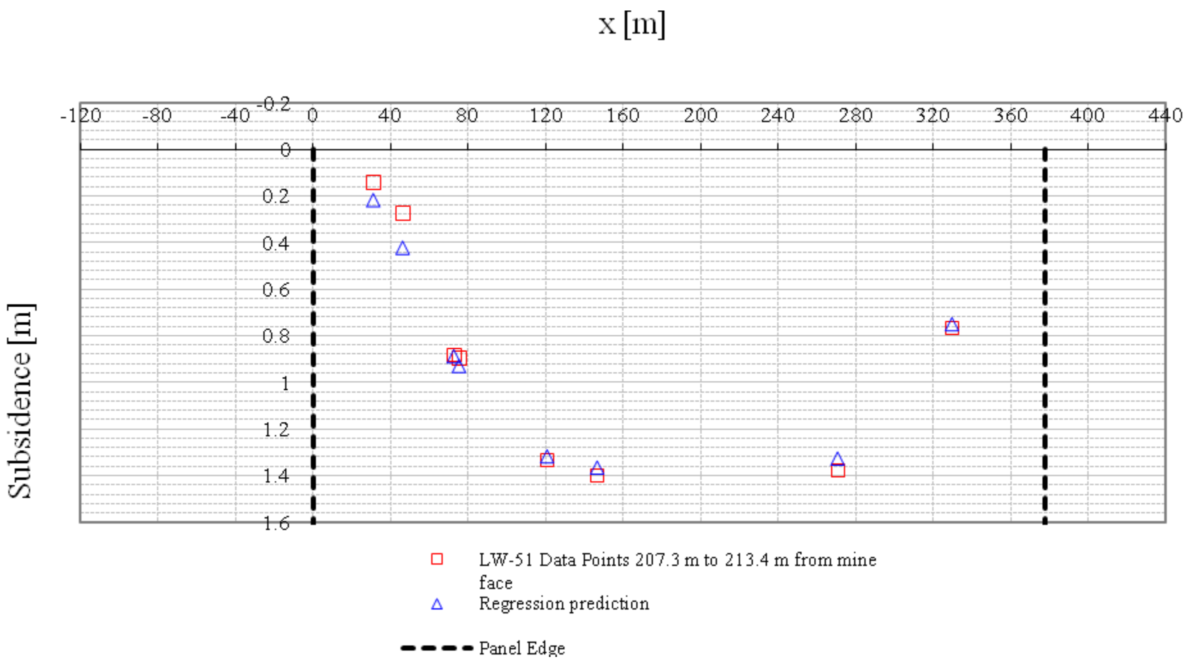

Figure 4-19 LW-51 subsidence prediction between 207.3 m and 213.4 m from mine face

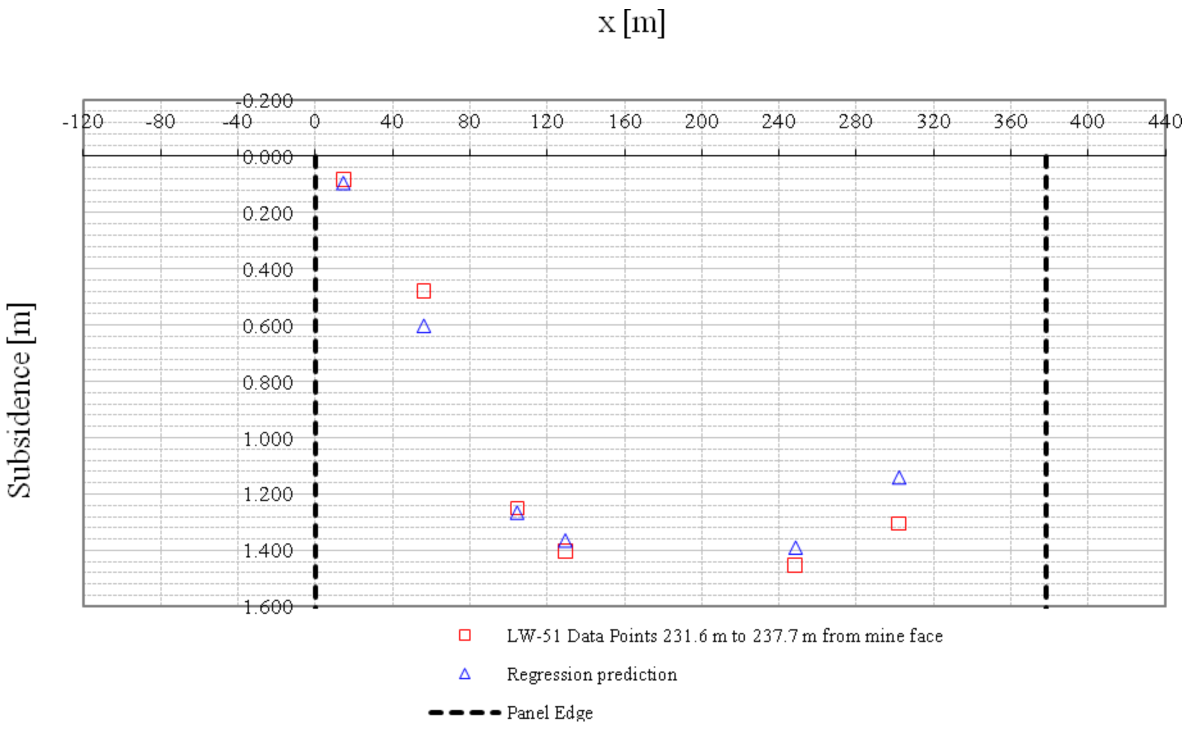

Figure 4-20 LW-51 subsidence prediction between 231.6 m and 237.7 m from mine face

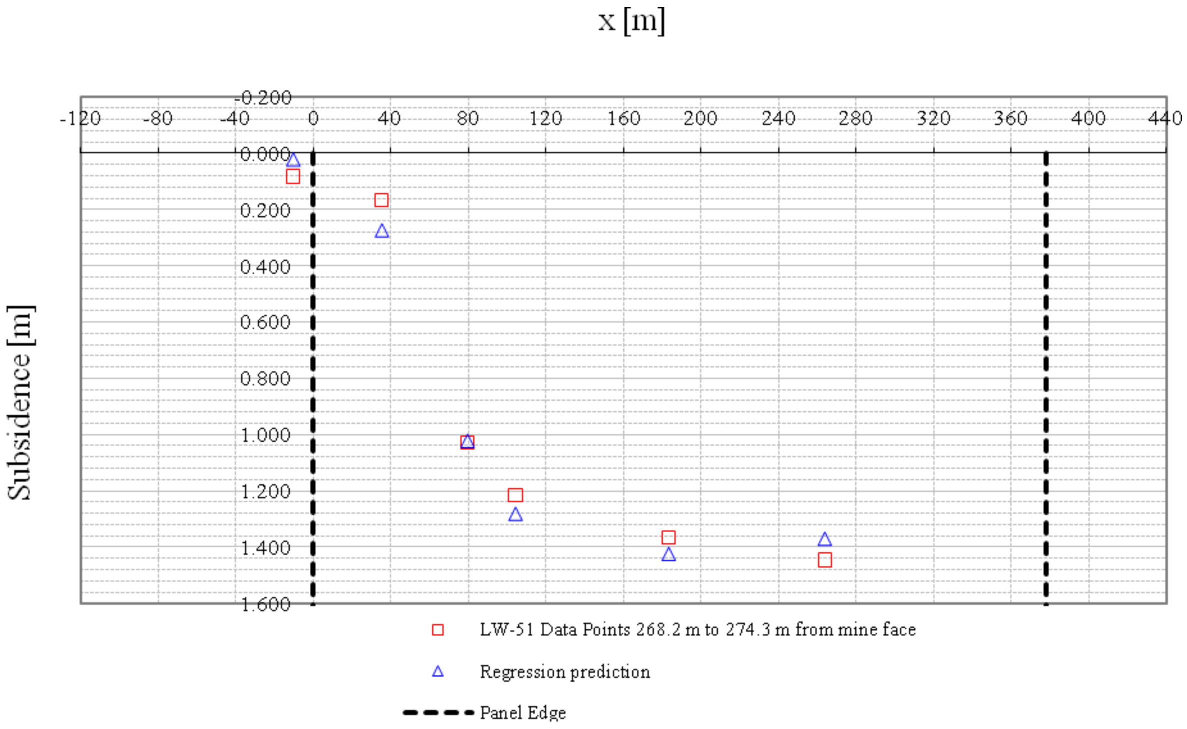

Figure 4-21 LW-51 subsidence prediction between 268.2 m and 274.3 m from mine face

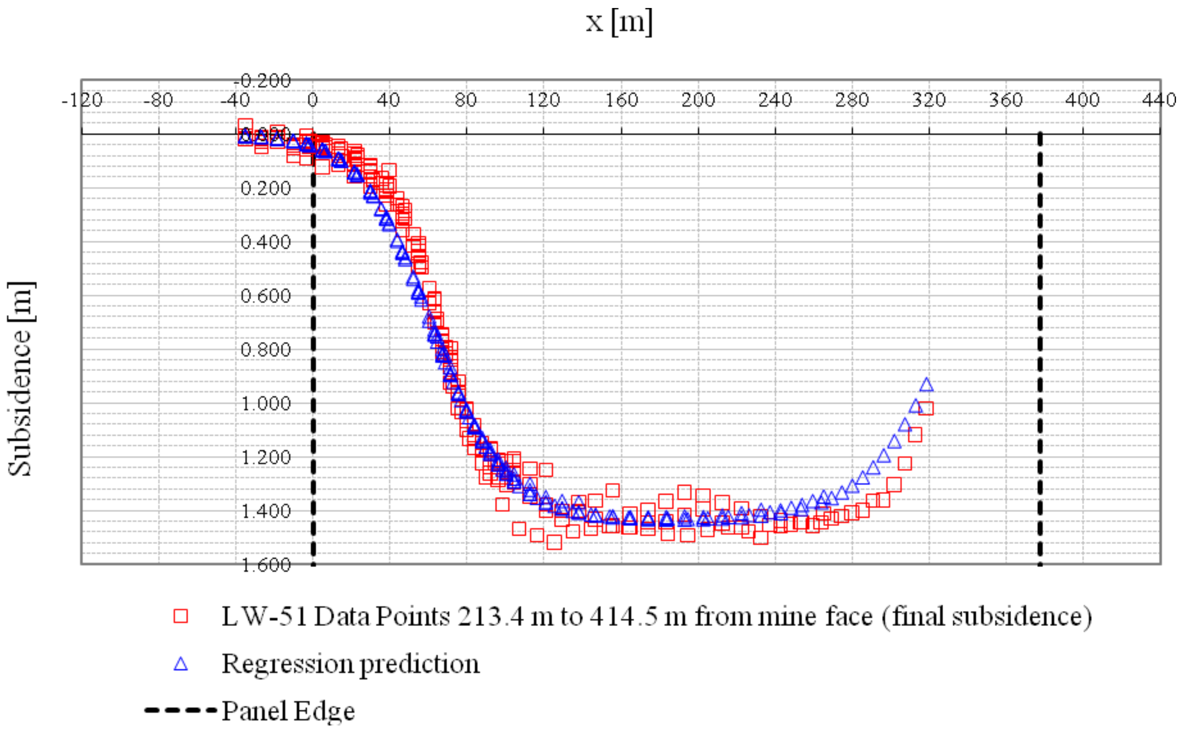

Figure 4-22 LW-51 subsidence prediction between 213.4 m and 414.5 m from mine face

4.5 TEMPORAL DISTRIBUTION OF SUBSIDENCE

One apparent feature of the way the trough is obtained is that the trough front, as it is described, experiences the dynamic effect of subsidence. In other words, if the non-linear regression that describes the trough is evaluated at the panel center and a central longitudinal profile is obtained, that longitudinal profile is nothing but the dynamic subsidence profile. Provided the geology is the same, the shape of the dynamic subsidence profile is influenced by the rate of advance of the mine face and it can be gentle for high rates of advance or sharp for slow rates (Kratzsch 1983; Jarosz, Karmis et al. 1990; Kratzsch 2008; Agioutantis and Karmis 2009).

The data upon which the 3D model is based comes from three panels, LW-49, LW-51, and LW-52, which experienced an average constant rate of advance of roughly 17 m/day. As a result, the non-linear regression here obtained represents the magnitude of or close magnitudes to that rate of advance. The difference between the dynamic profile shape and the permanent deformation shapes on the sides of the panel, or static profiles as they are often called, is clear if Figure 4-2 and Figure 4-3 are compared. One way to deal with intermediate values of rate of advance between 0 and 17 m/day would be to consider profiles interpolated within these two limits. For rates of advance higher than 17 m/day, the prediction could be less reliable, although conclusions on this may not be drawn due to a lack of data.

In temporal subsidence prediction, a useful task is to predict deformation for a given point in terms of a time scale that can be set to zero for the position of the mine face. The basic assumption for both spatial and temporal subsidence prediction is that the rate of mine face advance is constant, and in this case equal to 17 m/day. Therefore, the longitudinal coordinate, *z*, can be expressed as a function of the rate of advance, *v*, as $z = vt$.

$$\frac{S}{S*} = \frac{1}{\left[1+e^{-\left(-2.79+11.60\frac{x}{H}\right)}\right]^{1.24}\left[1+e^{-\left(-1.94+101.83\frac{t}{H}\right)}\right]^{1.23}} \qquad \textbf{4-6}$$

Since *v* = 17 m/day, the spatial coordinate *z* is replaced by 17*t*, and the model in 4-6 is obtained. Since *t* = 0 corresponds to the mine face position, *t* < 0 corresponds to points ahead of the mine face, whereas *t* > 0 corresponds to points behind the mine face. For example, if there are concerns about a point *P* that is estimated to be reached by the mine face in 4 days, its deformation can be predicted for the days before and after the mine face passes by plugging in *t* = -3, -2, -1, 0, 1, 2, 3. It is important to note that the model 4-6 has the spatial coordinate *x* as one of its independent variables. This is useful since the point *P* of concern could be located anywhere within the width of the panel, even outside the edges. Also, complete transverse profiles could be predicted for different times.

Another way the temporal subsidence may be looked at is in the prediction of long-term subsidence, for which researchers have proposed decay functions (Whittaker and Reddish 1989). This work is not concerned with this type of prediction since the available data was obtained soon after the mine face passed the surveyed stations.

4.6 SUBSIDENCE DEFORMATION INDICES

Definitions of subsidence deformation indices were introduced in section 1.3 and illustrated in Figure 1-3. Information indices are important for damage prediction. If the subsidence profile or trough is known, these can be easily obtained.

From the general model, left half:

$$S = \frac{S*}{\left[1+e^{-\left(a_1+a_2\frac{x}{H}\right)}\right]^{a_3}\left[1+e^{-\left(a_4+a_5\frac{z}{H}\right)}\right]^{a_6}} \tag{4-7}$$

the following parts may be defined:

$$C_X = \frac{S*}{\left[1+e^{-\left(a_1+a_2\frac{x}{H}\right)}\right]^{a_3}} \tag{4-8}$$

$$C_Z = \frac{S*}{\left[1+e^{-\left(a_4+a_5\frac{z}{H}\right)}\right]^{a_6}} \tag{4-9}$$

$$S_X = \frac{1}{\left[1+e^{-\left(a_1+a_2\frac{x}{H}\right)}\right]^{a_3}} \tag{4-10}$$

$$S_Z = \frac{1}{\left[1+e^{-\left(a_4+a_5\frac{z}{H}\right)}\right]^{a_6}} \tag{4-11}$$

The first and second derivatives of 4-10 and 4-11 are required for the deformation indices. The expressions for the case of the transversal direction, *x*, left half, are:

$$S'_X = \frac{a_2 a_3}{H}\frac{e^{-\left(a_1+a_2\frac{x}{H}\right)}}{\left[1+e^{-\left(a_1+a_2\frac{x}{H}\right)}\right]^{a_3+1}} \tag{4-12}$$

$$\begin{aligned} S''_X = {} & -\frac{a_2{}^2 a_3}{H^2} e^{-\left(a_1+a_2\frac{x}{H}\right)}\left[1+e^{-\left(a_1+a_2\frac{x}{H}\right)}\right]^{-a_3-1} + \\ & \frac{(a_3+1)a_2{}^2 a_3}{H^2} e^{-2\left(a_1+a_2\frac{x}{H}\right)}\left[1+e^{-\left(a_1+a_2\frac{x}{H}\right)}\right]^{-a_3-2} \end{aligned} \tag{4-13}$$

For the right half:

$$S'_X = -\frac{a_2 a_3}{H}\frac{e^{-\left[a_1+a_2\frac{(W-x)}{H}\right]}}{\left[1+e^{-\left[a_1+a_2\frac{(W-x)}{H}\right]}\right]^{a_3+1}} \tag{4-14}$$

$$\begin{aligned} S''_X = {} & -\frac{a_2{}^2 a_3}{H^2} e^{-\left[a_1+a_2\frac{(W-x)}{H}\right]}\left[1+e^{-\left[a_1+a_2\frac{(W-x)}{H}\right]}\right]^{-a_3-1} + \\ & \frac{(a_3+1)a_2{}^2 a_3}{H^2} e^{-2\left[a_1+a_2\frac{(W-x)}{H}\right]}\left[1+e^{-\left[a_1+a_2\frac{(W-x)}{H}\right]}\right]^{-a_3-2} \end{aligned} \tag{4-15}$$

The same expressions may be obtained for the longitudinal direction, *z*. Based on these, the deformation indices are defined as follows:

$$Slope_X = \frac{\partial S}{\partial x} = C_Z S'_X \qquad \textbf{4-16}$$

$$Curvature_X = -\frac{\partial^2 S}{\partial x^2} = -C_Z S''_X \qquad \textbf{4-17}$$

As discussed in subsection 1.3.3, horizontal displacements are correlated to slope through a constant. The SDPS developers (Agioutantis and Karmis 2009) use a factor B_f defined as $B_f = B\frac{H}{tan\beta}$, where *B* is a fitting constant and $\frac{H}{tan\beta}$ is the radius of influence, where *H* is the overburden thickness and β is the angle of influence. The SDPS uses *B* = 0.35 for Northern Appalachia. From horizontal displacement figures, given by Figure 3-16, Figure 3-23, Figure 3-29, and Figure 3-35, however, and taking the resulting subsidence trough into account, a value for this constant *B* is set here equal to 0.15. Figure 4-23 through Figure 4-31 give a graphical example of the application of the new model in the symmetric case of LW-49.

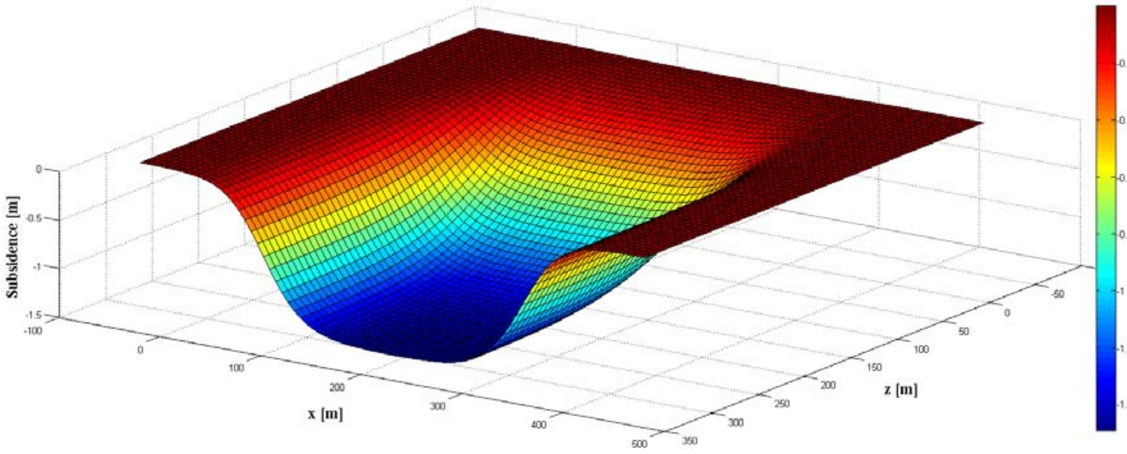

Figure 4-23 Subsidence trough of symmetric case LW-49 obtained with new model

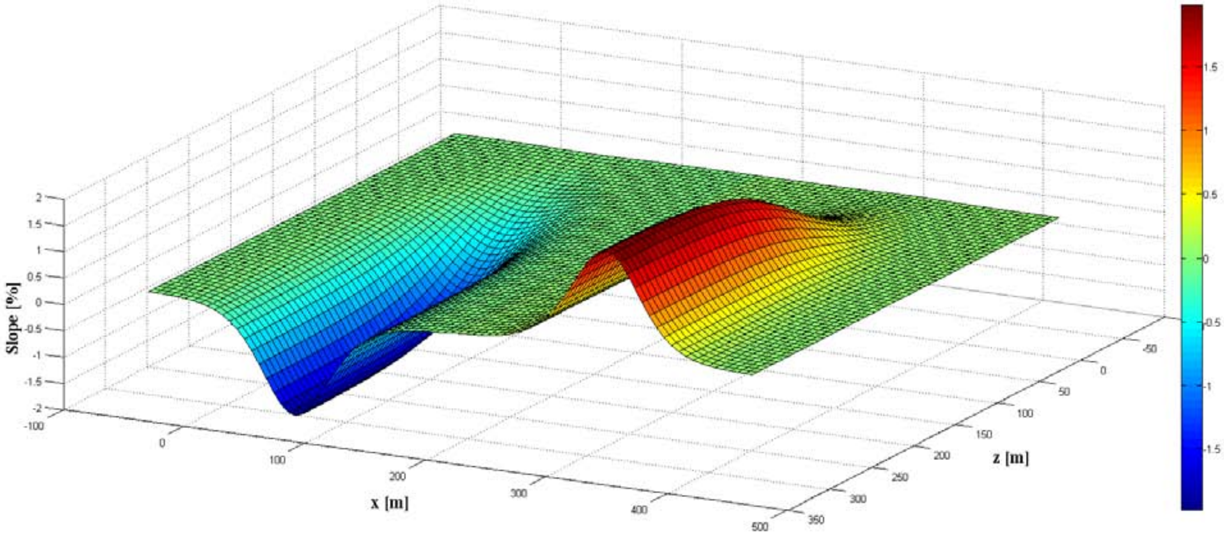

Figure 4-24 Distribution of transversal (*x*) slope for symmetric case LW-49

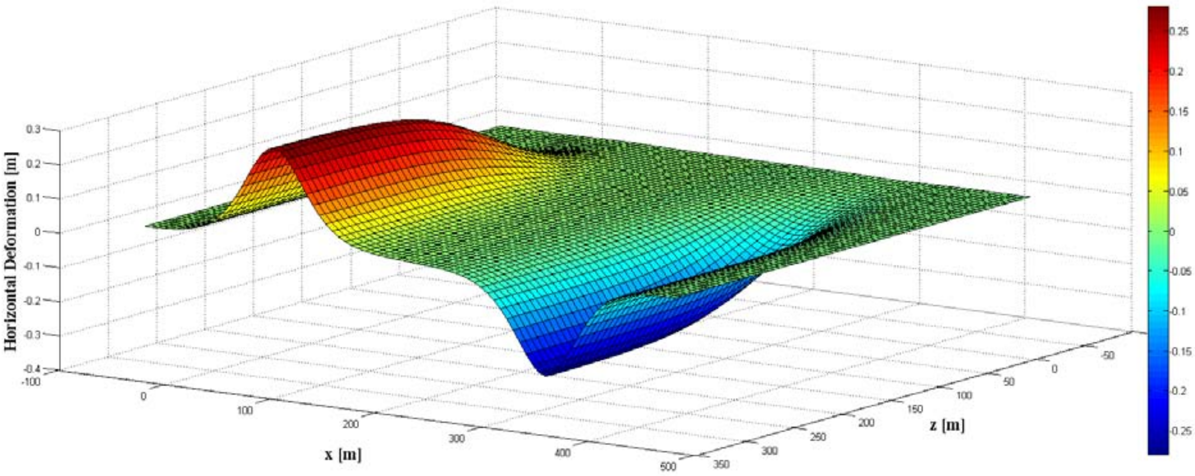

Figure 4-25 Distribution of transversal (*x*) horizontal deformation for symmetric case LW-49

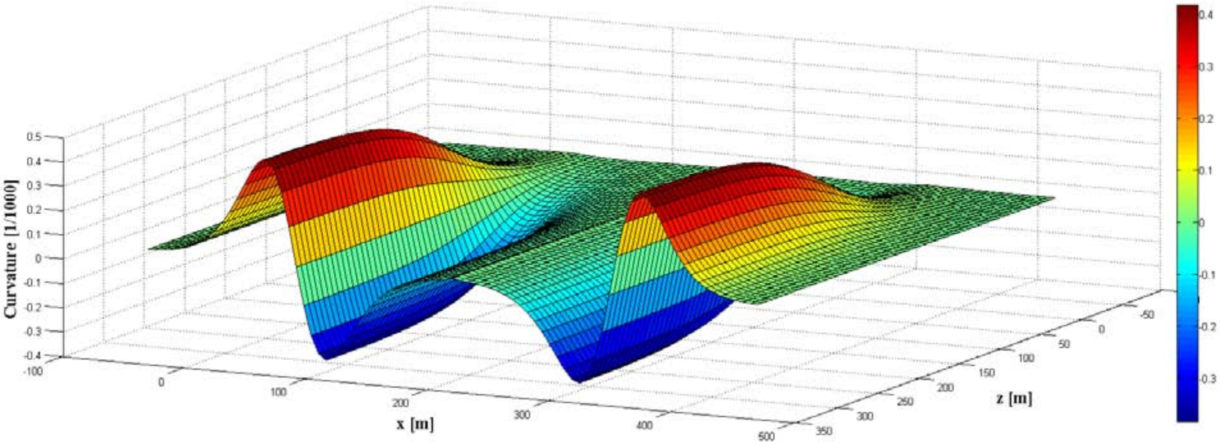

Figure 4-26 Distribution of transversal (*x*) curvature for symmetric case LW-49

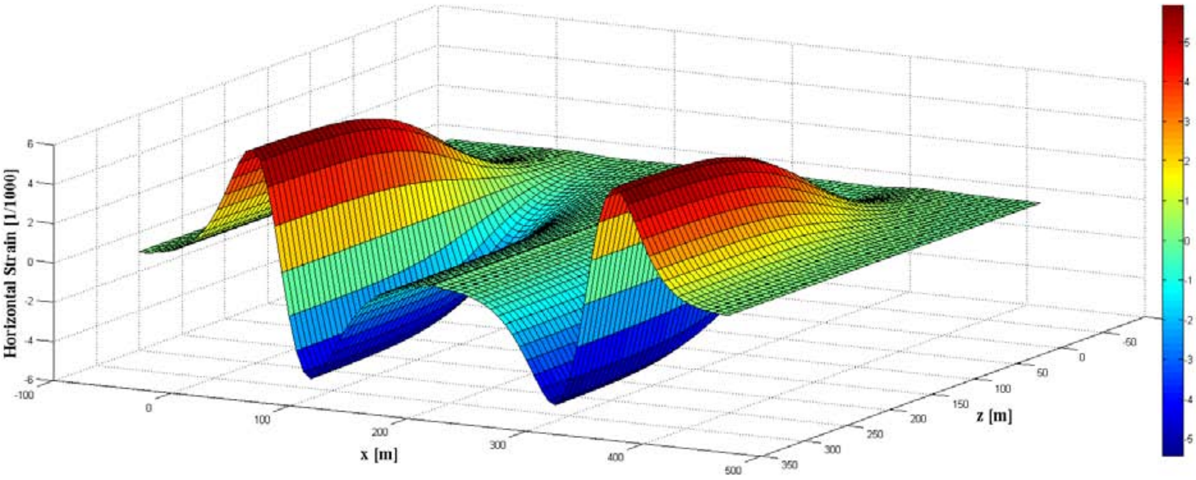

Figure 4-27 Distribution of transversal (*x*) horizontal strain for symmetric case LW-49

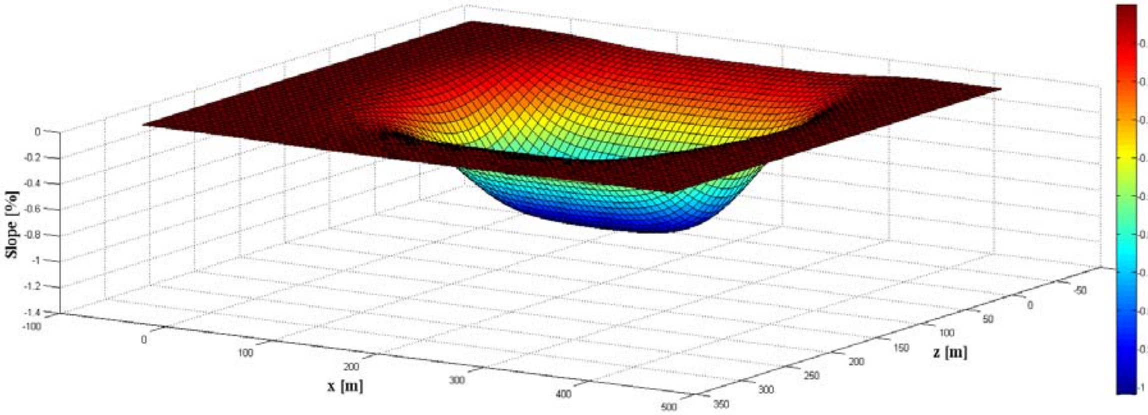

Figure 4-28 Distribution of longitudinal (*z*) slope for symmetric case LW-49

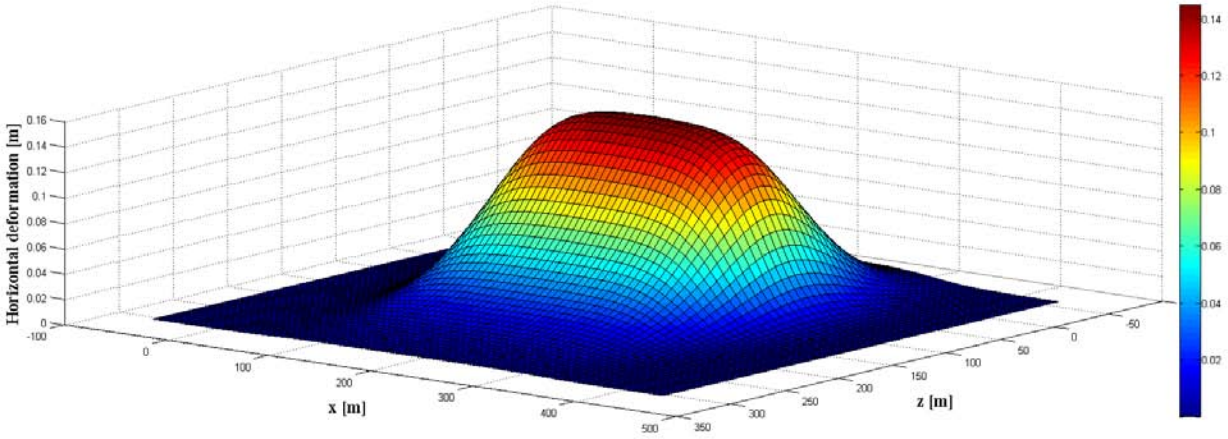

Figure 4-29 Distribution of longitudinal (*z*) hor. deformation for symmetric case LW-49

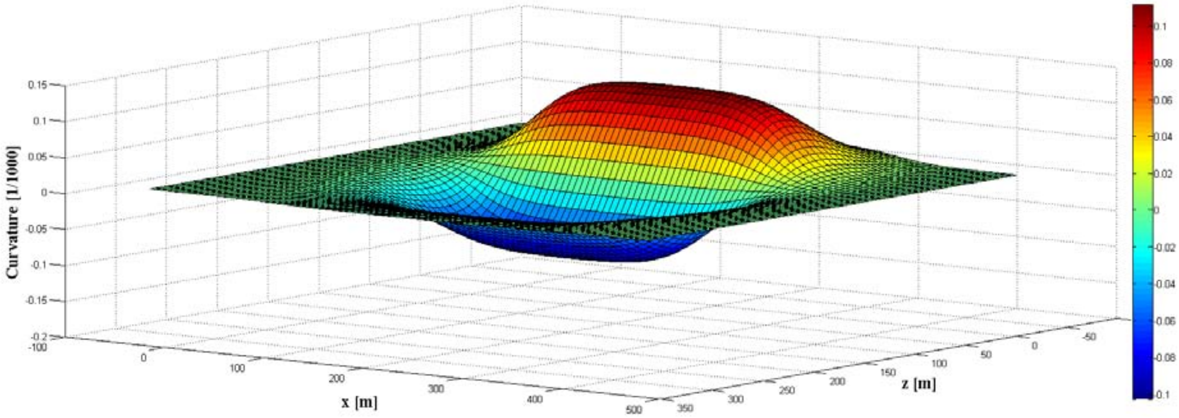

Figure 4-30 Distribution of longitudinal (*z*) curvature for symmetric case LW-49

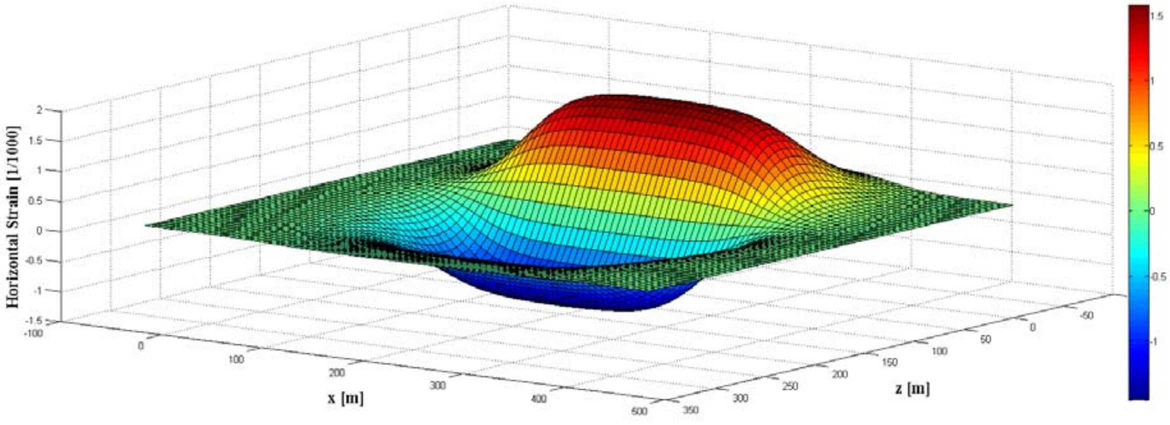

Figure 4-31 Distribution of longitudinal (*z*) horizontal strain for symmetric case LW-49

4.7 COMMENTS ON HORIZONTAL DISPLACEMENTS

A three-dimensional trough subsidence may be predicted as described in previous sections of this chapter. Section 4.6 introduced the traditional way horizontal displacements are dealt with. A linear correlation to slope yields horizontal displacement, an assumption so generalized that seems to have worked well for relatively flat terrain. Some researchers, however, have brought up the fact that this assumption is less reliable when hilly terrain is dealt with (Luo and Peng 1999), and have proposed methodologies to account for the inclination of terrain and its impact both on subsidence and horizontal displacements. Luo and Peng, for example, consider the proportionality factor G, which is the reciprocal of the safety factor against sliding of an infinite slope (Luo and Peng 1999). Their paper shows an example where this assumption seems to work. Basically, a relatively shallow topsoil above the bedrock is considered, and its tendency to slide as a function of the terrain slope, represented by the G factor, is considered in adjusting the subsidence movements caused by a flat terrain.

The behavior provided by the data of the present work, however, seems to be quite different, as suggested by Figure 3-16, Figure 3-23, Figure 3-29, and Figure 3-35. In general, it may be observed that horizontal displacements experienced by the highway foundation are sensitive to very gentle highway gradients of the order of 1 to 3 degrees. In cases where the direction of highway gradient is constant, that is, the whole highway segment above the panel width going uphill or downhill, it is possible that almost all surveyed points move in a single direction, namely the downhill direction. This behavior cannot be captured by the assumption that horizontal displacements may be correlated to the trough slope. Also, considering infinite slope stability does not seem to be the best approach since the behavior is dominated by complex irregular three-dimensional geometry. The complex behavior of horizontal displacements on top of highway foundations will be addressed in the numerical modeling part of this work.

5.0 HIGHWAY SUBSIDENCE FINITE ELEMENT MODEL

A Finite Element Model (FEM) for the problem of highway subsidence is proposed here. Table 5-1 gives a list of the actual rock layers encountered in the field, according to a 1955 boring log by Mott Core Drilling Company in Perry Township, Greene County, and their thicknesses, as well as a set of layers used in the finite element model.

Table 5-1 Boring log and FEM model layer thicknesses

Sub-layer No. (bottom-up)	Approx. thickness of individual layers [ft]	Approx. thickness of individual layers [m]	Depth [m]	Rock type	FEM Layer (bottom-up)	Total layer thickness [m]
55	5.0	1.5	1.5	Surface	29	4.0
54	6.0	1.8	3.4	Brown clay		
53	12.0	3.7	7.0	Gray shale	28	4.0
52	40.5	12.3	19.4	Gray sandy shale	27	12.0
51	17.5	5.3	24.7	Dark shale	26	5.0
50	3.4	1.0	25.7	Sandy shale	25	3.0
49	6.5	2.0	27.7	Gray shale		
48	1.4	0.4	28.1	Coal		
47	20.0	6.1	34.2	Dark shale	24	8.0
46	1.0	0.3	34.5	Coal	23	5.0
45	12.6	3.8	38.4	Sandy shale		
44	3.5	1.1	39.4	Dark shale		
43	52.5	16.0	55.4	Sandy lime	22	18.0
42	7.2	2.2	57.6	Sandstone		
41	10.3	3.1	60.8	Gray lime	21	7.0
40	2.5	0.8	61.5	Sandy lime		
39	7.0	2.1	63.7	Gray lime		
38	3.7	1.1	64.8	Coal		

Table 5-1 (Continued)

Sub-layer No. (bottom-up)	Aprox. thickness of individual layers [ft]	Aprox. thickness of individual layers [m]	Depth [m]	Rock type	FEM Layer (bottom-up)	FEM Total layer thickness [m]
37	4.6	1.4	66.2	Green lime	20	4.0
36	10.0	3.0	69.3	Green soft lime		
35	35.7	10.9	80.1	Sandstone	19	11.0
34	20.0	6.1	86.2	Dark shale	18	8.0
33	7.2	2.2	88.4	Coal		
32	10.0	3.0	91.5	Sandy shale	17	6.0
31	3.2	1.0	92.4	Sandstone		
30	5.0	1.5	94.0	Dark shale		
29	15.5	4.7	98.7	Gray lime	16	5.0
28	10.3	3.1	101.8	Green lime	15	5.0
27	5.5	1.7	103.5	White lime		
26	15.4	4.7	108.2	Green lime	14	5.0
25	10.3	3.1	111.3	White lime	13	7.0
24	14.2	4.3	115.7	Gray lime		
23	36.0	11.0	126.6	White lime	12	11.0
22	25.5	7.8	134.4	Sandy lime	11	8.0
21	7.3	2.2	136.6	White lime	10	12.0
20	32.7	10.0	146.6	Lime shale streaks		
19	12.0	3.7	150.3	White lime	9	4.0
18	4.4	1.3	151.6	Dark shale	8	9.0
17	10.4	3.2	154.8	Gray lime		
16	3.2	1.0	155.8	Green lime		
15	12.0	3.7	159.4	Gray lime		
14	13.0	4.0	163.4	Sandy shale	7	6.0
13	4.4	1.3	164.7	Dark shale		
12	3.8	1.2	165.9	Coal		
11	17.0	5.2	171.1	Dark shale	6	5.0
10	24.5	7.5	178.5	Sandy shale	5	7.0
9	3.0	0.9	179.4	Dark shale	4	5.3
8	2.0	0.6	180.0	Soft clay		
7	1.1	0.3	180.4	Coal		
6	2.0	0.6	181.0	Dark shale		
5	6.6	2.0	183.0	Gray lime	3	5.3
4	14.2	4.3	187.3	Dark shale		
3	7.6	2.3	189.6	Bone coal streaks		
2	7.4	2.3	191.9	Coal	2	2.4
1	131.2	40.0	231.9	Floor	1	40.0

5.1 GENERAL DESCRIPTION OF FEM MODEL

The layer partition of the FEM model was done such that the number of layers could be reduced for the ease of building and running the model. The use of a stack of layers in subsidence modeling is important because the relative displacement between layers and the relatively low bending stiffness of individual layers allow for realistic subsidence trough shapes. Su built a FEM with several layers and obtained accurate shape of the subsidence trough (Su 1991). Besides FEM, a laminated Boundary Element model also considered a stack of layers and was used in subsidence modeling (Heasley and Barton 1998).

The FEM model proposed here was developed using the software LS-DYNA. The model has been implemented mainly for linear elastic material. Between layers, a tiebreak contact definition and friction angle may be used. The basic strength parameters used in the tiebreak definition are tensile strength and shear strength. A contact failure criterion involves these two parameters. When the failure criterion is met, the bonds between the layers are broken and relative displacements occur between them.

5.1.1 FEM calibration criteria

Calibration of the FEM model was planned based on three criteria that are important in a subsidence model. The criteria are: subsidence trough shape, maximum subsidence magnitude, and post-mining vertical stress distribution in the abutment and gob areas of the panel. Getting reasonable results of these three characteristics is the main motivation behind the development of the model. A brief description of each of these is given here. The next sub-section explores the trade-offs between these criteria.

5.1.1.1 Subsidence trough shape

The shape of the subsidence trough is a very important feature in a prediction model. Underground extractions in materials that behave somewhat elastically will produce S-shapes in the surface when the extractions reach certain dimensions. However, the S-shaped subsidence curve needs to be accurate if the model is intended to serve prediction of surface deformations, as the location of critical deformations needs to be known. The key to the correct shape of subsidence troughs is the stacking of several thin layers that represent the geologic strata in the overburden rock. The correct shape of a subsidence trough can be calibrated trough appropriate number of layers, relative thickness of the layers with respect to overburden depth, mechanical properties of the layer material, and strength of the bonding between layers.

5.1.1.2 Maximum subsidence

The problem of predicting maximum subsidence has been discussed and a maximum subsidence model for the region has been proposed (see Figure 4-1). For this purpose, the ratio of maximum subsidence to extraction thickness, S^*/M, was used, which is always less than 1.0 and in the vicinity of 0.67. An important factor that contributes to this ratio being always less than 1.0 is the bulking factor. Peng defines the bulking factor as "the ratio of the volume of the broken rock strata to the original volume of the same strata before they are broken and cave." It continues: "Since the volume of the broken strata is always larger than that of the original intact strata, bulking factor is usually larger than one" (Peng 2008).

The average value of bulking factor measured by Peng was 1.28. The bulking behavior of broken rock is a feature not considered in the present FEM model. Even though LS-DYNA has the capabilities necessary to model damage in rock materials, its implementation in the problem of three-dimensional subsidence would be computationally extremely expensive and impractical.

Obtaining magnitudes of subsidence in supercritical troughs that are less than the extracted thickness is a very difficult task without considering the bulking factor. Even though it is still possible to get the correct value of the *S*/M* ratio if the roof of the extracted cavity is not allowed to touch the floor, the resulting distribution of vertical stress in the abutment and gob areas and the trough shape so obtained are not satisfactory.

5.1.1.3 Post-mining vertical stress distribution in abutment and gob areas

The model would be expected to give not only correct subsidence magnitude and shape, but also a reasonably correct redistribution of post-mining vertical stresses in the abutment and gob areas. This would consistently connect what is happening in the mine with what is happening in the surface. Otherwise, many different combinations of parameters could be used to produce correct subsidence magnitudes and shapes without truly representing the mechanics of the problem. Typical abutment and gob stress distributions are given in Figure 5-1 and Figure 5-2 (Morsy and Peng 2002).

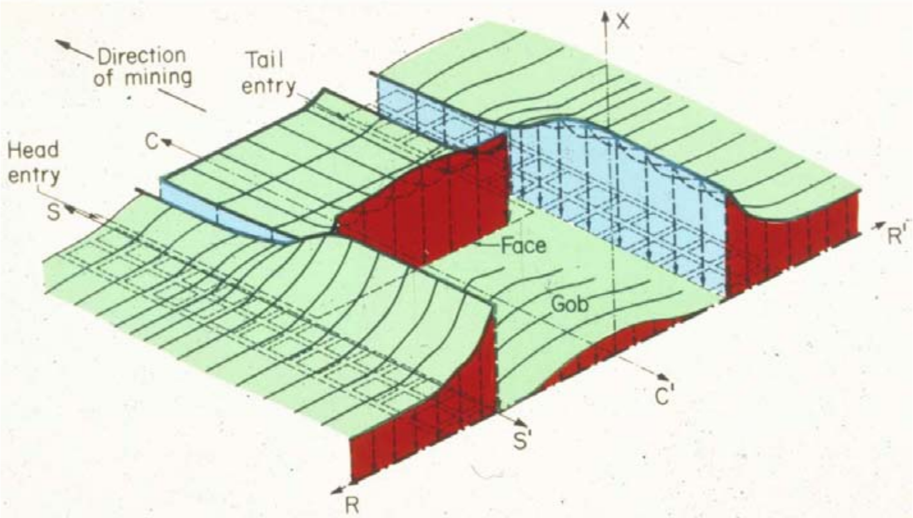

Figure 5-1 Qualitative abutment stress distribution

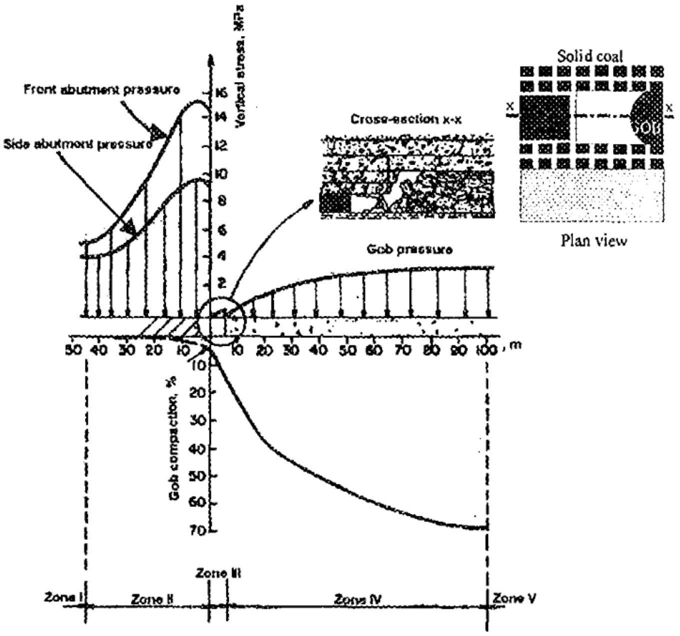

Figure 5-2 Probable distribution of strata pressure in the vicinity of the longwall face

(Morsy and Peng 2002)

5.1.2 Trade-off between subsidence shape, subsidence magnitude, and post-mining vertical stress redistribution

The model investigation begins with a stack of relatively thin layers whose thicknesses are given in Table 5-1. Several cases will be explored in which the role of each of the three calibration criteria is analyzed.

5.1.2.1 Case 1

The modulus of elasticity for all layers is equal to $1.48\text{x}10^{10}$ Pa and the Poisson's ratio is equal to 0.22. The tensile and shear interface bond strengths were varied linearly from the top to the bottom in the range $2.35\text{x}10^{6}$ Pa to $5.35\text{x}10^{6}$ Pa, for an average of $3.95\text{x}10^{6}$ Pa for the first case, roughly 10% of the compressive strength of a typical rock encountered in this region. This first model is given in Figure 5-3. *S*/M* turned out to be equal to 1.09 because the layers fall into the created extraction, thus fully closing the vertical gap. The readings of subsidence were corrected by subtracting the initial settlement due to the application of gravity to the whole model.

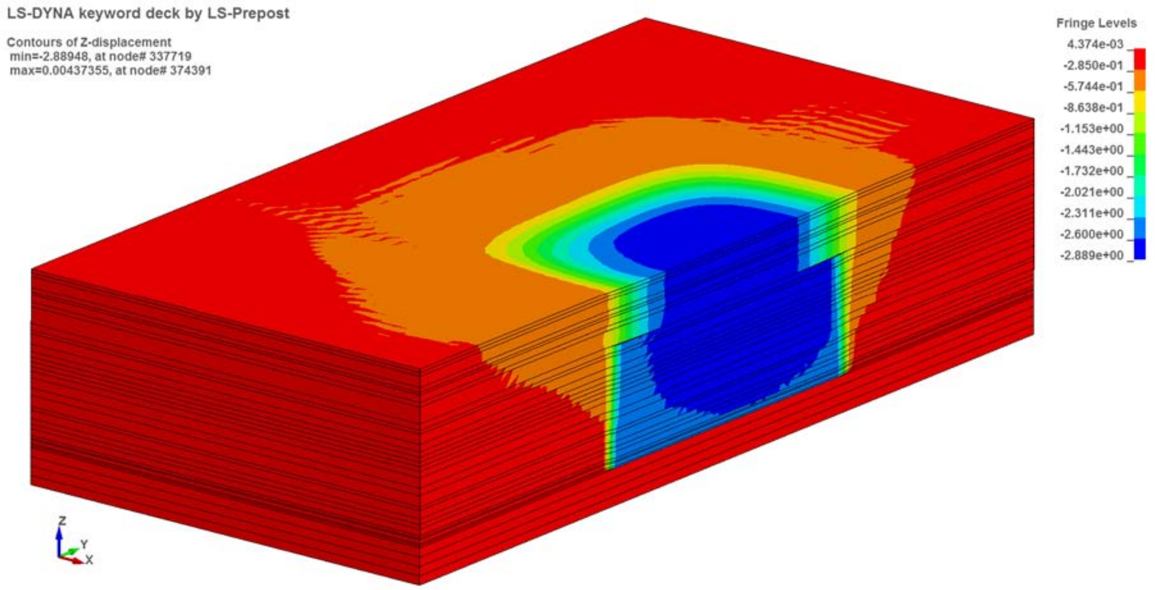

Figure 5-3 Subsidence for case 1

The shape of the trough obtained with this first model is given in Figure 5-4. In terms of shape, it can appreciated that the stacking of thin layers is very effective and a very accurate shape may be obtained.

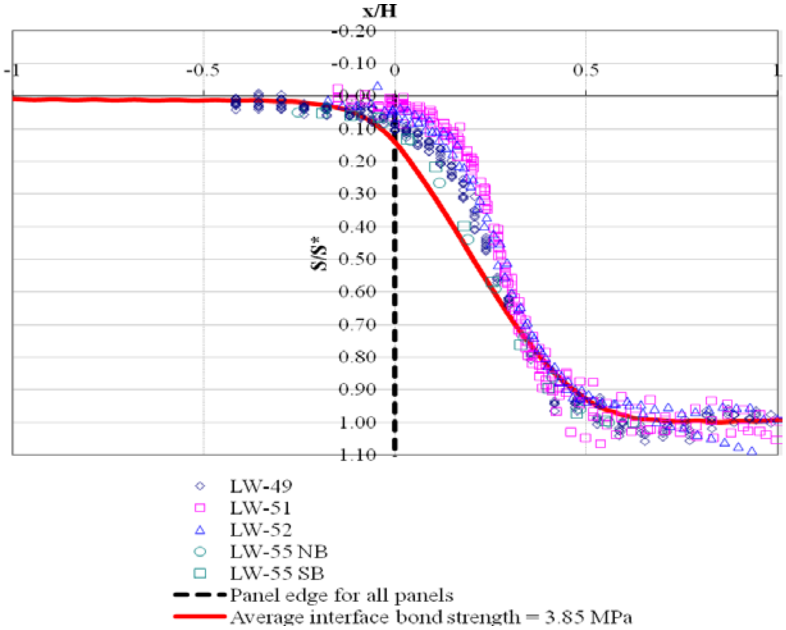

Figure 5-4 Shape of subsidence trough for case 1

The post-mining redistribution of stresses is given in Figure 5-5. Since the central portion of the stack of layers is allowed to fall downward with all of its weight applied on the floor of the cavity, the magnitude of the stresses is essentially the same in the gob as in the abutments.

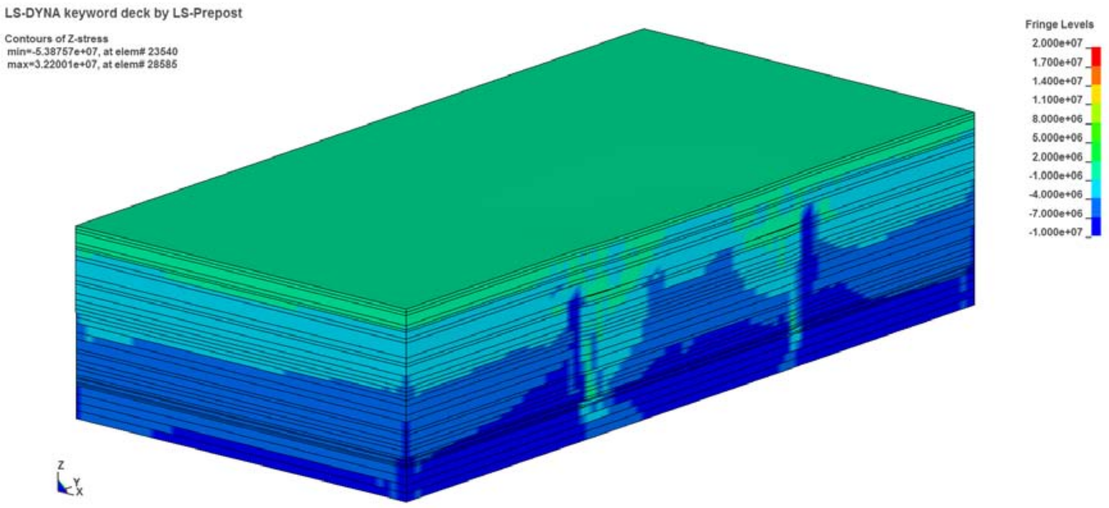

Figure 5-5 Post-mining vertical stress redistribution for case 1

5.1.2.2 Case 2

In case 2, the modulus of elasticity for all layers is also equal to 1.48x10^{10} Pa and the Poisson's ratio is equal to 0.22. The tensile and shear interface bond strengths were varied linearly from the top to the bottom in the range 2.40x10^{6} Pa to 5.60x10^{6} Pa, for an average of 4.00x10^{6} Pa for the first case, just a slight increase with respect to case 1. This second model is given in Figure 5-6. *S*/M* turned out to be equal to 1.07 because the layers fall into the created extraction, thus fully closing the vertical gap. The readings of subsidence were corrected by subtracting the initial settlement due to the application of gravity to the whole model.

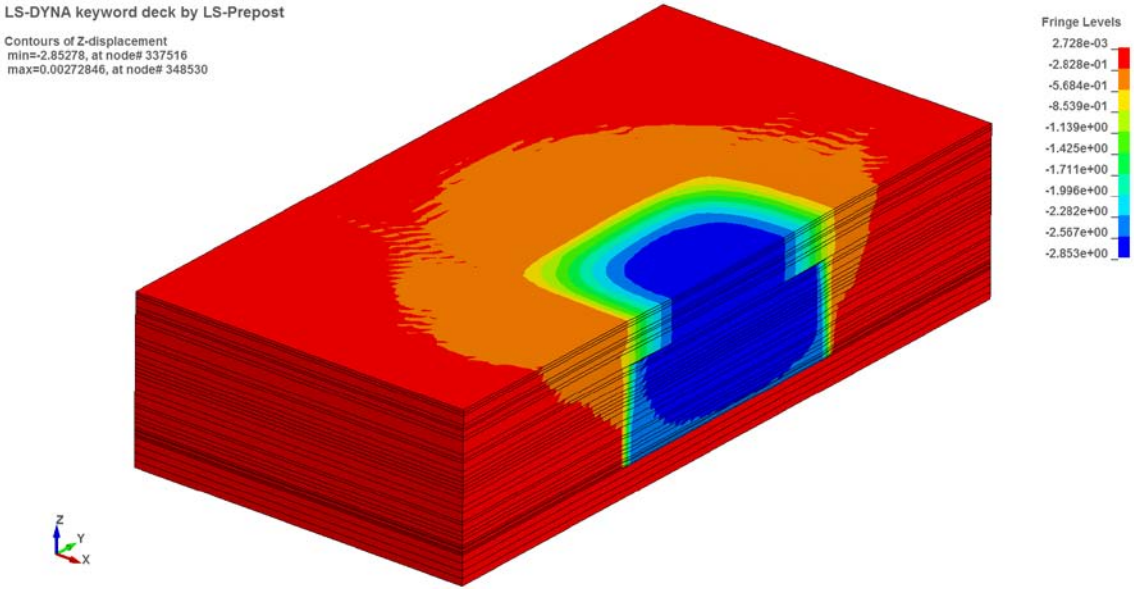

Figure 5-6 Subsidence for case 2

The shape of the trough obtained with the second model is given in Figure 5-7. In terms of shape, it can appreciated that the stacking of thin layers is very effective and a very accurate shape may be obtained.

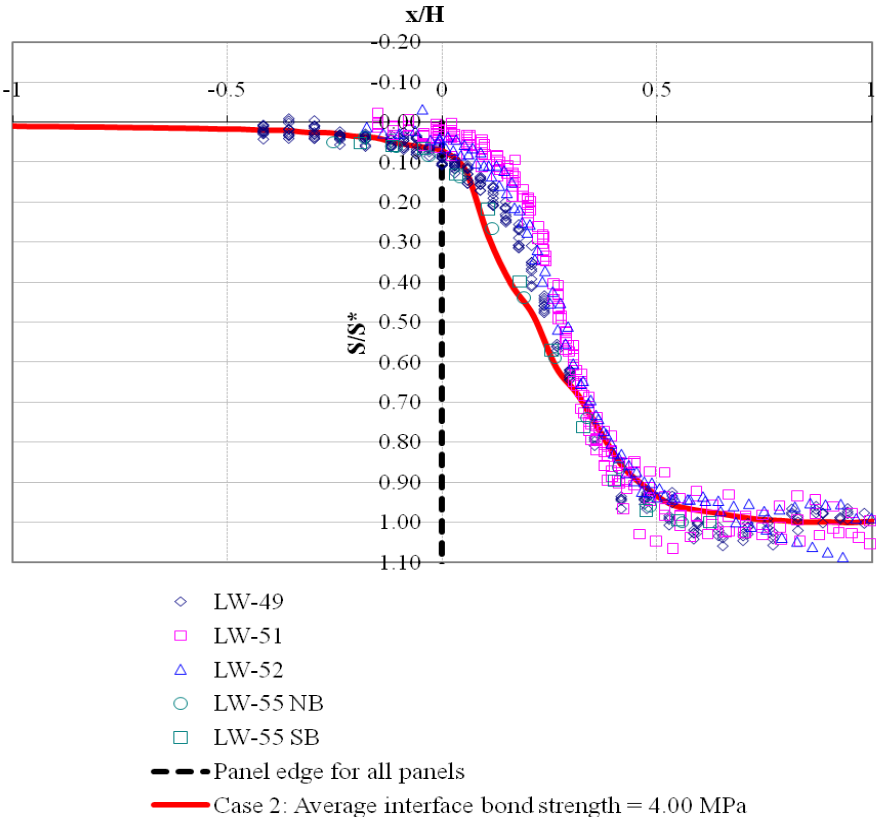

Figure 5-7 Shape of subsidence trough for case 2

The post-mining redistribution of stresses is given in Figure 5-8. Since the central portion of the stack of layers is allowed to fall downward with all of its weight applied on the floor of the cavity, the magnitude of the stresses is essentially the same in the gob as in the abutments.

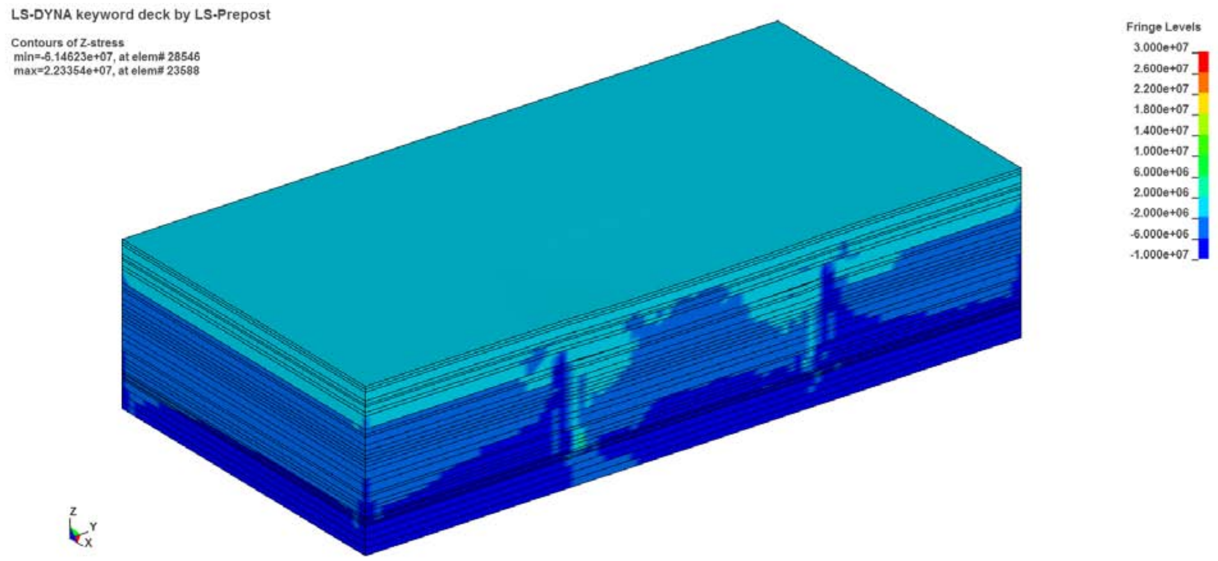

Figure 5-8 Post-mining vertical stress redistribution for case 2

5.1.2.3 Case 3

In case 3, the modulus of elasticity for all layers is also equal to 1.48×10^{10} Pa and the Poisson's ratio is equal to 0.22. The tensile and shear interface bond strengths were varied linearly from the top to the bottom in the range 2.45×10^{6} Pa to 5.65×10^{6} Pa, for an average of 4.05×10^{6} Pa for the first case, again a very slight increase with respect to case 2. This second model is given in Figure 5-6. *S*/M* in this model goes abruptly down to 0.24 as the whole stack of layers remains hanging in the central portion and supported only in the abutments. The readings of subsidence were corrected by subtracting the initial settlement due to the application of gravity to the whole model.

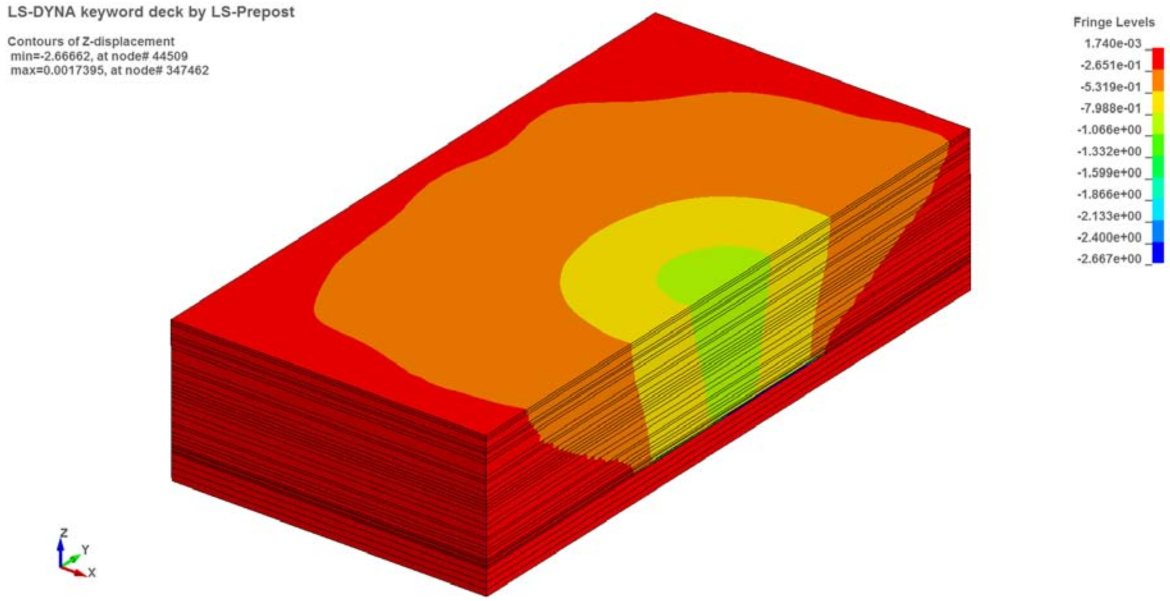

Figure 5-9 Subsidence for case 3

The shape of the trough obtained with the third model is very flat, as given in Figure 5-10.

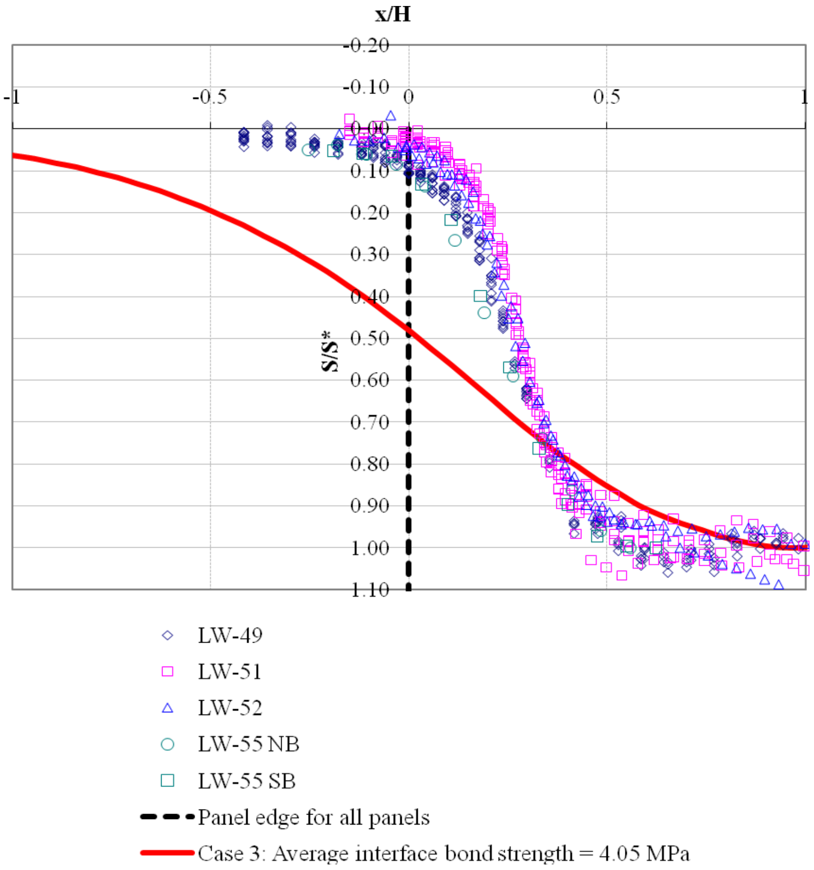

Figure 5-10 Shape of subsidence trough for case 3

The post-mining redistribution of stresses is given in Figure 5-11. Since the central portion of the stack of layers is not touching the floor of the cavity, the magnitude of the stresses in the abutments is high whereas the central part of the overburden is in tension.

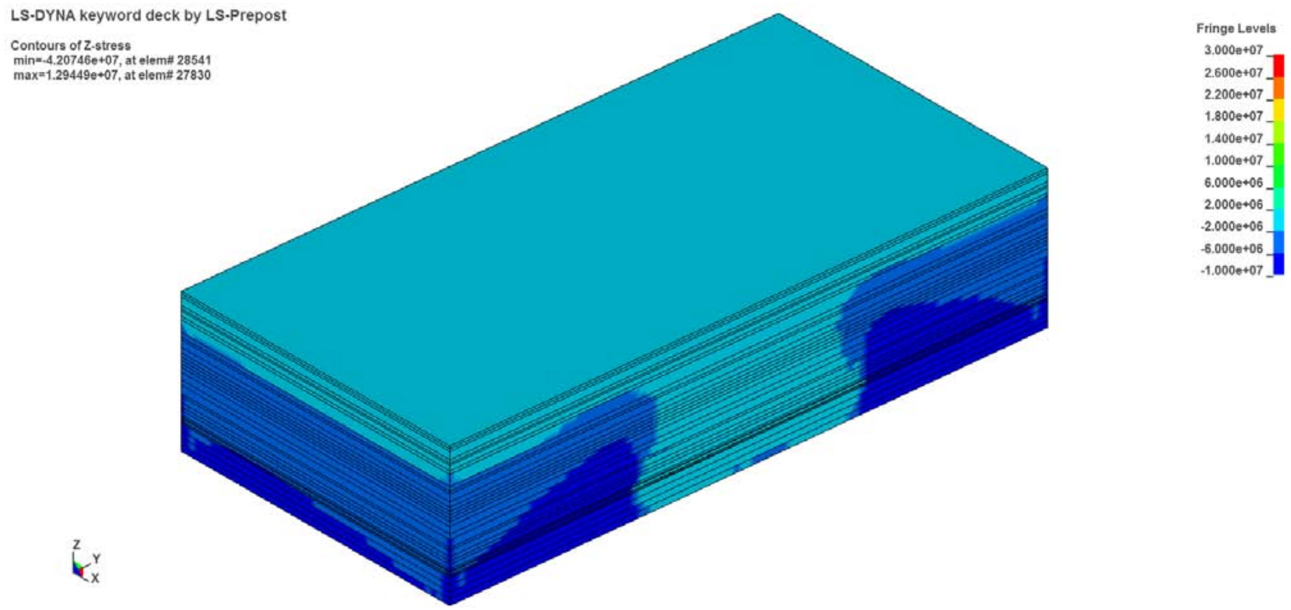

Figure 5-11 Post-mining vertical stress redistribution for case 3

5.1.2.4 Case 4

In case 4, the modulus of elasticity for all layers is also equal to 1.48x10^{10} Pa and the Poisson's ratio is equal to 0.22. A different treatment is given to the interface bonding. A sequence is used in which every third pair of layers are allowed to freely slide with respect to each other, whereas the layers in between are bonded through a high strength of 100 MPa. The sequence of sliding allowance in terms of 1 and 0 is 1001001 where 1 means "allowed to slide" and 0 gets the high bond strength of 100 MPa. This four model is given in Figure 5-12. *S*/M* in this model turns out to be equal to 1.12 as the whole stack of layers is allowed to fall on the central floor. The readings of subsidence were corrected by subtracting the initial settlement due to the application of gravity to the whole model.

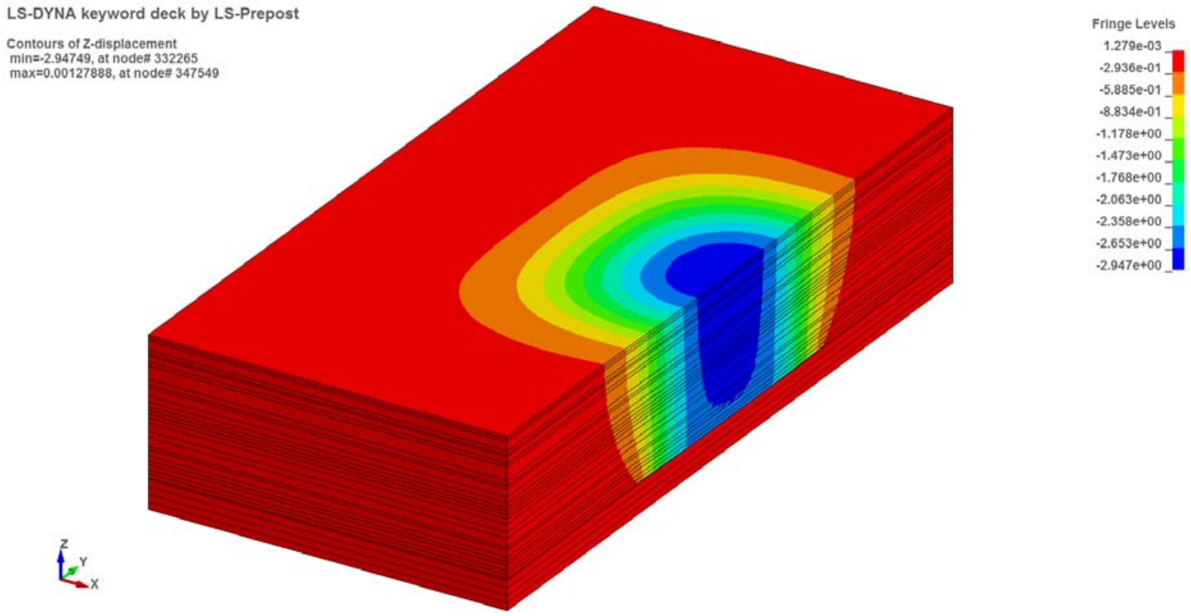

Figure 5-12 Subsidence for case 4

The shape of the trough obtained with the fourth model is given in Figure 5-13. The shape again looks correct as sliding is allowed in some interfaces and the central portion of the rock falls into the ground.

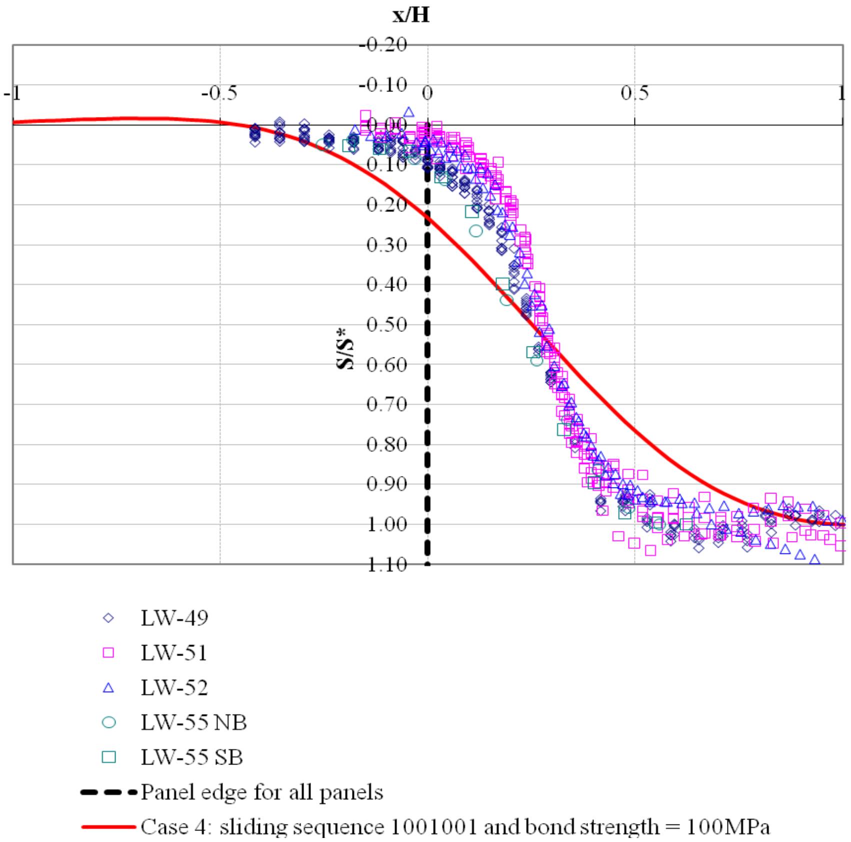

Figure 5-13 Shape of subsidence trough for case 4

The post-mining redistribution of stresses is given in Figure 5-14. Since the central portion of the stack of layers is allowed to fall downward with all of its weight applied on the floor of the cavity, the magnitude of the stresses is essentially the same in the gob as in the abutments.

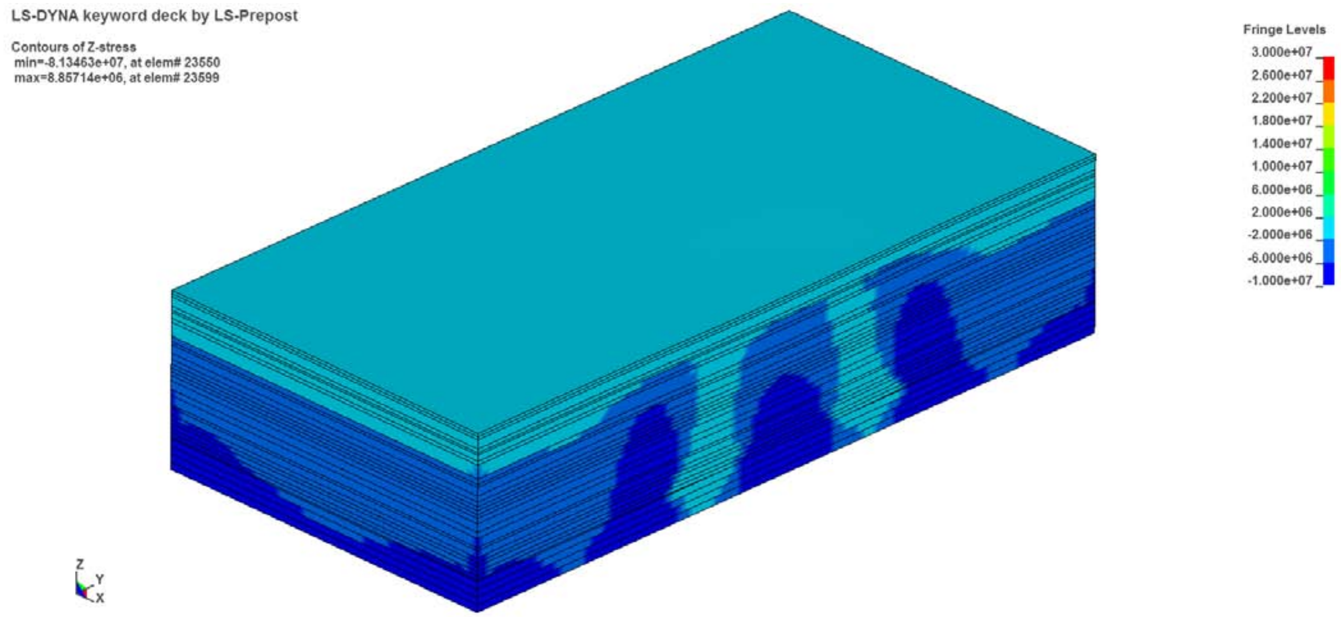

Figure 5-14 Post-mining vertical stress redistribution for case 4

5.1.2.5 Case 5

Case 5 is like case 4, except for the sequence of sliding allowance. In this case, this sequence is 100010001. This fifth model is given in Figure 5-15. *S*/M* in this model turns out to be equal to 1.06 as the whole stack of layers is still allowed to fall on the central floor. The readings of subsidence were corrected by subtracting the initial settlement due to the application of gravity to the whole model.

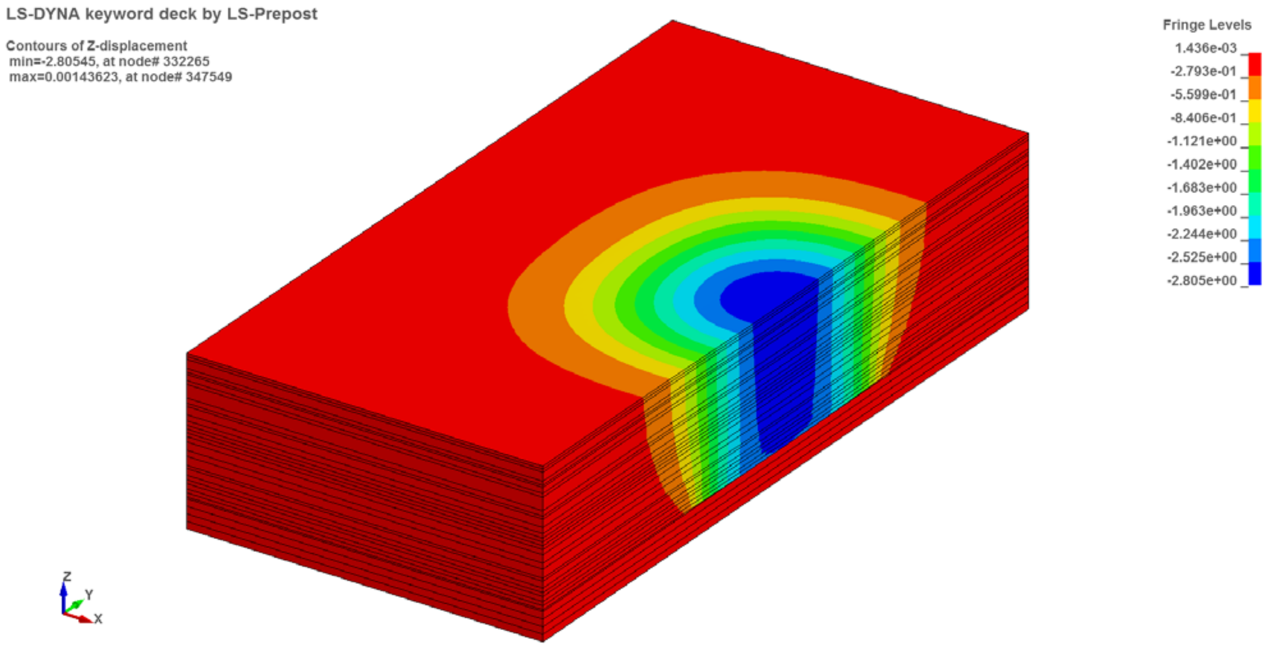

Figure 5-15 Subsidence for case 5

The shape of the trough obtained with the fifth model is given in Figure 5-16. The shape again looks correct as sliding is allowed in some interfaces and the central portion of the rock falls into the ground.

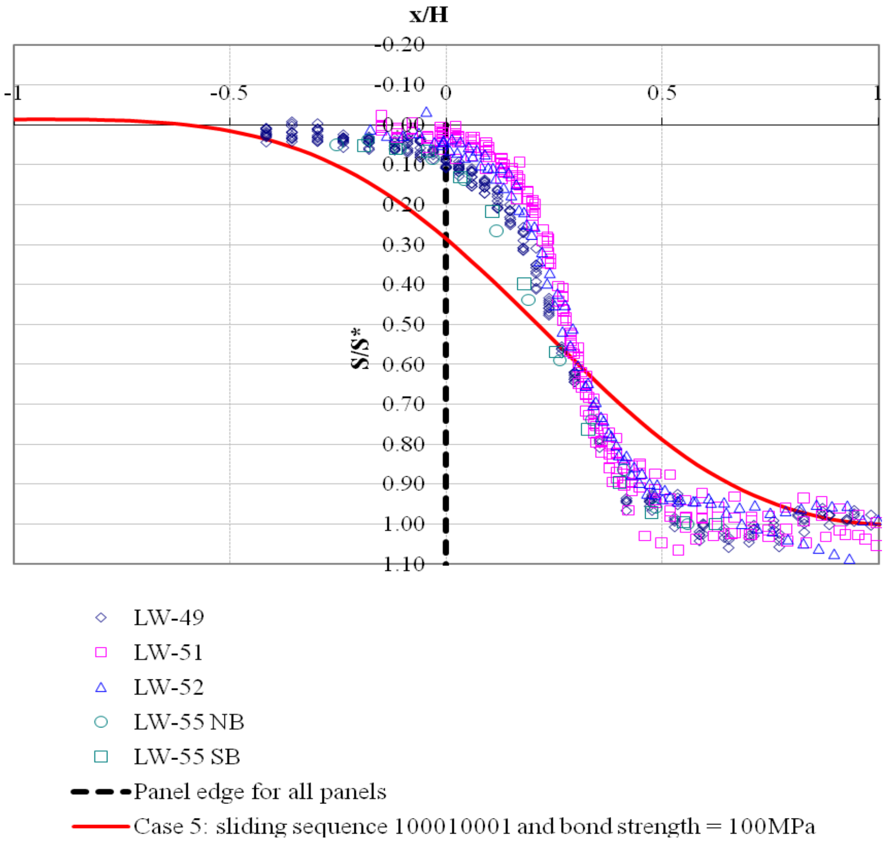

Figure 5-16 Shape of subsidence trough for case 5

The post-mining redistribution of stresses is given in Figure 5-17. Since the central portion of the stack of layers is allowed to fall downward with all of its weight applied on the floor of the cavity, the magnitude of the stresses is essentially the same in the gob as in the abutments. However, since the overall stiffness of the system was increased by increasing the spacing of interfaces with sliding allowance, the central region where stresses were high is smaller than in case 4.

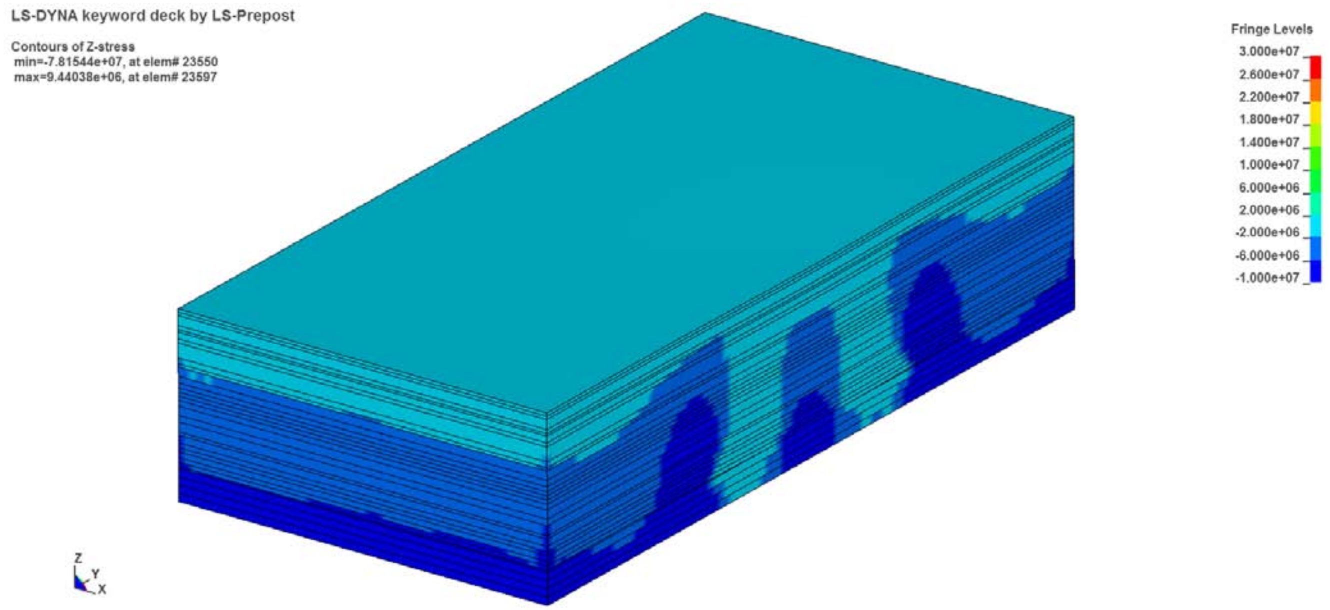

Figure 5-17 Post-mining vertical stress redistribution for case 5

5.1.2.6 Case 6

Case 6 differs from all previous cases in that the Young's modulus was increased to 30 GPa. All other features are those of case 5, including the sliding sequence of 100010001. This sixth model is given in Figure 5-18. *S*/M* in this model turns out to be equal to 0.66 as the whole stack of layers does not touch the floor. The readings of subsidence were corrected by subtracting the initial settlement due to the application of gravity to the whole model.

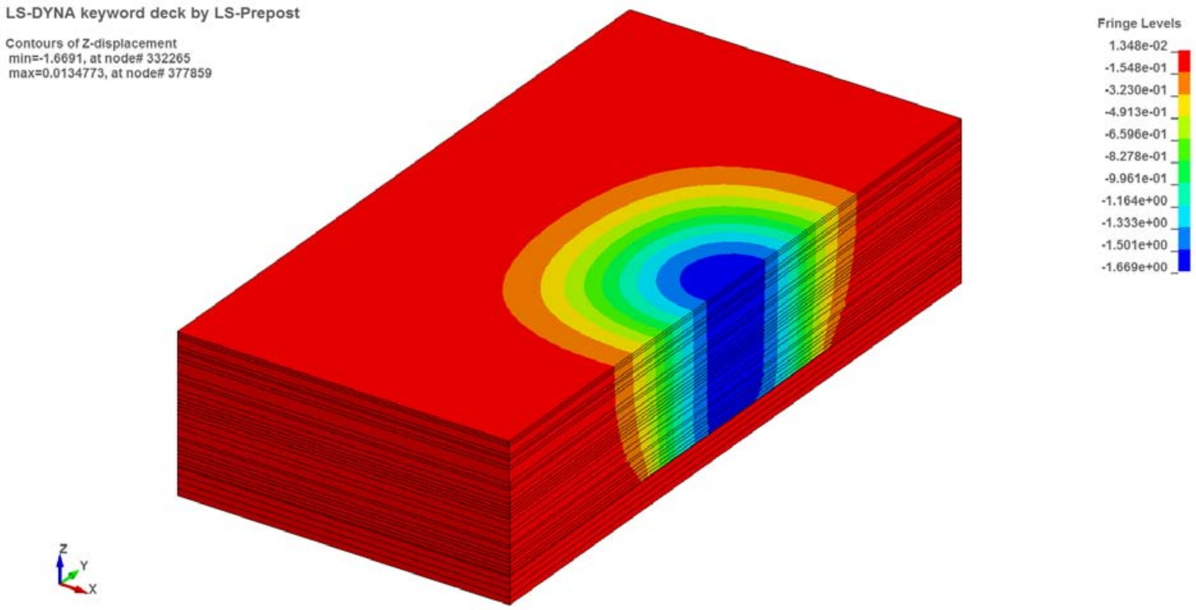

Figure 5-18 Subsidence for case 6

The shape of the trough obtained with the sixth model is given in Figure 5-19. The shape looks correct as sliding is allowed in some interfaces and the central portion of the rock falls into the ground.

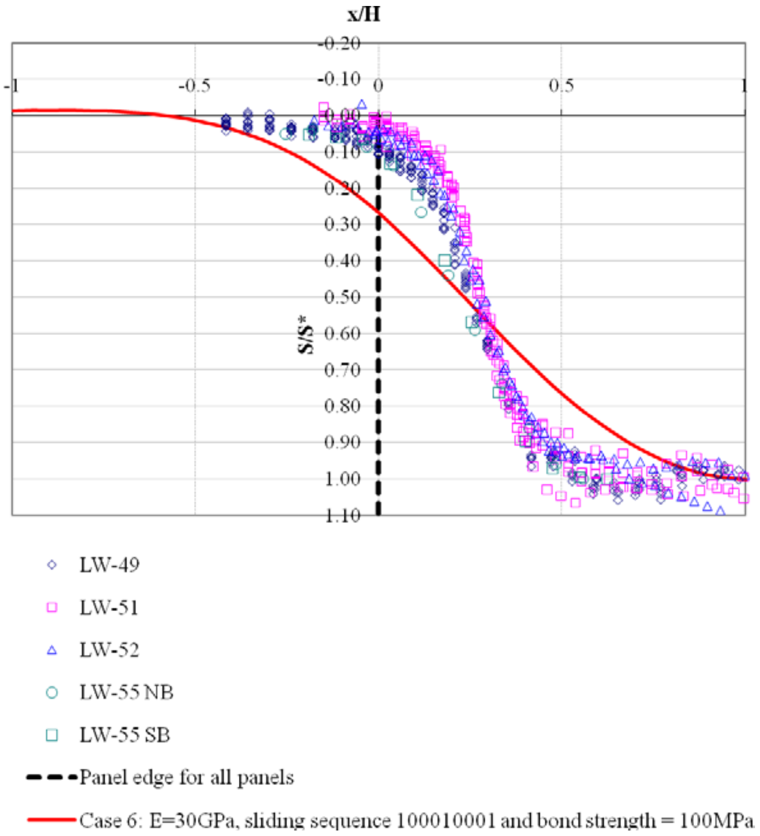

Figure 5-19 Shape of subsidence trough for case 6

The post-mining redistribution of stresses is given in Figure 5-20. Since the central portion of the stack of layers is not allowed to fall downward, the magnitude of the stresses is concentrated at the abutments. The magnitude of stress concentration is roughly 6 times higher than the pre-mining, roughly equal to 30 MPa, and the magnitude at the central hanging portion is roughly zero.

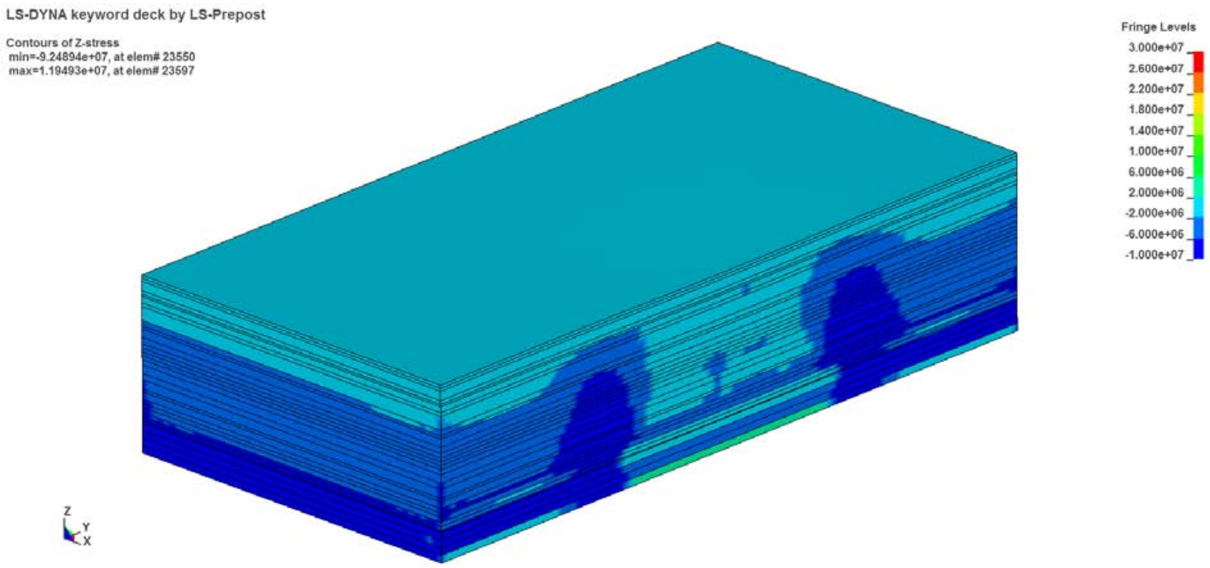

Figure 5-20 Post-mining vertical stress redistribution for case 6

5.1.2.7 Case 7

In case 7, tuning of the Young's modulus was done in order to improve the *S*/M* to approach the one measured in the field roughly equal to 0.7. The modulus was set equal to 23 GPa. All other features are those of case 6, including the sliding sequence of 100010001. This seventh model is given in Figure 5-21. *S*/M* in this model turns out to be equal to 0.7 as the whole stack of layers does not touch the floor. The readings of subsidence were corrected by subtracting the initial settlement due to the application of gravity to the whole model. The shape is reasonably good as in the previous case and the stresses have the same limitations as in the previous model.

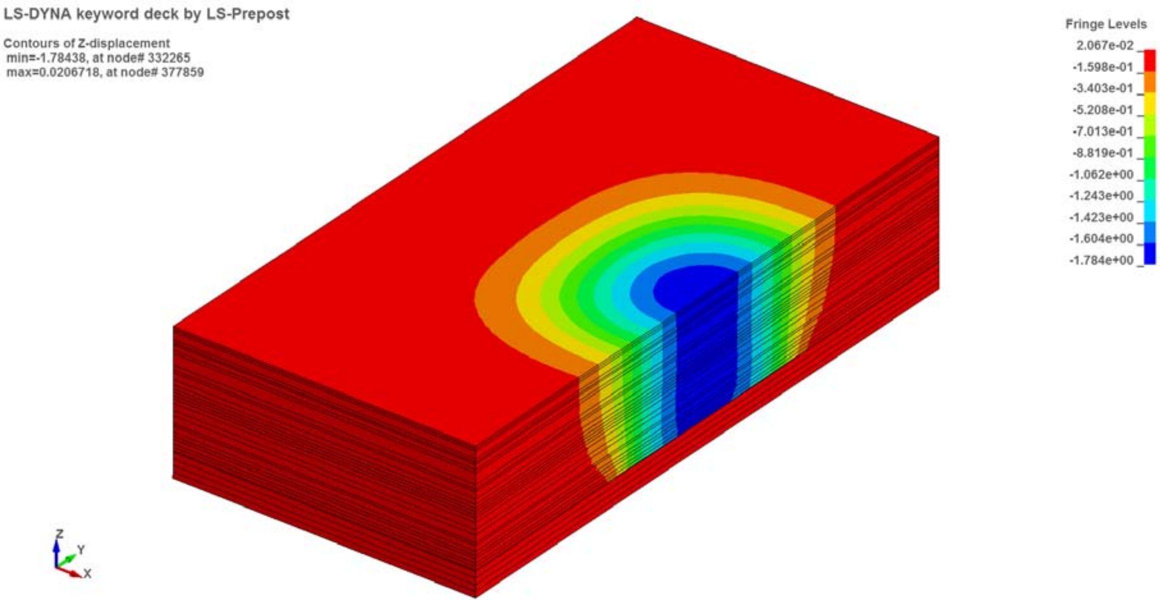

Figure 5-21 Subsidence for case 7

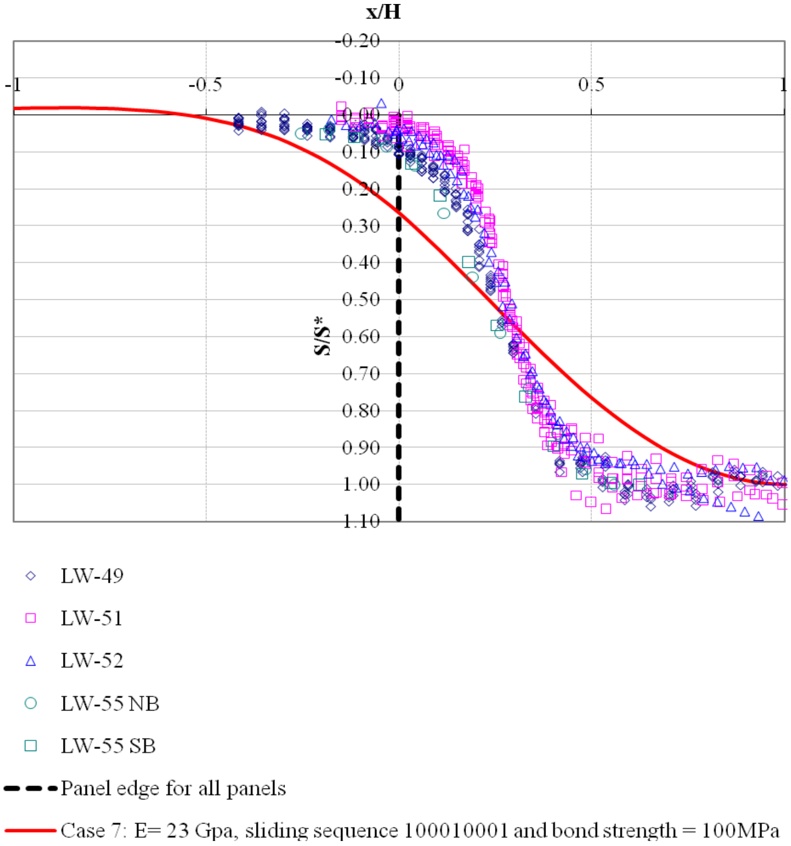

Figure 5-22 Shape of subsidence trough for case 7

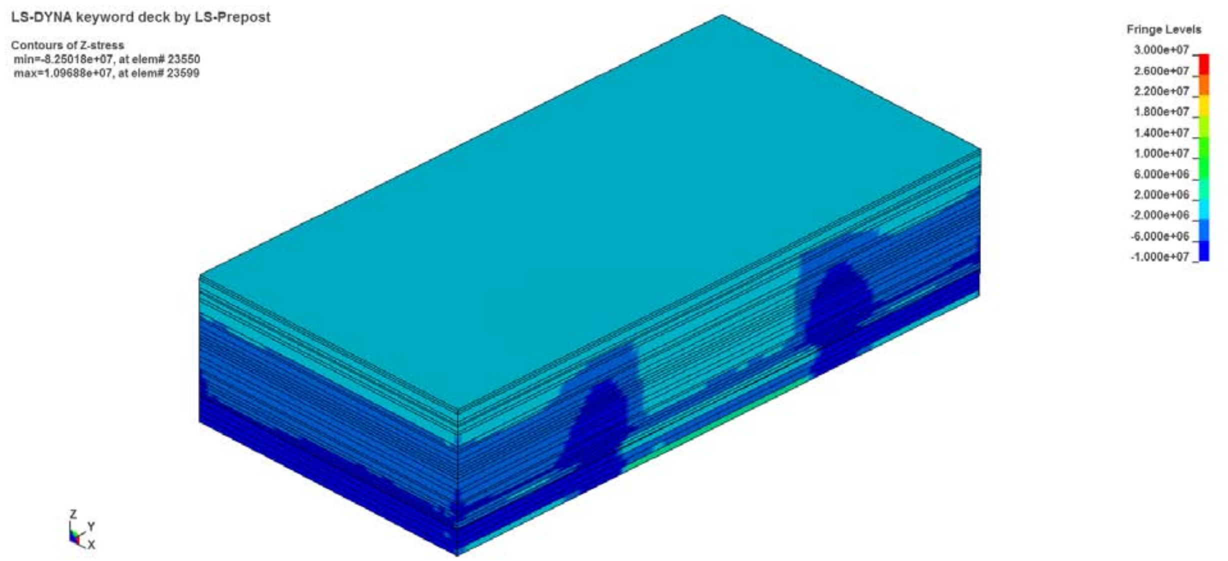

Figure 5-23 Post-mining vertical stress redistribution for case 7

5.1.3 The effect of horizontal in-situ stresses

Horizontal in-situ stresses can be extremely high in southwestern Pennsylvania, in cases reaching a ratio of 5:1 when compared to vertical stresses as illustrated in Figure 5-24 (Mark and Gadde 2008), where the circled data points correspond to eastern United States cases. A model with the properties contained in Table 5-2 is given in Figure 5-25. Figure 5-26 and Figure 5-27 provide details of the influence of the large horizontal pressure. The thin layers tend to warp, thus exerting a lifting effect that keeps the upper layers from freely falling downward. The subsidence factor obtained with this model was 0.83, and the vertical stress distribution and trough shape are given in Figure 5-28 and Figure 5-29, respectively.

Table 5-2 Mechanical properties of model considering horizontal stresses

Shear Modulus, G [GPa]	4.6
Density [kg/m3]	2650
Yield stress, σy [MPa]	28
Plastic stiffness, Ep [MPa]	0.1
Bulk Modulus, K [GPa]	7.7
Young's Modulus, E [GPa]	11.5

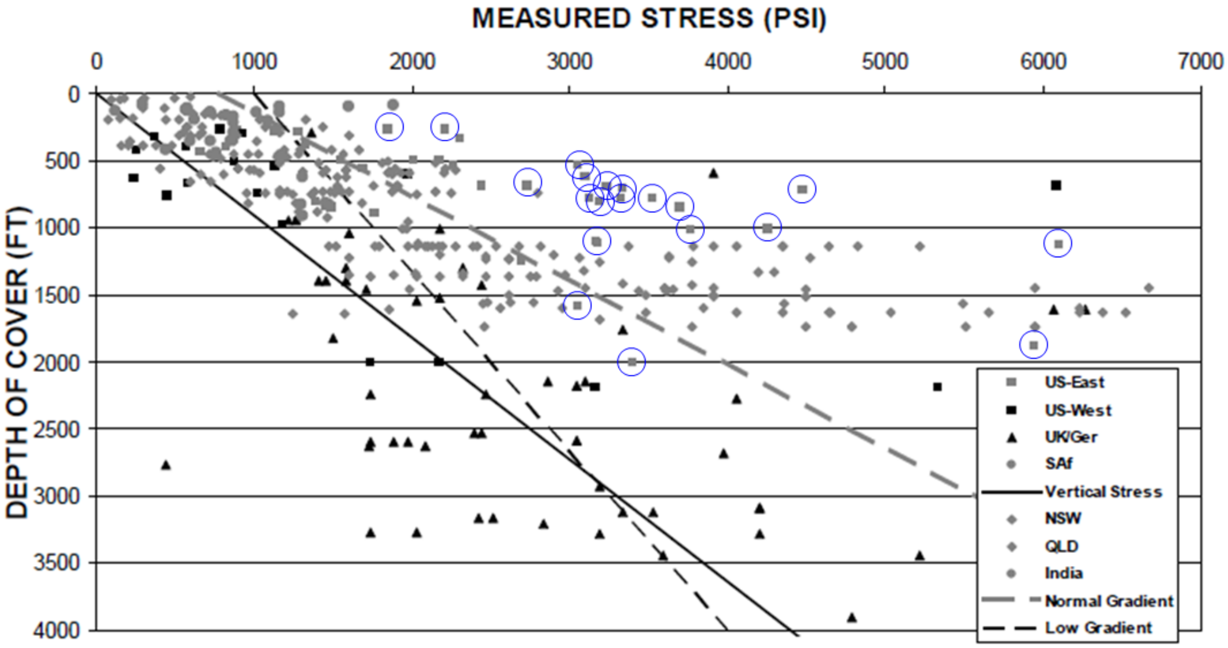

Figure 5-24 Horizontal in-situ stress database (Mark and Gadde 2008)

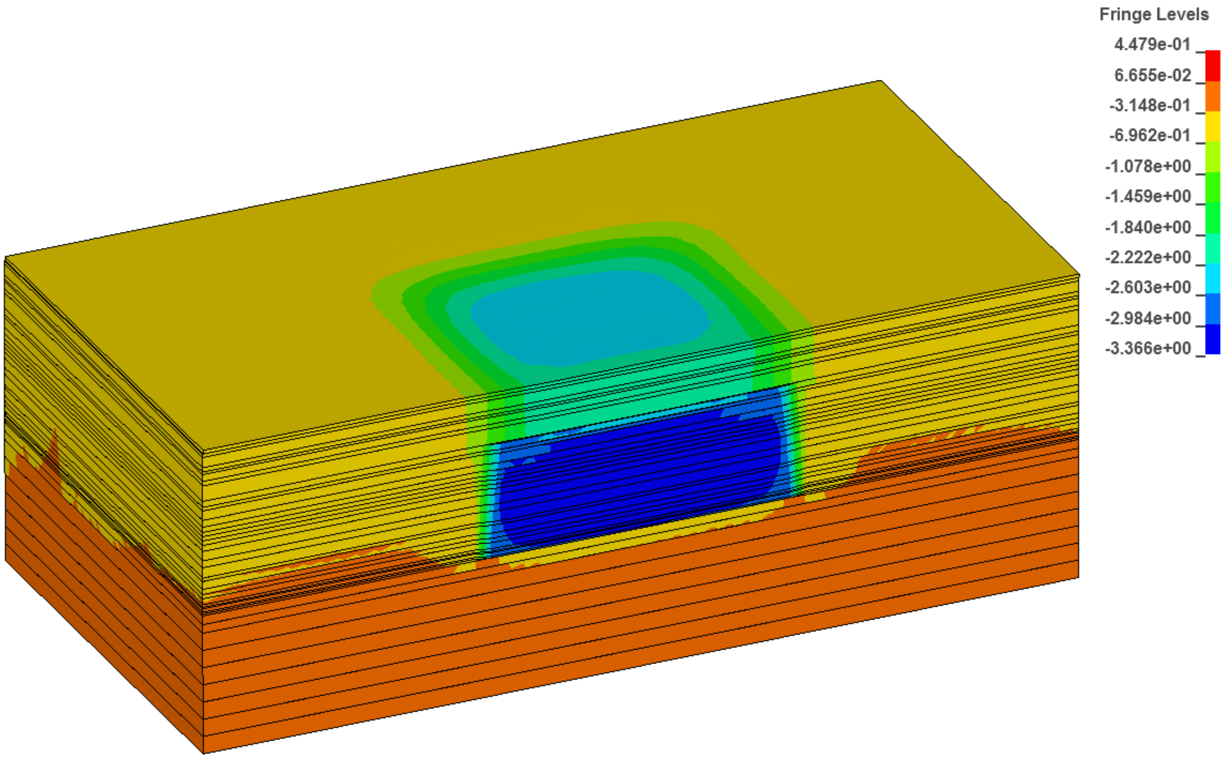

Figure 5-25 Subsidence considering the effect of horizontal in-situ stresses

Figure 5-26 View of post-mining gaps between layers and deformed surface

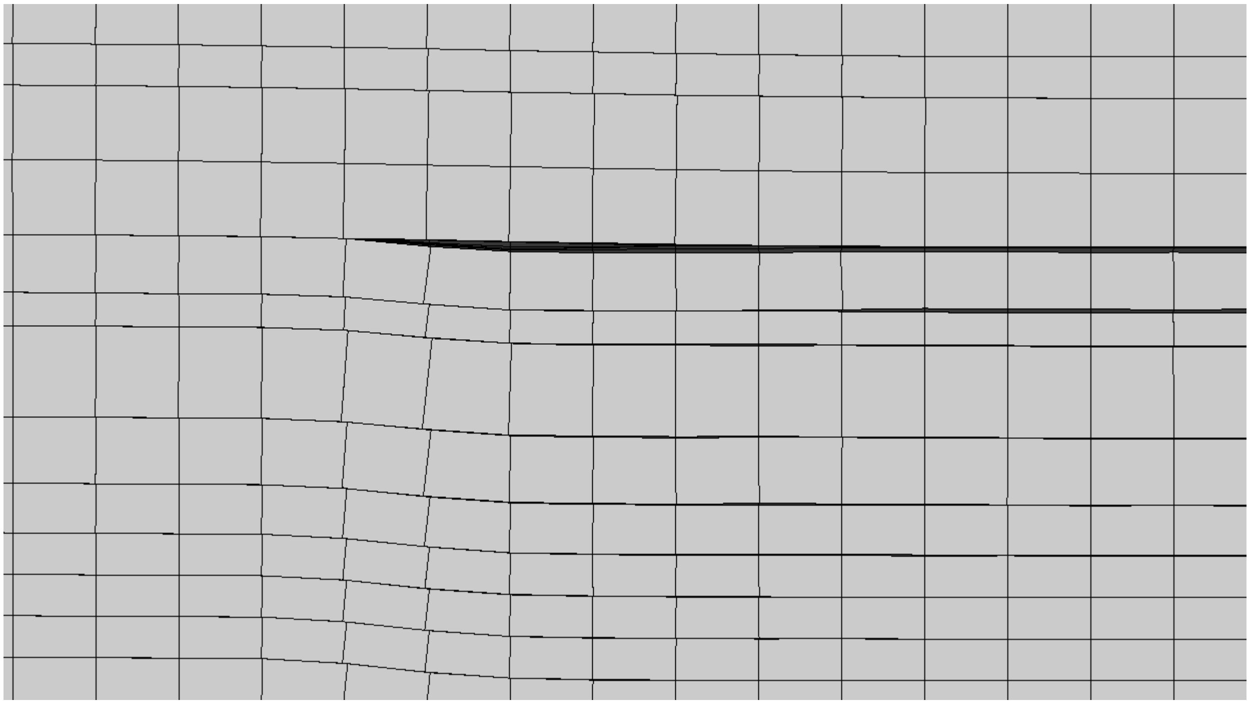

Figure 5-27 Detail of warped layers and gaps created due to high in-situ stress

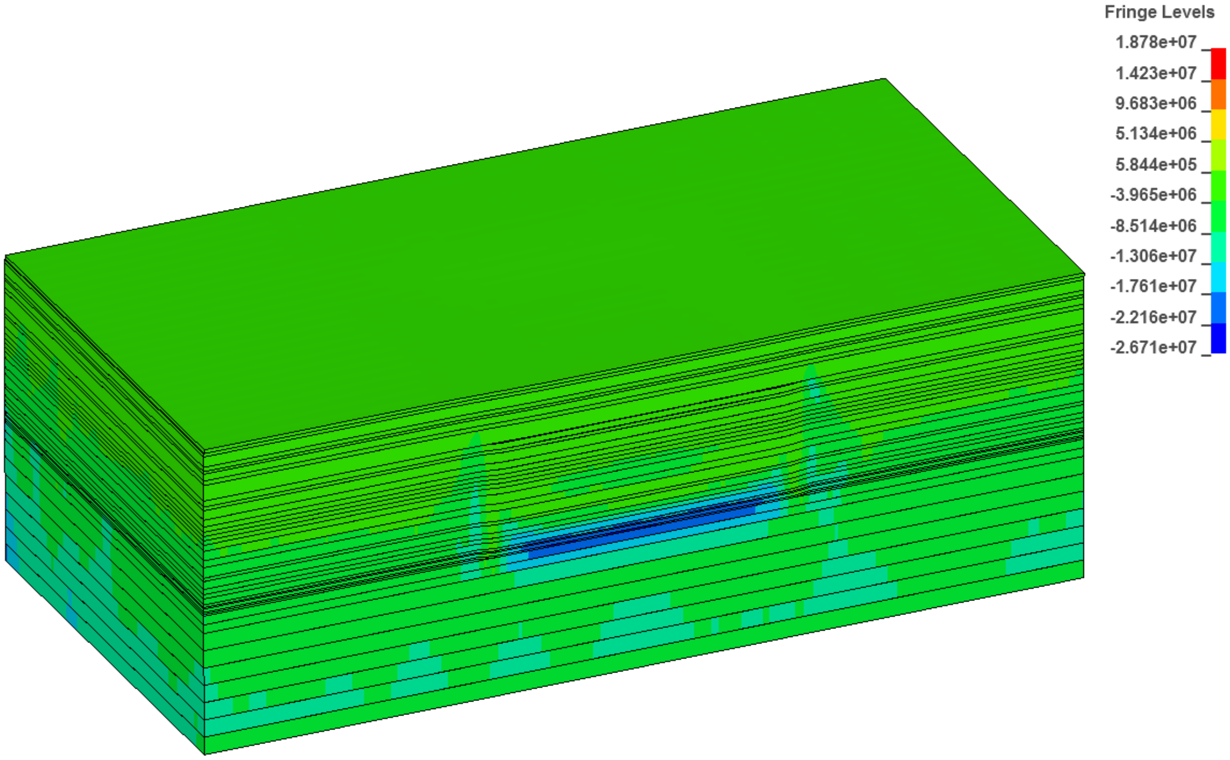

Figure 5-28 Vertical stresses at the end of extraction

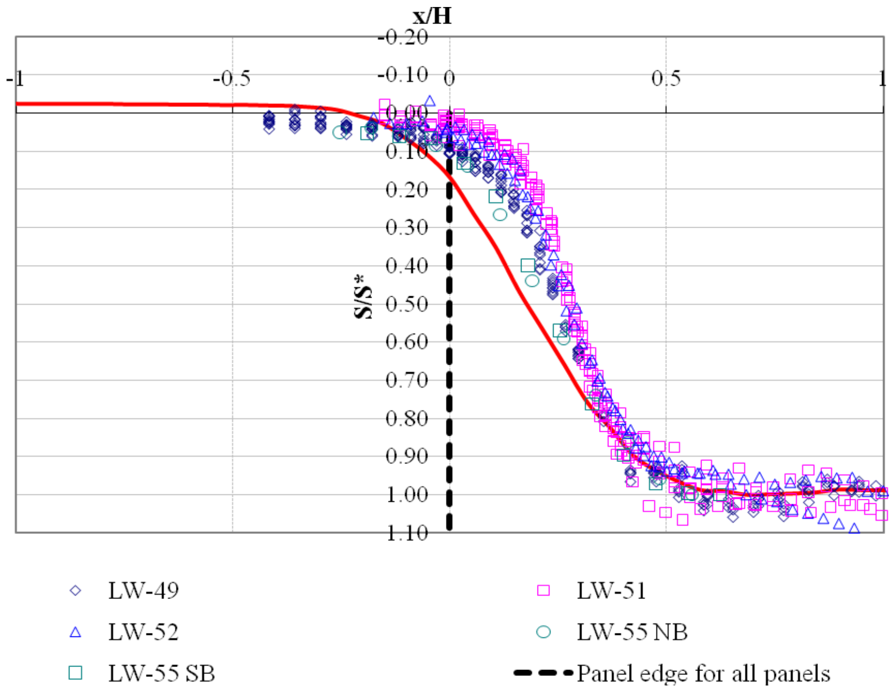

Figure 5-29 Normalized subsidence profile

5.1.4 Results including a highway embankment

For the general visualization of embankment behavior, a model with the properties shown in Table 5-3 and Table 5-4 was developed. Figure 5-30 shows that subsidence or vertical deformation is essentially independent of the presence of the embankment. This has been known to the subsidence community in that vertical deformations are not sensitive to hilly conditions. This fact also made it possible to develop the empirical model described in chapter 4.0 . On the other hand, horizontal deformations are very sensitive to the irregular shape of the highway embankment, and the asymmetry in horizontal deformation distribution is evident in Figure 5-31. Figure 5-32 shows two lines along which subsidence and horizontal deformations were calculated. The results are given in Figure 5-33 and Figure 5-34 and they demonstrate that under the special conditions of highway embankments, the general assumption that trough slope and horizontal deformation are linearly correlated, is not generally valid. Even though the embankment underwent a less steep deformation, the horizontal deformation was substantially higher than on the overburden. This would naturally be based on the fact that the overburden is formed by strong, confined rock, whereas the embankment is weaker, formed by compacted soils, and unconfined. Figure 5-34 also illustrates the asymmetry in the distribution of horizontal deformation as a consequence of the asymmetry in the embankment mass distribution. This finding is even clearer from the real data, as depicted for example in Figure 3-23 or Figure 3-25.

Table 5-3 Mechanical properties of model overburden

Shear Modulus, G [GPa]	9.4
Density [kg/m3]	2650
Yield stress, σy [MPa]	38
Plastic stiffness, Ep [MPa]	0.1
Bulk Modulus, K [GPa]	13.7
Young's Modulus, E [GPa]	23

Table 5-4 Mechanical properties of embankment

Shear Modulus, G [GPa]	0.2
Density [kg/m3]	2650
Yield stress, σy [MPa]	1.9
Plastic stiffness, Ep [MPa]	0.1
Bulk Modulus, K [GPa]	0.55
Young's Modulus, E [GPa]	0.535

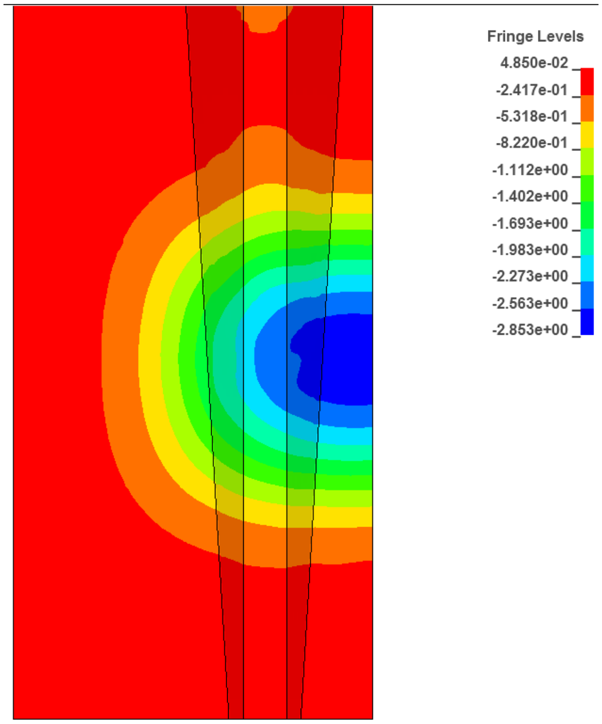

Figure 5-30 Top view of subsidence in 3D FEM model with embankment on top

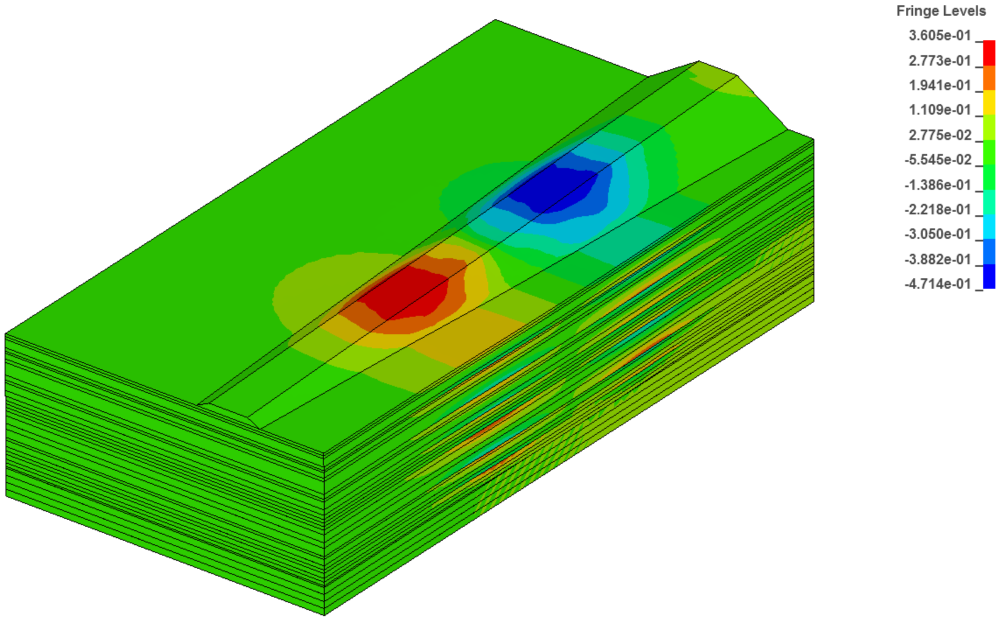

Figure 5-31 Lateral deformation distribution

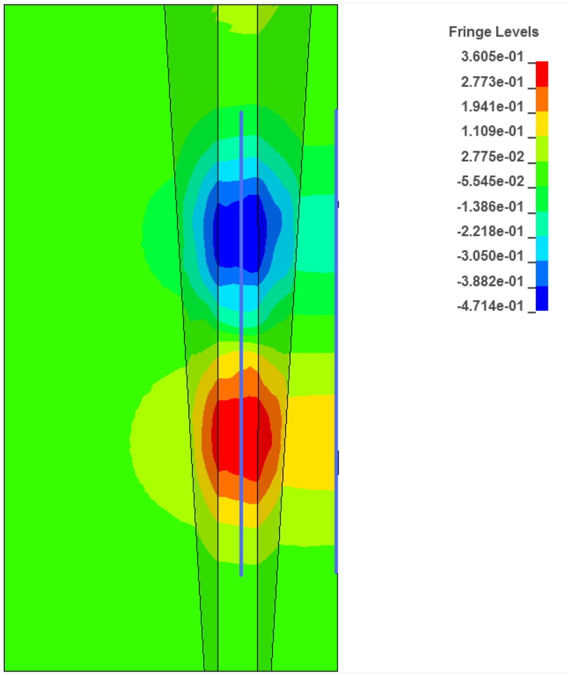

Figure 5-32 Profile lines on embankment and terrain for horizontal deformation

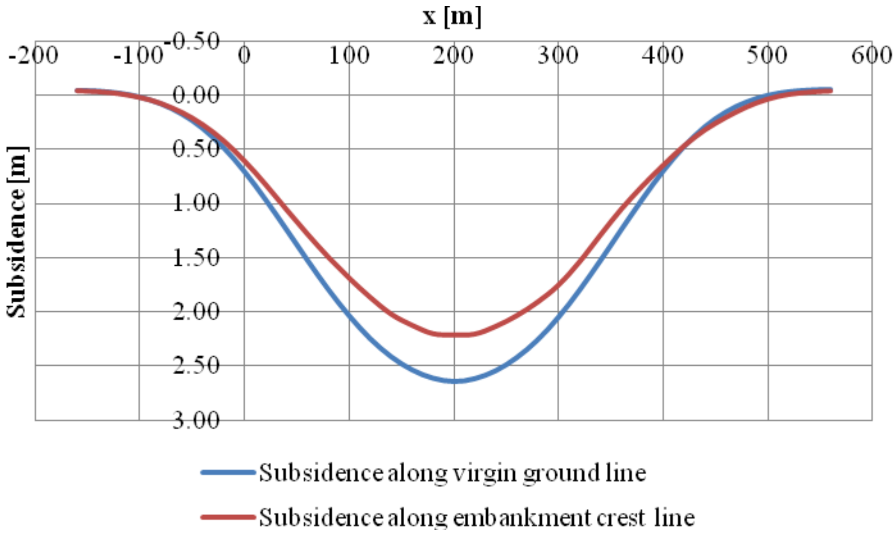

Figure 5-33 Subsidence profiles along embankment and virgin ground lines

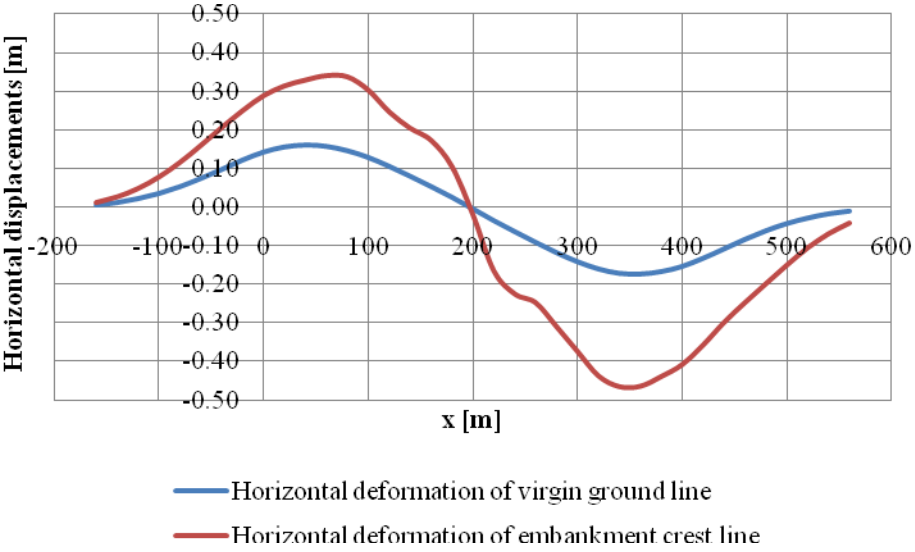

Figure 5-34 Horizontal deformation along embankment and virgin ground lines

6.0 CONCLUSIONS

From the development of the new subsidence model described in this work, four general conclusions may be drawn.

First, a clear relationship has been shown to exist between the subsidence factor, S^*/M, and the overburden thickness, H, whereby the subsidence factor decreases with overburden thickness. This variation exists for values of the width-to-depth ratio, W/H, that are well above the critical threshold of 1.2. This means that, even for supercritical cases, the subsidence factor of a specific region may still vary as different mining depths are considered. It is important to note that this contradicts a common notion that the subsidence factor in a given region approaches a constant value for $W/H > 1.2$.

Second, an extension of the so called profile functions has been presented for three dimensions, for which in the past influence functions have been employed. The influence function is more restricted. For instance, a profile can be too sharp to be described by influence functions.

Third, a simultaneous description of the so called static and dynamic subsidence was made through the methodology described. This was possible because the data were both spatially and temporally considered. This is useful in that a complete final and in-progress description of the subsidence trough can be made in three dimensions in a single model.

Fourth, the use of mathematical functions made it possible to derive the subsidence information indices. Moreover, the function, as shown, applies to both symmetric and asymmetric subsidence profiles.

From the development of the numerical subsidence model described in this work, four general conclusions may be drawn.

First, in order for a FEM model to correctly simulate the complete mechanism associated to mine subsidence, fracturing of the material would need to be implemented. This would be the most direct way to reproduce the so-called bulking factor that has a remarkable influence on the subsidence factor. Since this is impractical due to the extremely expensive computational cost, some conditions need to be imposed, such as the remaining elements on the floor that account for the bulking factor in an indirect way.

Second, the horizontal in-situ stresses seem to play a role on the subsidence factor, especially when they are very high. These stresses seem to be particularly high in this region of the world, where the typical subsidence factors also happen to be very low. Obviously, without a sound modeling of the fracturing of the rock and its consequent bulking, it is very difficult to draw conclusions on the importance of the role of in-situ stresses on subsidence. Nevertheless, the observed results would suggest that there is a connection between in-situ stresses and subsidence magnitudes.

Third, the behavior of horizontal deformations of earthen structures was demonstrated through a simple example. This quick result is in good agreement with observations and unfortunately suggests that the use of current empirical subsidence tools to predict lateral deformations would be extremely unreliable when applied to embankments or earth dams. In such cases, detailed numerical models should be encouraged.

Fourth, the FEM developed here brought the important results obtained in the past in 2D to a sound 3D version that serves as an excellent platform for further research. Beyond the case of embankments, any structure could be modeled in a flexible way.

BIBLIOGRAPHY

1. Agioutantis, Z. and M. Karmis (2009). Surface Deformation Prediction System for Windows Virginia Polytechnic Institute and State University.

2. Agioutantis, Z., M. Karmis, et al. (1987). Prediction of surface subsidence and strain in the Appalachian coalfields using numerical methods. *7th International Conference on Ground Control in Mining*, Morgantown, WV, USA, West Virginia University.

3. Alejano, L. R., P. Ramírez-Oyanguren, et al. (1999). "FDM predictive methodology for subsidence due to flat and inclined coal seam mining." *International Journal of Rock Mechanics and Mining Sciences* **36**(4): 475-491.

4. Coulthard, M. A. and A. J. Dutton (1988). Numerical modelling of subsidence induced by underground coal mining. *The 29th U.S. Symposium on Rock Mechanics (USRMS)*. Minneapolis, MN, A. A. Balkema, Rotterdam. Permission to Distribute - American Rock Mechanics Association.

5. Earth (2006). S.R. 0079 Longwall Mining Emerald Mine Panel B-4 Greene County, PA. Harrisburg, Pennsylvania, USA, Pennsylvania Department of Transportation.

6. Edmunds, W. E. (1999). Chapter 11: Pennsylvanian-Permian Transition and Permian. *Geology of Pennsylvania*. C. H. Schultz. Harrisburg, Pittsburgh, Pennsylvania Geological Survey Pittsburgh Geological Society**:** 171-177.

7. Edmunds, W. E., V. W. Skema, et al. (1999). Chapter 10: Pennsylvanian. *Geology of Pennsylvania*. C. H. Schultz. Harrisburg, Pittsburgh, Pennsylvania Geological Survey Pittsburgh Geological Society**:** 156.

8. GeoTDR (2001). Effects of undermining Interstate Route 70, South Strabane Township, Washington County, Pennsylvania. Westerville, Ohio, USA.

9. Graybill, F. A. and H. K. Iyer (1994). *Regression Analysis: Concepts and Applications*. Belmont, California, USA, Dusbury Press An Imprint of Wadsworth Publishing Company.

10. Gutiérrez, J. J., L. E. Vallejo, et al. (2010). A study of highway subsidence due to longwall mining using data collected from I-79. Pittsburgh, Pennsylvania, Pennsylvania Department of Transportation**:** 402.

11. Heasley, K. A. and T. M. Barton (1998). Subsidence Prediction Using a Laminated, Boundary-Element Program. *3rd North American Rock Mechanics Symposium*. Cancun, Mexico**:** 381-390.

12. Jarosz, A., M. Karmis, et al. (1990). "Subsidence development with time - experiences from longwall operations in the Appalachian coalfield." *International Journal of Mining and Geological Engineering*: 261-273.

13. Jeran, P. and V. Adamek (1988). Subsidence due to undermining of sloping terrain: A case study. *Report of Investigations*, United States Department of Interior Bureau of Mines.

14. Karmis, M. (1987). Prediction of ground movements due to underground mining in the Eastern United States coalfields. Blacksburg, VA, USA, Virginia Polytechnic Institute and State University.

15. Karmis, M., Z. Agioutantis, et al. (2008). Enhancing mine subsidence prediction and control methodologies. *27th International Conference on Ground Control in Mining*, Morgantown, WV, USA, West Virginia University.

16. Karmis, M., C. Haycocks, et al. (1992). The prediction of ground movement caused by mining. *3rd Subsidence Workshop Due to Underground Mining*, Morgantown, WV, USA, West Virginia University.

17. Karmis, M., T. Triplett, et al. (1983). Mining Subsidence And Its Prediction In The Appalachian Coalfield. *The 24th U.S. Symposium on Rock Mechanics (USRMS)*. College Station, TX, The Association of Engineering Geologists. Permission to Distribute - American Rock Mechanics Association.

18. Kratzsch, H. (1983). *Mining Subsidence Engineering*. Berlin Heidelberg New York, Springer-Verlag.

19. Kratzsch, H. (2008). *Bergschadenkunde*. Bochum, Deutscher Markscheider-Verein e.V.

20. Luo, Y. and S. S. Peng (1999). "Integrated approach for predicting mining subsidence in hilly terrain." *Mining Engineering*: 100-104.

21. Luo, Y., S. S. Peng, et al. (1996). Identification of factors affecting horizontal displacement in subsidence process. *15th International Conference on Ground Control in Mining*, Golden, CO, USA.

22. Mark, C. and M. Gadde (2008). Global Trends in Coal Mine Horizontal Stress Measurements. *27th International Conference on Ground Control in Mining*, Morgantown, WV, West Virginia University.

23. Mine Subsidence Engineering Consultants (2007). "Introduction to longwall mining and subsidence." Retrieved 08/19/2009, 2009, from www.minesubsidence.com.

24. Mohammad, N., P. W. Lloyd, et al. (1997). Longwall surface subsidence prediction through numerical modeling. *16th International Conference on Ground Control in Mining*, Morgantown, WV, USA, West Virginia University.

25. Morsy, K. and S. S. Peng (2002). Numerical modeling of the gob loading mechanism in longwall coal mines. *21st International Conference on Ground Control in Mining*, Morgantown, WV, West Virginia University.

26. NCB (1975). *Subsidence Engineer's Handbook*, National Coal Board.

27. OSMRE (1986). Guidance manual on subsidence control, United States Department of Interior.

28. Oyler, D., C. Mark, et al. (2004). Performance of roof support under high stress in a U.S. coal mine, NIOSH.

29. Peng, S. S. (1992). *Surface Subsidence Engineering*. Littleton, CO, USA, Society for Mining, Metallurgy, and Exploration, Inc.

30. Peng, S. S. (2008). *Coal Mine Ground Control*. Morgantown, WV, Department of Mining Engineering, College of Engineering and Mineral Resources, West Virginia University.

31. Peng, S. S. and H. S. Chiang (1984). *Longwall Mining*. New York, John Wiley & Sons.

32. Stone, R. W. (1932). *Geology and mineral resources of Greene County Pennsylvania*. Harrisburg, Pennsylvania, USA, Pennsylvania Geological Survey.

33. Su, D. (1991). Finite element modeling of subsidence induced by underground coal mining: The influence of material nonlinearity and shearing along existing planes of weakness. *10th International Conference on Ground Control in Mining*, Morgantown, WV, USA, West Virginia University.

34. Szostak-Chrzanowski, A. (1988). An iterative modeling of ground subsidence using non-linear elastic finite element analysis. *5th International Symposium on Deformation Measurements*, Fredericton, N.B., University of New Brunswick.

35. Tajdus, K. (2009). "New method for determining the elastic parameters of rock mass layers in the region of underground mining influence." *International Journal of Rock Mechanics and Mining Sciences* **46**(8): 1296-1305.

36. VPI&SU (1987). Prediction of ground movements due to underground mining in the Eastern United States coalfields. Blacksburg, VA, USA, Virginia Polytechnic Institute and State University**:** 205.

37. Whittaker, B. N. and D. J. Reddish (1989). *Subsidence: Occurrence, Prediction, and Control*, Elsevier Science Publisher B.V.